
This is an electronic reprint of the original article.
This reprint may differ from the original in pagination and typographic detail.

Multia, Jenna; Karppinen, Maarit

Atomic/Molecular Layer Deposition for Designer's Functional Metal–Organic Materials

Published in:
Advanced Materials Interfaces

DOI:
[10.1002/admi.202200210](https://doi.org/10.1002/admi.202200210)

Published: 23/05/2022

Document Version
Publisher's PDF, also known as Version of record

Published under the following license:
CC BY-NC-ND

Please cite the original version:
Multia, J., & Karppinen, M. (2022). Atomic/Molecular Layer Deposition for Designer's Functional Metal–Organic Materials. *Advanced Materials Interfaces*, 9(15), Article 2200210. <https://doi.org/10.1002/admi.202200210>

This material is protected by copyright and other intellectual property rights, and duplication or sale of all or part of any of the repository collections is not permitted, except that material may be duplicated by you for your research use or educational purposes in electronic or print form. You must obtain permission for any other use. Electronic or print copies may not be offered, whether for sale or otherwise to anyone who is not an authorised user.

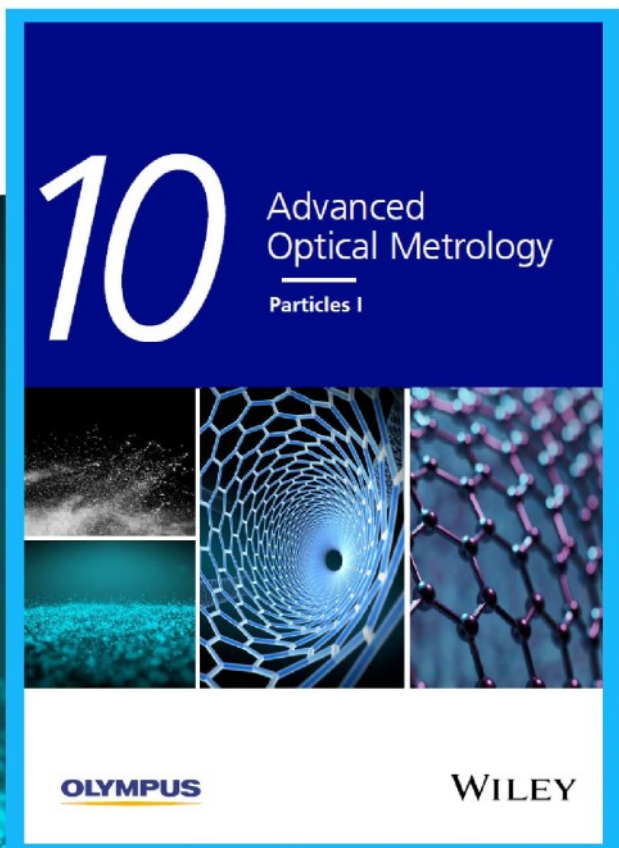


Particles I

Access the latest eBook →

Particles: Unique Properties,
Uncountable Applications

**Read the latest eBook and
better your knowledge with
highlights from the recent
studies on the design and
characterization of micro-
and nanoparticles for
different application areas.**



Access Now

This eBook is sponsored by

OLYMPUS

WILEY

Atomic/Molecular Layer Deposition for Designer's Functional Metal–Organic Materials

Jenna Multia and Maarit Karppinen*

Atomic layer deposition (ALD) for high-quality conformal inorganic thin films is one of the cornerstones of modern microelectronics, while molecular layer deposition (MLD) is its less-exploited counterpart for purely organic thin films. Currently, the hybrid of these two techniques, i.e., ALD/MLD, is strongly emerging as a state-of-the-art gas-phase route for designer's metal–organic thin films, e.g., for the next-generation energy technologies. The ALD/MLD literature comprises nearly 300 original journal papers covering most of the alkali and alkaline earth metals, 3d transition metals, and lanthanides as the metal component and a variety of aliphatic, aromatic, and natural organic components. Some of these ALD/MLD processes yield *in situ* crystalline coordination-polymer- or metal–organic-framework-like structures. Another attractive aspect is that many of the metal–organics realized through ALD/MLD are fundamentally new materials, and even unaccessible through conventional synthesis. Here, the current state of research in the field is presented, by i) providing a comprehensive account of the ALD/MLD processes so far developed, ii) addressing the constraints/possibilities for growing *in situ* crystalline metal–organic films, iii) highlighting some intriguing ALD/MLD materials and their application potential, and iv) making a brief outlook to the future perspectives and challenges in the field.

organic ligands act as bridges between the metal centers to form infinite 1D, 2D, or 3D structures. These materials are often referred to as coordination polymer (CP)^[1] or metal–organic framework (MOF)^[2] materials; the latter term is used when the metal–organic material is crystalline and highly porous.^[3] The research field of CP- and MOF-type materials has grown tremendously over the last two decades. The structural and chemical diversity of these materials has served as a continuous source of scientific excitement; the same diversity has also triggered huge technological interest as these materials possess enormous potential to be tailored for a wide variety of applications ranging from gas capture, storage, and separation to sensing, catalysis, optics, electronics, and energy storage.^[4–7]

Most of the targeted application breakthroughs of metal–organics require that these materials can be produced as high-quality thin films and coatings, which can be integrated with the other components

1. Introduction to Metal–Organic Materials and Combined Atomic Layer Deposition/Molecular Layer Deposition (ALD/MLD) Technique

Combining metal species with small organic molecules is a rather common concept in chemistry, viz. the entire field of conventional coordination complexes where the central metal atom/ion is connected to organic ligands through coordination bonds. Currently, the research interest is increasingly expanding to polymeric metal–organic complexes in which the

in the actual device configuration. The possibility to deposit such thin films in an industry-feasible manner on the substrate types needed, would be a major step forward in the field.^[8] Traditionally, solvent-based processes such as liquid-phase epitaxy, Langmuir–Blodgett, layer-by-layer, and electrochemical deposition techniques have been used for metal–organic thin films.^[9–11] These are, however, incompatible with the requirements set by the possible integration of the materials in microelectronics. This is due to corrosion and contamination risks, and the problems in patterning and precise deposition on high-aspect-ratio features. Hence, it is vital to develop solvent-free thin-film deposition routes for the metal–organic material family. In the optimal case, these deposition methods should allow conformal coatings on large-area and high-aspect-ratio substrates.

The currently strongly emerging ALD/MLD technique is uniquely suited to address the challenge in a scientifically elegant yet industrially feasible way. This technique is derived from the two parent gas-phase thin-film techniques: ALD for inorganic materials (mostly binary metal oxides, sulfides, and nitrides),^[12–14] and its counterpart MLD for purely organic thin films (e.g., polyimides and polyamides).^[15] In both cases, the attractive film growth characteristics are derived from the unique way of separating the different precursor gas pulses. Currently, ALD is the standard thin-film technology in many

J. Multia, M. Karppinen
Department of Chemistry and Materials Science
Aalto University
Aalto FI-00076, Finland
E-mail: maarit.karppinen@aalto.fi

 The ORCID identification number(s) for the author(s) of this article can be found under <https://doi.org/10.1002/admi.202200210>.

© 2022 The Authors. Advanced Materials Interfaces published by Wiley-VCH GmbH. This is an open access article under the terms of the Creative Commons Attribution-NonCommercial-NoDerivs License, which permits use and distribution in any medium, provided the original work is properly cited, the use is non-commercial and no modifications or adaptations are made.

DOI: 10.1002/admi.202200210

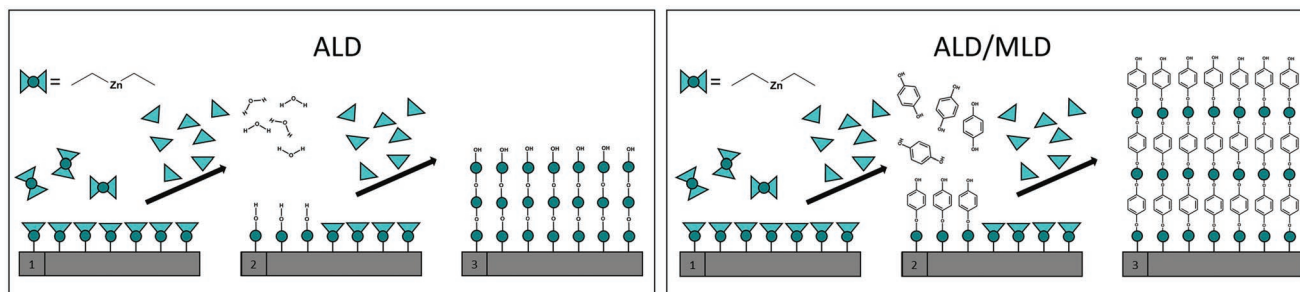


Figure 1. Schematics of the ALD and ALD/MLD processes: 1) metal precursor (e.g., diethyl zinc) + N₂ purge, 2) coreactant for ALD (e.g., H₂O) or organic precursor for ALD/MLD (e.g., hydroquinone) + N₂ purge. This precursor/purge pulse sequence is repeated to grow 3) the targeted inorganic or metal–organic thin film.

advanced applications in microelectronics and beyond (viz. the fabrication of HfO₂-based gate dielectrics in Intel's Xeon microprocessors since 2007^[16]), while MLD – first demonstrated in early 1990s^[15] – has only recently started to attract wider interest. Along with this recent interest, the MLD material library has been expanded from the polyimides^[15,17–22] and polyamides^[23–28] to many other polymers.^[29–44]

Both the parent techniques, ALD and MLD, are based on chemical surface reactions between two different gaseous (or vaporized) precursors sequentially pulsed into a vacuum reactor. The combined ALD/MLD technique for the hybrid metal–organic thin films involves a metal precursor similar to those used in ALD and an organic precursor that matches with the metal precursor (**Figure 1**).^[45–47] To facilitate the gas–surface reactions, the two precursors need to be mutually reactive. This requires that the metal precursor has reactive counterparts (e.g., halogenide ions or organic ligands) attached to the metal atom/ion and that the organic precursor has reactive functional groups attached to the organic backbone. Like its parent technologies for the purely inorganic and organic thin films, the ALD/MLD technique for the hybrids relies on self-limiting gas–surface reactions and yields high-quality thin films with excellent precision for the film thickness and composition. Another common fact with ALD and MLD is that the as-deposited films may be either amorphous or crystalline, depending on the material and the deposition conditions.

Since the first ALD/MLD papers for the hybrid inorganic–organic thin films appeared,^[45–49] there has been a growing interest not only in the combined ALD/MLD approach but also in MLD,^[50–52] see **Figure 2**. Initially the variety of the metal (Al, Ti, and Zn) and organic (e.g., ethylene glycol) components in the ALD/MLD films remained narrow and conventional,^[53] but in recent years, a rich variety of hybrid materials with different metals (alkali metal, alkaline earth metal, 3d transition metal, lanthanide) and organic (allyl, aryl, pyridine, nucleobase, etc.) constituents have been fabricated. As an evidence of the application potential of these newly discovered hybrid materials, exciting functional properties have already been demonstrated for these thin films, related to, e.g., textile-integrable thermoelectrics,^[54,55] barrier layers,^[33,56] photoluminescence,^[57,58] Li-ion battery,^[59] and other electrochemical applications.^[60]

The growth of in situ crystalline metal–organic thin films by ALD/MLD was demonstrated in 2016, first for copper terephthalate films,^[61] and soon after for several other metal and organic components.^[62] Some of these crystalline metal–organic films were of previously known CP- or MOF-type structures, but not all, underlining the possibility to exploit the ALD/MLD technique for synthesizing entirely new materials as well.^[63] Moreover, since both ALD and MLD are modular in principle, it is possible to create new hybrid materials by mixing different ALD and MLD cycles with arbitrary frequencies into elaborated superlattices (regular or irregular),^[54,64] nanolaminates,^[65,66]

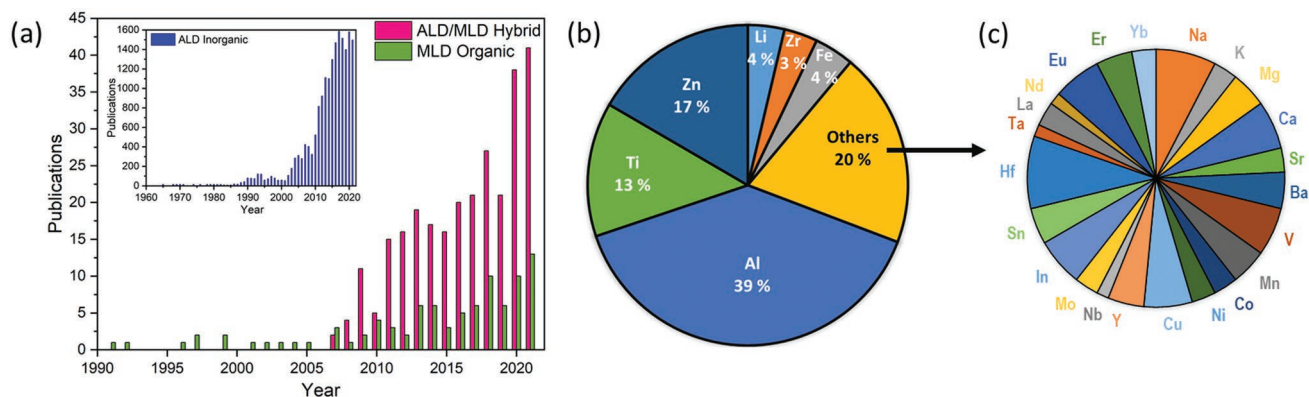


Figure 2. a) Annually published papers on MLD (organics; green) and ALD/MLD (metal–organics; pink); the inset displays similar records for ALD (inorganics; blue). b) Different metal components (and their frequencies) in ALD/MLD publications. c) Metal components constituting the group “others” in (b).

and heterostructures^[67] not necessarily attainable with conventional synthesis techniques.

There are many excellent review papers on ALD/MLD published over the years; these are collected in Table S1 (Supporting Information).^[11,12,33,47,53,68–102] In the early reviews by George et al.,^[12,47] Lee et al.,^[87] and Zhou and Bent,^[33] the ALD/MLD approach was thoroughly introduced. The two comprehensive accounts of the ALD/MLD precursors and processes are from the years 2014 and 2017.^[53,102] There are also reviews on more specific aspects of the topic, such as porous films obtained from ALD/MLD films through calcination or water etching,^[77] different high-surface-area substrates and reactor configurations used,^[74] and the so-called vapor-phase infiltration processes where inorganic precursors are infiltrated into porous polymers or fibers.^[75] Also, some of the reviews focus on specific applications of the ALD/MLD films, in particular on different Li-ion battery and other energy applications,^[69,70,76,91–93,101,103] but also on drug delivery encapsulation.^[99] Moreover, Weimer^[98] describes different ALD and MLD processes over nanoparticles, nanotubes, and polymer particles, and Cai et al.^[100] categorize the ALD/MLD processes based on their dimensionality, i.e., 0D, 1D, 2D, or 3D. In the most recent review, the different alkali-metal-based ALD/MLD processes and their application possibilities are summarized.^[94]

In this comprehensive review, our intension is to present the current state of research in the field; we i) provide a full account of the ALD/MLD processes so far developed, ii) address the constraints and possibilities for growing in situ crystalline metal–organic films, iii) highlight some intriguing ALD/MLD materials and their application potential, and iv) make a brief outlook to the future perspectives and challenges in the field.

2. Particular Features of ALD/MLD Processes

Like in conventional ALD, the precursor design is highly important in ALD/MLD. The technique is based on gaseous precursors (or liquids/powders that are readily vaporized within the deposition conditions), and in particular for the larger organic precursors, the low volatility may be a major issue.^[104] Then, for the efficient and ideal film growth itself, the main requirement concerns the optimal balance between the reactivities and thermal stabilities of the precursors. The metal-bearing precursors employed in ALD/MLD are typically very similar to those used in

ALD for the inorganic thin films. For the organic precursor, the design scheme (as discussed in a more detailed way in Section 3) covers not only the optimal functional groups to achieve the surface reactions with the metal precursor but also the need to bring the desired functionality to the resultant hybrid thin film through the backbone of the precursor molecule.

The overall deposition process is typically examined and evaluated by monitoring the film growth rate as a function of different deposition parameters (precursor and purge pulse lengths, deposition temperature, etc.). The growth rate is expressed as a so-called growth-per-cycle (GPC) value calculated from the total film thickness divided by the number of precursor cycles applied. For ideal ALD and MLD processes, expected is to see a saturation behavior for the GPC value with increasing precursor pulse length (for both precursors), and also a linear dependence of the film thickness on the number of deposition cycles (Figure 3).^[105]

Most straightforwardly, one might assume that the GPC value in ALD/MLD would correspond to the metal–organic unit length, i.e., the metal cation size plus the length of the organic backbone. In practice, however, significantly lower GPC values are often seen. In conventional ALD, the lower than monolayer growth rates are often attributed to the steric hindrance of the spacious ligands of the metal precursor.^[106] In ALD/MLD, additional issues are likely to arise when the metal-bearing precursor is combined with an organic precursor (Figure 4).^[23,24,47] Organic molecules are characteristically large but flexible and (in particular, those with lengthy alkyl chains) prone to tilt. The resultant nonperpendicular orientation of the molecule increases its steric hindrance effect on the surface. Moreover, the bending of the organic molecule increases its probability to react twice, i.e., through both of its reactive groups, with the film surface, which eventually lowers the number of reactive surface sites and decreases the growth rate, see Figure 4b. Another rather opposite implication of the larger organic backbone is that the metal–metal distance in the resultant metal–organic thin film naturally increases; this creates larger spacing between the binding sites on the surface and makes them less affected by the different steric hindrance effects. Saturation of the film growth with bulkier organic precursors typically takes longer time than for the smaller metal precursors. One plausible explanation here is that the large molecules may initially block the neighboring binding sites, causing the saturation to take longer, see Figure 4c.^[106]

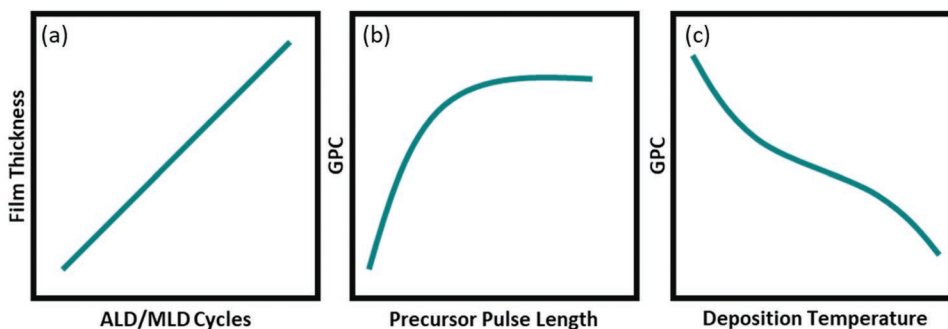


Figure 3. An ideal ALD/MLD process shows a) linear dependence of the film thickness on the number of precursor pulsing cycles, and b) saturation of the GPC value with increasing precursor pulse lengths. On the other hand, c) differently from the conventional ALD processes, the ALD/MLD processes typically do not show any constant-GPC temperature window, but the GPC value often decreases with increasing deposition temperature.

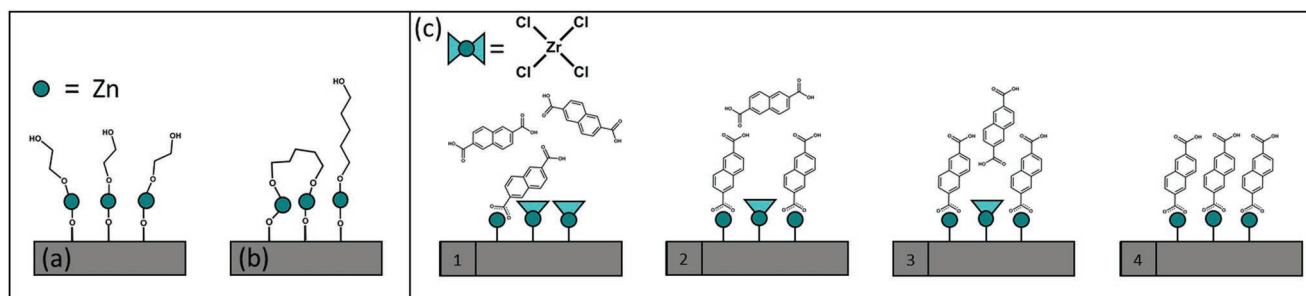


Figure 4. Different surface reaction modes demonstrated for two example ALD/MLD processes based on diethyl zinc (DEZ) as the inorganic precursor, a) DEZ + EG, and b) DEZ + DAH, illustrating the possibility of surface termination with the longer organic precursor. c) Possible stages of surface saturation demonstrated for the relatively large 2,6-NDC organic precursor molecule which may initially block the neighboring binding sites causing saturation to take longer time. Adapted with permission.^[106] Copyright, 2020, Royal Society of Chemistry.

By smart design of the organic precursor (backbone and functional groups), it may be possible to affect the aforementioned film growth issues.^[23,24] Most straightforwardly, by selecting a rigid aryl-based organic backbone (e.g., hydroquinone,^[107] 1,3,5-benzenetriol,^[46] or *p*-phenylenediamine^[108]) instead of a more flexible alkyl backbone, it may be possible to diminish the bending and thereby the unwanted double surface reactions. Then, considering the functional groups, it has been demonstrated that heterofunctional organic precursors (e.g., amino alcohols or hydroxyl compounds with vinyl groups) could be beneficial over their homofunctional counterparts, as with two different reactive groups, the precursor is likely to react with preference through the more reactive one, leaving the other group unreacted as long as there are similar heterofunctional precursor molecules freely available in the gas phase.^[47] To go even further along this strategy, the heterofunctional precursor can be modified by activating the surface after the precursor pulsing cycle transforming the second group into a more reactive group; as an example, vinyl groups have been successfully activated with ozone and peroxides to form reactive carboxylic acid or aldehyde groups.^[24,45] Another strategy to avoid double reactions is to utilize ring-opening reactions; this would yield new hydroxyl, amine, or carboxylic acid groups for the further film growth.^[24,109]

For most of the ALD/MLD processes, the GPC value depends on the deposition temperature (T_{DEP}), typically decreasing with increasing T_{DEP} , as was schematically shown in Figure 3c. There are multiple possible explanations for this (possibly all contributing simultaneously): i) tendency of organic precursors to decompose and/or desorb at high temperatures,^[110] ii) stickiness of organic molecules at low temperatures toward remaining in the growing film as a kind of reservoir and additional reaction site during the metal precursor pulses,^[23,24,56,111–114] and iii) physisorption of metal precursor molecules within the porous organic material at low temperatures.^[56,111–114] Finally, it should be noted that like in conventional ALD, the choice of the substrate may have an effect on the film as well. For example, Zn–ethylene glycol (EG) films were deposited on two different metal oxide substrates, SiO_2 and Al_2O_3 , to investigate the binding-energy-dependent growth behavior and surface properties of the films. Initially, the film was found to grow faster on SiO_2 , but after 100 ALD/MLD cycles, the growth rates were similar on both SiO_2 and Al_2O_3 .^[115]

The ALD-/MLD-grown metal–organic thin films are typically characterized by multiple techniques, as summarized in Figure 5. Some but not all of the films have been found air-sensitive or chemically/thermally unstable. One of the reasons could be the fact that these films are typically more porous and less dense than the inorganic films based on the same

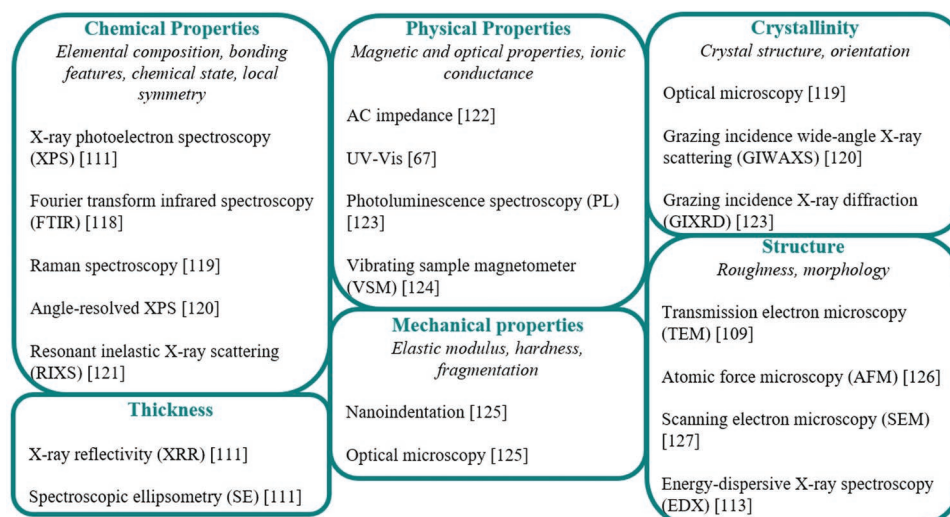


Figure 5. Characterization techniques commonly employed for the ALD-/MLD-grown thin films.

metal constituent. For example, the following densities have been reported for the two Al-bearing thin films fabricated using trimethyl aluminum (TMA) as the inorganic precursor: $\approx 1.5 \text{ g cm}^{-3}$ for Al-EG^[111] and $\approx 3.0 \text{ g cm}^{-3}$ for Al₂O₃.^[116]

3. Organic Precursors in ALD/MLD

As already mentioned in the previous section, the design/choice of the organic precursor in ALD/MLD is important for various reasons. First, the functional groups should be reactive toward the ligands in the inorganic (metal-bearing) precursor. For example, the rather common metal diketonate precursors based on the 2,2,6,6-tetramethyl-3,5-heptanedionate (thd) ligands are highly stable in air and hence easy to handle, but at the same time, the low reactivity of these complexes poses stricter requirements for the second precursor in terms of reactivity. In ALD, for metal oxide films, the second precursor combined with metal diketonates is typically ozone (instead of water),^[127] while in ALD/MLD, carboxylic acids serve the same purpose (instead of alcohols).^[61,128,129] Another option but little exploited so far is 1,4-benzenedisulfonic acid (BDS); it is significantly (six orders of magnitude)^[130] more acidic than the corresponding 1,4-benzenedicarboxylic acid (BDC), and could therefore enable the use of the least reactive inorganic precursors.^[131,132]

The second issue concerns the fact that most of the organic precursors are solids with relatively high sublimation temperatures, hence requiring higher precursor source temperatures compared to the metal precursors used in ALD. Typically, the use of a too low source temperature leads to the need of longer pulse lengths, thus elongating the deposition process. On the contrary, a too high source temperature may lead to the unwanted gas-phase decomposition of the precursor and uncontrollable film growth. Thermogravimetric (TG) analysis has been utilized as a convenient practical tool to find the optimized organic precursor source temperatures (Figure 6).^[104] The observed onset temperature for the weight loss upon heating can be used to predict the optimal precursor source temperature in ALD/MLD, which is typically lower by $\approx 14\%$

than the onset temperature where the weight loss starts in a TG experiment. In case no TG data are available, it is noteworthy that even the melting point values seem to reflect relatively well the required precursor source temperature values. However, strong hydrogen bonds within the material tend to increase the melting point, but not necessarily the required MLD sublimation temperature.^[104]

The third aspect – an additional degree of freedom – in the organic precursor design is the choice of the backbone which provides us an intriguing possibility to bring new functionalities to the final metal–organic hybrid material. As exciting examples, the organic component could contribute to the charge-carrier doping (e.g., hydroquinone (HQ) for n-type doping, BDC for p-type doping),^[133] act as a photoresponsive moiety (e.g., azobenzene),^[134] or show antimicrobial effects (e.g., curcumin).^[135] From the sustainability and/or biocompatibility points of view, interesting organic precursor candidates are also the different nucleobases,^[58,136] i.e., constituents of DNA and RNA.

New organic components have also been developed for the purely organic MLD processes; the MLD material library already includes, besides the initially introduced polyimides^[15,17–22,137–143] and polyamides,^[15,23–28,144–149] many other polymers: polyurea,^[29,30,37,38,51,150–164] polythiourea,^[52] polyurethane,^[165,166] polyazomethine,^[167–172] poly(3,4-ethylenedioxythiophene),^[173–177] polyimide–polyamide,^[141] poly(ethylene terephthalate) (PET),^[50,178–180] and others.^[31,32,39–44,176,181–200] In recent years, the organic precursor library has been rapidly expanding. We have collected in Table 1 the organic precursors so far used in ALD/MLD processes, together with the heating temperatures employed for their evaporation in the corresponding process conditions;^[17,18,32,40,46,51,57–59,61,63,64,66,81,105–108,114,118,119,121,122,125,129,134–136,139,141,142,156,164,168,189,201–284] molecular structures of these precursors are shown in Figure 7.

4. Brief Account of ALD/MLD Processes Developed

The early ALD/MLD studies were mostly based on the three metal components, Al, Ti, and Zn. This is understandable,

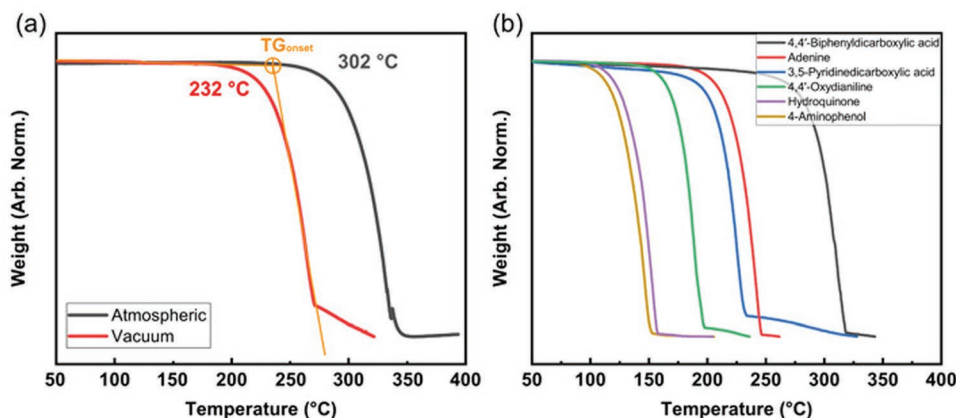


Figure 6. TG curves recorded a) for 1,4-benzenedicarboxylic acid under vacuum ($\approx 4 \text{ mbar}$) and atmospheric pressure (the corresponding onset temperature ($T_{G_{\text{onset}}}$) values and their definition are also indicated) and b) for other selected organics under vacuum (the weight scale is normalized). Reproduced with permission.^[104] Copyright 2020, AIP Publishing.

Table 1. Organic precursors employed in ALD/MLD processes and their commonly used source temperatures.

| Abbreviation | Full name (aromatic molecules) | Source temperature [°C] | Abbreviation | Full name (linear molecules) | Source temperature [°C] |
|-------------------------------|---|---|-------------------|--|---|
| BDC | 1,4-Benzenedicarboxylic acid | 185 ^[57,59,61,129,201–206] | | Oxalic acid | 100 ^[207] |
| 3,5-PDC | 3,5-Pyridinedicarboxylic acid | 190 ^[57,118,208] | DAH | 1,6-Diaminohexane | 40 ^[209] |
| 2,6-PDC | 2,6-Pyridinedicarboxylic acid | 235 ^[57] | | Succinic acid | 140 ^[210] |
| 8-HQ | 8-Hydroxyquinoline | 100 ^[46,211–213] | ED | Ethylenediamine | RT ^[46,51,164] |
| 2,3-PZD | 2,3-Pyrazinedicarboxylic acid | 145 ^[214] | | Propargyl alcohol | [215,216] |
| | Thymine | 207 ^[136,217] | GL | Glycerol | 60 ^[218–220] |
| | Adenine | 210 ^[58,136,217] | | Suberic acid | 139 ^[221] |
| | Uracil | 207 ^[58,136,217,222,223] | | Glycine | 200 ^[210,217] |
| 2-Amino-1,4-BDC | 2-Amino-1,4-benzenedicarboxylic acid | 225, ^[224] 185 ^[225] | 7-OTS | 7-Octenyltrichlorosilane | 100 ^[226–228] |
| 2,6-NDC | 2,6-Naphthalenedicarboxylic acid | 250, ^[229] 225 ^[106,122] | EG | Ethylene glycol | 30 ^[220,230,231] |
| ODA | 4,4'-Oxydianiline | 140 ^[17,18,32,139,141,142,206,232,233] | | L-glutamic acid | 165 ^[234] |
| BDT | 1,4-Benzenedithiol | 35 ^[206] | HDD | 2,4-Hexadiyne-1,6-diol | 80 ^[81,228,235] |
| PPDA | <i>p</i> -Phenylenediamine | 70 ^[108,168,206] | TCNE | Tetracyanoethylene | RT ^[236,237] |
| 4-AP | 4-Aminophenol | 111 ^[105,233,238,239] | | Sebacic acid | 147 ^[221] |
| PMDA | Pyromellitic dianhydride | 150 ^[209] | | Maleic acid | 130 ^[46,240] |
| PDIC | 1,4-Phenylene diisocyanate | 90 ^[241] | EDT | 1,2-Ethanedithiol | RT ^[242,243] |
| | 4-Aminobenzoic acid | [46] | | 1,4-Butanedithiol | RT ^[243] |
| HQ | Hydroquinone | 90 ^[46,59,63,64,66,107,244–252] | | Arginine | 200 ^[217] |
| 1,2-BDC | 1,2-Benzenedicarboxylic acid | 177 ^[114] | | Glutaric acid | 199 ^[253] |
| | 1,3,5-Benzenetriol | [46] | | Tricarballic acid | 135 ^[114,234] |
| 1,2,4,5-BTC | 1,2,4,5-benzenetetracarboxylic acid | 190 ^[46,114] | | Fumaric acid | 150, ^[46,240] 172 ^[254] |
| TC | Terephthaloyl chloride | 90 ^[40] | | (2 <i>E</i> ,4 <i>E</i>)-hexa-2,4-dienedioic acid | [46] |
| FHQ | Tetrafluorohydroquinone | [230] | TEA | Triethanolamine | 148 ^[255,256] |
| 4MP | 4-Mercaptophenol | 100 ^[257] | BD | 1,4-Butanediol | 80 ^[156,189,258] |
| IR-806 | 2-[2-(2-Chloro-3-[2-[1,3-dihydro-3,3-dimethyl-1-(4-sulfobutyl)-2 <i>H</i> -indol-2-ylidene]-ethylidene]-1-cyclopenten-1-yl]-ethenyl]-3,3-dimethyl-1-(4-sulfobutyl)-3 <i>H</i> -indolium hydroxide | 245 ^[259] | Bdy | 1,4-Butynediol | 50 ^[258] |
| 4,4'-BPDC | 4,4'-Biphenyldicarboxylic acid | 250 ^[106] | | Aconitic acid | 114 ^[234] |
| 1,3-BDC | 1,3-Benzenedicarboxylic acid | 212 ^[114] | EA | Ethanolamine | 80 ^[260,261] |
| 1,3,5-BTC | 1,3,5-Benzenetricarboxylic acid | 245 ^[205] | MC | Malonyl chloride | RT, ^[262] 28 ^[261] |
| AZO | 4,4'-Azobenzenedicarboxylic acid | 310 ^[134,263] | | Lactic acid | 115 ^[264] |
| Cur | Curcumin | 260 ^[135,265] | | Pimelic acid | 139 ^[221] |
| 1,4-NDC | 1,4-Naphthalenedicarboxylic acid | 200 ^[266] | DEG | Diethylene glycol | 100 ^[267] |
| ADA | 9,10-Anthracenedicarboxylic acid | 240 ^[266] | HD | 1,6-Hexanediol | 85 ^[125] |
| Qz | Quinizarin | 130 ^[268] | DD | 1,10-Decanediol | 120 ^[269] |
| BDS | 1,4-Benzenedisulfonic acid | 190 ^[121] | H ₄ Pe | Pentaerythritol | 160 ^[268] |
| DHTP | 2,5-Dihydroxyterephthalic acid | 190 ^[270] | PD | 1,3-Propanediol | 100 ^[271] |
| PMDA | 1,2,4,5-Benzenetetracarboxylic anhydride | 150 ^[209] | L-Cys | L-Cysteine | [217,272] |
| Abbreviation | Full name (ring-opening) | Source temperature [°C] | L-Ala | L-Alanine | [217] |
| | Phenol | 80 ^[273,274] | L-Lys | L-Lysine | [217] |
| 3F | 3-(Trifluoromethyl)phenol | 80 ^[273,274] | | Malonic acid | 125 ^[221] |
| 4F | 2-Fluoro-4-(trifluoromethyl)benzaldehyde | 60 ^[273,274] | | L-aspartic acid | 225 ^[210] |
| GLY | Glycidol | 60 ^[275,276] | DMD | <i>N,N'</i> -dimethyldithioamide | 60 ^[119] |
| AZ | <i>N</i> -(2-aminoethyl)-2,2,4-trimethyl-1-aza-2-silacyclopentane | 55 ^[277] | PDT | 1,5-Pentanedithiol | 55 ^[278] |
| LAC | ϵ -Caprolactone | 60 ^[279] | D-Cys | D-Cysteine | [272] |
| V ₄ D ₄ | 2,4,6,8-Tetramethyl-2,4,6,8-tetravinylcyclotetrasiloxane | 75 ^[280,281] | MMA | Methyl-methacrylate | RT ^[282] |
| MA | Maleic anhydride | 80 ^[260,277,283] | | | |
| V ₃ N ₃ | 2,4,6-Trimethyl-2,4,6-trivinylcyclotrisilazane | 80 ^[284] | | | |

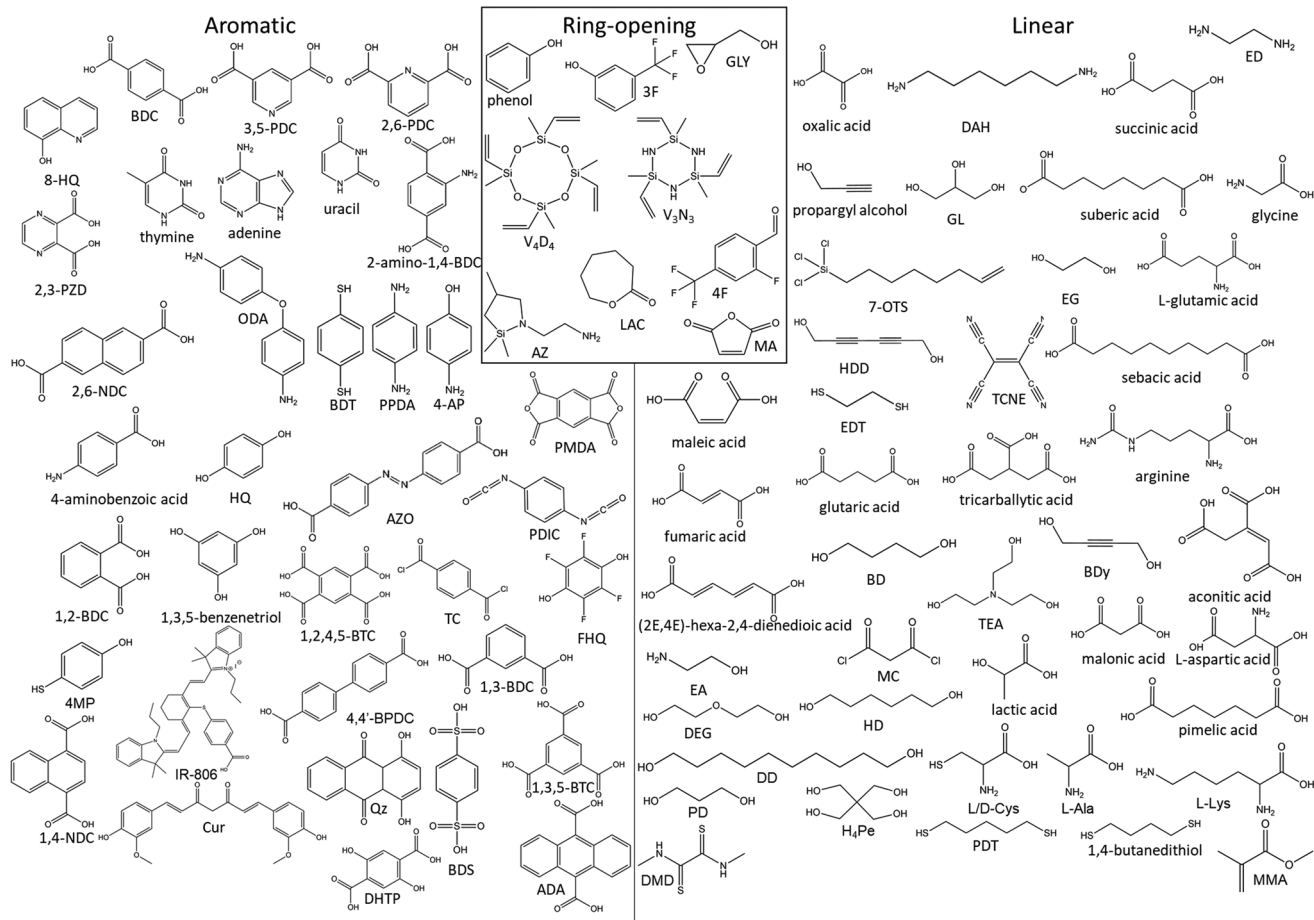


Figure 7. Molecular structures of organic precursors used in ALD/MLD processes.

as these three metals are also the most common elements in conventional ALD.^[70,285,286] For example, Nilsen et al.^[46,56,211] deposited metal quinolone films by coupling 8-HQ with all the most common ALD precursors, TMA, diethyl zinc (DEZ), and TiCl_4 , to yield Alq_3 , Znq_2 , and Tiq_4 films. More recently, the ALD/MLD material library has rapidly expanded to cover tens of different metal components, from all the parts of the periodic table, i.e., s-block, d-block, f-block, and p-block, see **Figure 8**.

To develop a new ALD/MLD process, several choices need to be made. The first one is naturally the metal node, which could bring to the resultant metal–organic thin film various desired functionalities (e.g., alkali metal \rightarrow battery, d-block metal \rightarrow magnetism or catalysis, lanthanide \rightarrow luminescence). Then, to realize the gas–solid surface reactions for the film growth, the choice of the ligands in the metal-bearing precursor becomes important. The variety of different ligands employed is also already relatively large, as summarized in **Figure 8**. For some of the metals, well-behaving precursors with several different ligand types have been demonstrated, for example, for iron: iron chloride (FeCl_3), iron *tert*-butoxide ($\text{Fe}_2(\text{O}^t\text{Bu})_6$), iron acetylacetonate ($\text{Fe}(\text{acac})_3$), cyclopentadienyl iron dicarbonyl dimer ($\text{Cp}_2\text{Fe}_2(\text{CO})_4$), and iron β -diketonate-diamine complex ($\text{Fe}(\text{hfa})_2\text{TMEDA}$, hfa = 1,1,1,5,5,5-hexafluoro-2,4-pentanedionate, TMEDA = *N,N,N',N'*-tetramethyl-ethylenediamine).

In the following subsections, a comprehensive account of the ALD/MLD processes so far developed is given, organized according to the metal component.

4.1. Aluminum-, Zinc-, and Titanium-Based Processes

Aluminum-based processes were the first ALD/MLD processes reported, and even now, they constitute a major part of the ALD/MLD processes. The prototype process is the one with TMA and EG.^[111,231,287–332] However, TMA works very well with many other organics as well.^[40,46,54,108,109,114,125,148,211–213,218,219,221,226,228,230,234,240,244,245,249,252,255,256,258,260,262,264,267–269,273–277,279–284,325,333–369]

The bulkier dimethyl aluminum isopropoxide precursor has been successfully used with EG as well.^[323] Different TMA + organic processes have been investigated, e.g., to elucidate the effect of the organic backbone length, i.e., long (1,10-decanediol) or short (1,6-hexanediol), on the mechanical properties; indeed, as expected, with the increasing chain length, the stretchability was enhanced.

Diethylzinc is the most common precursor for zinc in the ALD/MLD processes; it is often combined with HQ,^[54,55,66,107,133,230,244–247,250,361,366,370–378] but also with many other organic components.^[46,48,115,134,211,212,226,228,233,238,239,241,265,272,278,324,345,349,379–390] The DEZ + HQ process has been

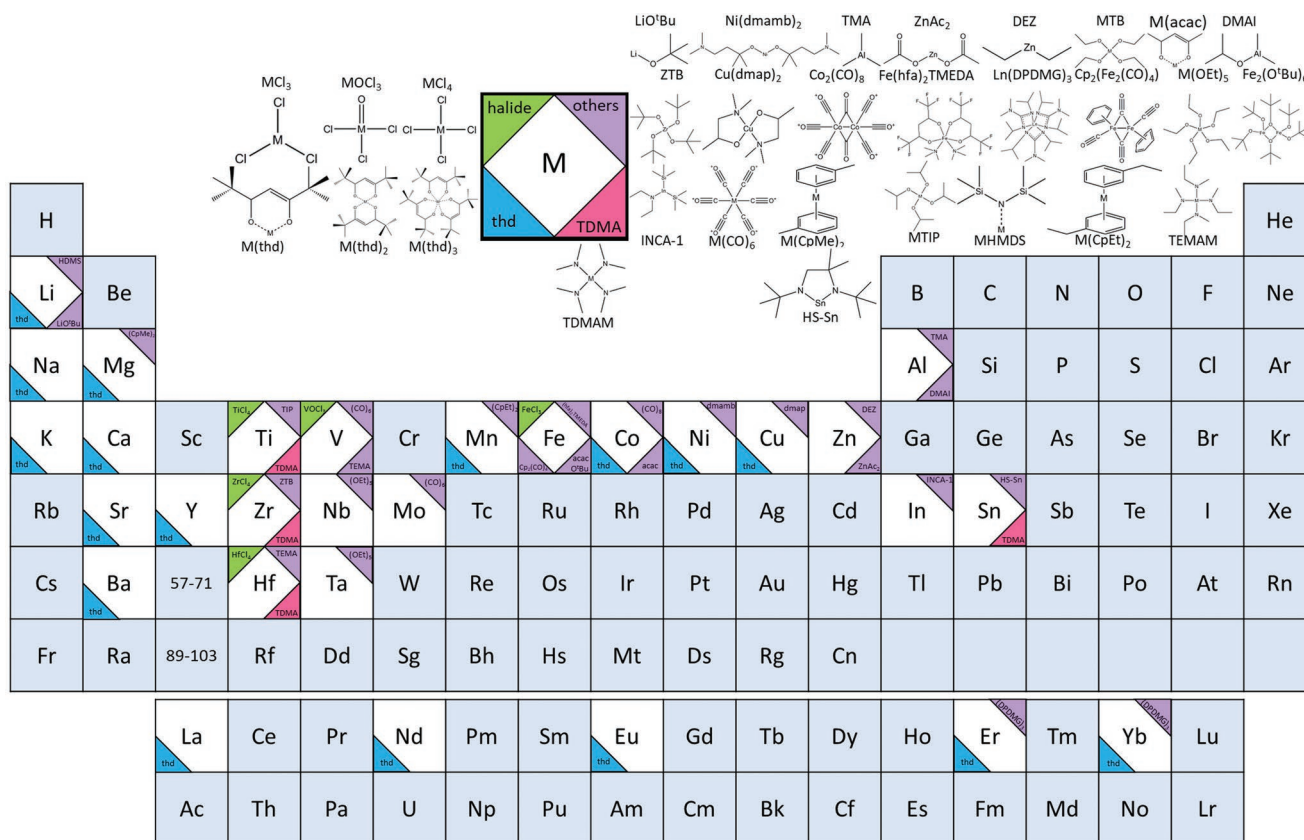


Figure 8. Inorganic precursors applied in ALD/MLD processes.

widely utilized for the growth of different superlattice structures in which the Zn–HQ layers are combined with thicker ZnO layers grown with ALD cycles with DEZ plus H₂O. Another zinc precursor employed in ALD/MLD is zinc acetate.^[117,229]

For titanium, the most common precursor is TiCl₄, extensively used with EG,^[179,293,391–400] and other organics.^[46,49,105,112,122,211,230,232,235,248,254,255,336,378,390,401–408] For example, the combination, TiCl₄ plus maleic anhydride has been utilized to deposit thin films with biologic synaptic functions.^[401] Besides the TiCl₄ precursor, also titanium tetra-isopropoxide^[45,135,136,210,217,227,265,351,409] and tetrakis(dimethylamido) titanium^[112] precursors have been successfully employed.

We have collected the numerous ALD/MLD processes developed and extensively investigated for aluminum, zinc, and titanium in Tables S2–S4 (Supporting Information).

4.2. Alkali-Metal-Based Processes

The first ALD processes for alkali-metal-based inorganic thin films were reported as late as in 2009.^[410] These processes were for lithium and motivated by the prospective Li-ion battery applications. Similarly, the first alkali-metal-based ALD/MLD process from the year 2016 was for lithium, and aiming at battery application.^[128] The somewhat slow emergence of the alkali-metal-based ALD/MLD processes is presumably due to the challenges related to the common alkali metal chemistry features, including the fact that alkali metals are monovalent

and their precursors mostly monoleptic. On the other hand, an intriguing feature of the alkali-metal-based ALD/MLD processes is that most of them yield in situ crystalline thin films.^[94]

Among the alkali metals, the precursor arsenal is the widest for lithium, comprising the thd-,^[67,118,121,128,129,225,270,411] O^tBu-,^[271,412] and bis(trimethylsilyl)amide (HMDS)-^[59,63,413] based precursors, which have been combined with BDC,^[59,128,129,225,411] 3,5-pyridinedicarboxylic acid (PDC),^[118,411] 2-amino-1,4-BDC,^[225] 1,3-propanediol (PD),^[271] EG,^[412,413] 4,4'-azobenedicarboxylic acid (AZO),^[67,411] HQ,^[59,63] 2,6-naphthalenedicarboxylic acid (2,6-NDC),^[411] 4,4'-biphenyldicarboxylic acid (4,4'-BPDC),^[411] 2,5-dihydroxyterephthalic acid (DHTP),^[270] and BDS^[121] as organic precursors. Interestingly, lithium ethylene carbonate thin films have been deposited as well; in this process, CO₂ was employed as the third precursor.^[413] Another intriguing process is based on Li(thd) and DHTP precursors; the special feature of this process is that the product, Li₂DHTP, or Li₄DHTP (both being potential ambipolar electrode materials), is controlled by adjusting the precursor pulsing times.^[270]

For sodium and potassium, all the reported ALD/MLD processes are based on the thd-based metal precursors, which have been combined with BDC,^[129] uracil,^[58,222,223] adenine,^[58] and 3,5-PDC^[118] in the case of sodium, and with BDC^[129] and 3,5-PDC^[118] in the case of potassium.

Deposition temperatures for the alkali-metal-based films range typically between 200 and 300 °C, the highest temperatures reported for the uracil-, adenine-, and AZO-based films. An outlier is the Li–EG films which have been deposited at as

Table 2. ALD/MLD processes based on alkali metals.

| 3 Lithium | Organic | GPC [Å per cycle] | T_{DEP} [°C] | In situ cryst. | Year | Ref. |
|---------------------|--|--|--|--|------|-------|
| LiOtBu | EG | 2.6 | 135 | | 2020 | [412] |
| | PD | 0.23 | 140–200 | Yes | 2020 | [271] |
| Li(thd) | DHTP | ≈4–8 (Li ₂ DHTP), ≈13 (Li ₄ DHTP) | 200–250 | Yes (Li ₂ DHTP), hyd. (Li ₄ DHTP) | 2022 | [270] |
| | BDS | 2.0–2.3 | 200–260 | Yes | 2021 | [121] |
| | BDC, 3,5-PDC, 2,6-NDC, 4,4'-BPDC, AZO | 2.5 (3,5-PDC), 3.0 (BDC), 2.3 (2,6-NDC), 7.0 (4,4'-BPDC), 7.0 (AZO) | 220 (BDC, 3,5-PDC, 2,6-NDC), 240 (4,4'-BPDC), 270 (AZO) | Yes | 2020 | [411] |
| | AZO | 7.0 | 270 | Yes | 2020 | [67] |
| | 2-Amino-1,4-BDC (BDC ref.) | 3.6 (2-amino-1,4-BDC), 3.0 (BDC) | 200 | Yes | 2020 | [225] |
| | 3,5-PDC | 2.5 | 190–300 | Yes | 2019 | [118] |
| | BDC | 3 | 200–280 | Yes | 2017 | [129] |
| | | | 3 | 200–280 | Yes | 2016 |
| Li(HMDS) | EG (+CO ₂) | 2.5–3 | 80 | | 2020 | [413] |
| | BDC, HQ | 3 | 200 (BDC), 160 (HQ) | Yes | 2018 | [59] |
| | HQ | 4.5 | 105–280 | Yes | 2017 | [63] |
| 11 Sodium | | | | | | |
| Na(thd) | 3,5-PDC | 3.7 | 190–300 | Yes | 2019 | [118] |
| | BDC | 3 | 190–300 | Yes | 2017 | [129] |
| | Uracil, adenine | 4.8 (uracil), ≈10 (adenine) | 260–320 | Yes | 2017 | [58] |
| | Uracil | 4.8 | 300 | Yes | 2017 | [222] |
| | | 4.8 | 300 | Yes | 2016 | [223] |
| 19 Potassium | | | | | | |
| K(thd) | 3,5-PDC | 3.5 | 190–300 | Yes | 2019 | [118] |
| | BDC | 2.5 | 220–300 | Yes | 2017 | [129] |

low temperatures as ≈100 °C. From **Table 2**, the growth rates range typically from 2 to 5 Å per cycle for most of the alkali-metal-based processes except for those based on the particularly long AZO and 4,4'-BPDC organic molecules for which GPC values up to 7 Å per cycle have been reached. In the other end, for the Li–PD process, a GPC value as low as 0.23 Å per cycle was seen, possibly due to the self-terminated reaction happening during the growth.^[271] Most of the alkali-metal-based films have been in situ crystalline, except for the Li–EG and Li₄DHTP films.

4.3. Alkaline-Earth-Metal-Based Processes

Most of ALD/MLD processes of alkaline earth metals involve thd-based metal precursors (**Table 3**), but Mg-based films have been deposited also from (MeCp)₂.^[56] As organic precursors, both linear (EG and glycerol (GL))^[56] and aromatic (BDC,^[62,67,129] 3,5-PDC,^[118] and AZO^[67]) molecules have been employed, and in the case of barium, also uracil and adenine have been challenged.^[58] The deposition temperature range is typically around 200–300 °C with the exception of the Mg–EG and Mg–GL films deposited in the temperature range of 100–200 °C. The Ca–BDC process is interesting in the sense that it yielded high-quality thin films over a remarkably wide deposition temperature range of 200–420 °C. The typical GPC values range from 2 to 4 Å per cycle.

4.4. 3d-Transition-Metal-Based Processes

The 3d-metal-based hybrid films are interesting candidates for a number of frontier applications. The films based on the late 3d metals (Mn, Fe, Co, Ni, Cu) with partially filled d orbitals are intriguing candidates for magnetically, electrically, optically, and catalytically active materials. Among the early 3d-metal-based films, the vanadium–organic films have been considered for room temperature (RT) organic magnets.^[236,237]

There is a good selection of possible metal precursors for the 3d metals (**Table 4**). Vanadium-based films have been deposited from VOCl₃,^[293] tetrakis(ethylmethyamido)vanadium (TEMAV),^[113] and V(CO)₆,^[237] precursors in combination with EG,^[113,293] GL,^[113] and tetracyanoethylene (TCNE),^[236,237] manganese-based films from Mn(thd)₃ together with BDC,^[201] and from bis(ethylcyclopentadienyl)manganese(II) (Mn(CpEt)₂) with EG,^[60,230] GL, HQ, and tetrafluorohydroquinone (FHQ),^[230] and nickel-based films from Ni(dmamb)₂ and Ni(thd)₂ together with 4-mercaptophenol (4MP)^[257] and BDC.^[120] For Fe, Co, and Cu, the precursor varieties are significantly wide, as iron-based films have been deposited from FeCl₃,^[67,123,124,203,215,216,263,414] Fe(acac)₃,^[203] Cp₂Fe₂(CO)₄,^[251] Fe₂(O^tBu)₆,^[261,415] and Fe(hfa)₂TMEDA^[207] together with HQ,^[251] propargyl alcohol,^[215,216] BDC,^[67,123,124,202,203] AZO,^[67,263,414] EG,^[415] ethanolamine (EA),^[261,415] malonyl chloride (MC),^[261,415] and oxalic acid,^[207] cobalt-based films from Co(thd)₂,^[201] Co(acac)₂,^[201] and Co(CO)₈,^[236] combined with BDC^[201] and TCNE,^[236] and

Table 3. ALD/MLD processes based on alkaline earth metals.

| 12 Magnesium | Organic | GPC [Å per cycle] | T_{DEP} [°C] | In situ cryst. | Year | Ref. |
|-----------------------|-----------------|-----------------------------|-----------------------|----------------|------|-------|
| Mg(MeCp) ₂ | EG, GL | 2–3 | 100–250 | | 2020 | [56] |
| Mg(thd) ₂ | 3,5-PDC | 2.4 | 190–300 | hyd. | 2019 | [118] |
| | BDC | 3.5 | 200–300 | Yes | 2017 | [129] |
| 20 Calcium | | | | | | |
| Ca(thd) ₂ | AZO, BDC | 3.4 (AZO) | 280–320 | Yes | 2020 | [67] |
| | 3,5-PDC | 3.7 | 190–300 | hyd. | 2019 | [118] |
| | BDC | 3.5 | 190–300 | Yes | 2017 | [129] |
| | | 3.5 | 200–420 | Yes | 2016 | [62] |
| 38 Strontium | | | | | | |
| Sr(thd) ₂ | 3,5-PDC | 4.2 | 190–300 | hyd. | 2019 | [118] |
| | BDC | 2.5 | 190–300 | Yes | 2017 | [129] |
| 56 Barium | | | | | | |
| Ba(thd) ₂ | 3,5-PDC | 3.6 | 190–300 | hyd. | 2019 | [118] |
| | BDC | 3.5 | 220–300 | Yes | 2017 | [129] |
| | Uracil, adenine | 2.8 (uracil), 3.4 (adenine) | 260–300 | Yes (uracil) | 2017 | [58] |

copper-based films from Cu(thd)₂,^[61,121] and Co(dmap)₂^[119,206] combined with *N,N'*-dimethyldithiooxamide (DMD),^[119] BDC,^[61,206] BDS,^[121] HQ, 4,4'-oxydianiline (ODA), *p*-phenylenediamine (PPDA), and 1,4-benzenedithiol (BDT).^[206]

Deposition temperatures typically range from 80 up to 300 °C, but even room temperature processes exist for some hybrids (V–TCNE and Co–TCNE). Some of the processes work within a wide temperature range such as the Fe(hfa)₂TMEDA + oxalic acid process (125–350 °C). The GPC values vary widely for the reported processes, for Cu–BDC and Cu–DMD, the values being exceptionally low (0.7 and 0.45 Å per cycle, respectively), while for Fe–AZO, exceptionally high (25 Å per cycle). Regarding the crystallinity, most of the as-grown films have been amorphous, the exceptions being some Cu- and Fe-based films (Fe–BDC, Cu–BDC, Fe–AZO, Fe–oxalic acid, Cu–PPDA, Cu–HQ, Cu–DMD, Cu–BDS).

In **Figure 9**, the GPC versus deposition temperature behaviors are shown for four BDC-based processes, Mn(thd)₃ + BDC, Co(thd)₂ + BDC, Ni(thd)₂ + BDC, and Cu(thd)₂ + BDC, carried out under similar experimental conditions.^[61,120,201] For all these processes, GPC decreases with increasing temperature. However, in overall, the GPC values are clearly the lowest for the Mn(thd)₃ + BDC process. This can be explained by the more pronounced steric hindrance caused by the bulky thd ligands left after the reaction of the metal precursor on the substrate surface: in the case of Mn(thd)₃, two thd ligands are left, while in the case of the other three precursors, only one thd ligand remains.

4.5. 4d- and 5d-Transition-Metal-Based Processes

The 4d and 5d transition metals have so far remained little exploited in ALD/MLD research (**Table 5**), except in the cases of hafnium and zirconium for which processes with different precursor combinations have already been developed. Among these, the Zr-based processes are especially interesting as zirconium is a common constituent of MOF materials.

Zirconium-based ALD/MLD films have been deposited from ZrCl₄,^[106,122,204,224,416] and also from tetrakis(dimethylamido) (TDMA).^[65] and tetra-*tert*-butoxide (ZTB).^[126,230,417–419] based precursors together with a variety of different organic precursors. Likewise, Hf-based films have been deposited from TDMAH,^[230,262,324,420] HfCl₄,^[122] and TEMAH^[367] together with various organics. In the few additional studies involving the 4d or 5d transition metals, Nb-based films have been deposited from Nb(OEt)₅ in combination with HQ.^[421] Mo-based films from molybdenum hexacarbonyl together with 1,2-ethanedithiol (EDT),^[242,243] 1,4-butanedithiol, and BDT,^[243] and In-based films from bis(trimethylsilyl)amidodiethylindium (INCA-1) and HQ.^[369,422,423] The as-deposited In–HQ films showed a structural change upon exposure to ambient air and were found promising as flexible transparent films.^[424] Tin-based hybrid

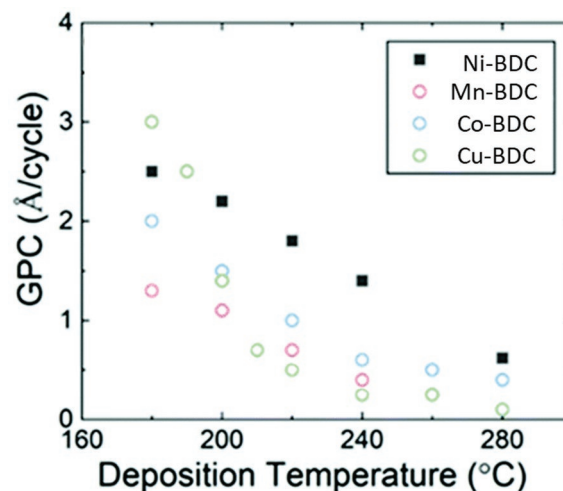


Figure 9. GPC values at different deposition temperatures for four different 3d transition metal–BDC processes; data depicted from refs. [61, 120, 201] and figure Reproduced with permission.^[120] Copyright 2021, Royal Society of Chemistry.

Table 4. ALD/MLD processes based on 3d transition metals.

| 23 Vanadium | Organic | GPC [Å per cycle], *mass gain [ng cm ⁻²] | T _{DEP} [°C] | In situ cryst. | Year | Ref. |
|---|--|---|-----------------------|--------------------------|------|-------|
| VOCl ₃ | EG | *15.2 | 90–135 | | 2018 | [293] |
| TEMAV | GL (EG) | 1.2 | 80–180 | | 2017 | [113] |
| V(CO) ₆ | TCNE | *≈150 | RT | | 2014 | [236] |
| | | 9.8 | RT | | 2012 | [237] |
| 25 Manganese | | | | | | |
| Mn(thd) ₃ | BDC | ≈1.0 | 160–280 | | 2016 | [201] |
| Mn(CpEt) ₂ | EG | 0.9 | 120–220 | | 2019 | [60] |
| | EG, HQ, FHQ, GL | – | 150 | | 2013 | [230] |
| 26 Iron | | | | | | |
| Fe ₂ (OtBu) ₆ | EA (B), MC (C) (four-step ABCB) | – | 150 | | 2021 | [261] |
| | EG (two-step AB), EA, MC (four-step ACDC) | 0.9 (EG), 2.1 (EA, MC) | 120 | | 2019 | [415] |
| FeCl ₃ (+H ₂ O) | AZO | – | 280 | | 2021 | [414] |
| | BDC | 0.83 (ε-Fe ₂ O ₃), 8.3 (Fe–BDC) | 280 | Yes (Fe–BDC) | 2021 | [124] |
| | | – | 280–300 | | 2020 | [123] |
| | | 0.65 (Fe ₂ O ₃), 0.69–1.5 (SL), 11 (Fe–BDC) | 280 | | 2018 | [202] |
| FeCl ₃ , Fe(acac) ₃ | BDC | 11 | 240–260 | Yes (FeCl ₃) | 2018 | [203] |
| Cp ₂ Fe ₂ (CO) ₄ (+H ₂ O) | HQ | 2.5 (Fe ₃ O ₄), ≈3.7 (Fe–HQ) | 150–190 | | 2015 | [251] |
| Fe(hfa) ₂ TMEDA | Oxalic acid | ≈4 | 125–350 | Yes | 2015 | [207] |
| FeCl ₃ | AZO, BDC | 25 (AZO) | 280 | Yes | 2020 | [67] |
| | AZO | 25 | 250–290 | Yes | 2019 | [263] |
| | Propargyl alcohol | ≈10 | 200 | | 2009 | [215] |
| | | – | 200 | | 2007 | [216] |
| 27 Cobalt | | | | | | |
| Co(acac) ₃ , Co(thd) ₂ | BDC | 1.0–1.2 (Co(acac) ₃), 1.5 (Co(thd) ₂) | 160–280 | | 2016 | [201] |
| Co ₂ (CO) ₈ | TCNE | *≈145 | RT | | 2014 | [236] |
| 28 Nickel | | | | | | |
| Ni(thd) ₂ | BDC | 2.3 | 180–320 | | 2021 | [120] |
| Ni(dmamb) ₂ | 4MP | 2.26 | 100 | | 2019 | [257] |
| 29 Copper | | | | | | |
| Cu(dmap) ₂ | DMD | ≈0.45 | 80 | Yes | 2021 | [119] |
| | HQ, BDC, ODA, PPDA, BDT | 1.0–2.6 | 140–240, <120 (HQ) | hyd. (HQ), yes (PPDA) | 2018 | [206] |
| Cu(thd) ₂ | BDS | – | 210 | Yes | 2021 | [121] |
| | BDC | 0.7 | 180–280 | Yes | 2016 | [61] |

films have been deposited from Sn–TDMA together with GL,^[220,425] and EG,^[220] and also from HS–Sn with HQ.^[426] Also, Ta₂O₅/polyimide nanolaminated structures have been deposited using Ta(OEt)₅ and water as precursors for Ta₂O₅ and pyromellitic dianhydride (PMDA) and 1,6-diaminohexane (DAH) as precursors for polyimide.^[209]

Growth rates for the 4d- and 5d-metal-based processes vary significantly, the lowest GPC value being 0.1 Å per cycle for the TDMASn + EG and TDMASn + GL processes and the highest being 13 Å per cycle for the processes with the longer and bulkier organic precursor 4,4'-BPDC. The deposition temperature range is wide as well, the lowest deposition

temperature applied being 75 °C for the TDMASn + GL process, and the highest yet usable deposition temperature found to be 390 °C for the processes of ZrCl₄ in combination with 2-amino-1,4-BDC or BDC.

4.6. Rare-Earth-Element-Based Processes

Robust ALD/MLD processes have also been developed for yttrium and other rare earth elements (R), often motivated by their potential applications as photoluminescent or upconverting coatings.^[57,208,427] Most of these processes are

Table 5. ALD/MLD processes based on 4d and 5d transition metals.

| 40 Zirconium | Organic | GPC [Å per cycle] | T_{DEP} [°C] | In situ cryst. | Year | Ref. | |
|--|-----------------------------|---|-----------------------|----------------|--------------|-------|-------|
| ZrCl ₄ | 2,6-NDC | ≈150–175* | 260 | | 2021 | [122] | |
| | 2,6-NDC, 4,4'-BPDC | ≈8 (2,6-NDC), ≈9–13 (4,4'-BPDC) | 290 | Yes | 2020 | [106] | |
| | 2-Amino-1,4-BDC | | – | 265 | Post-treated | 2021 | [416] |
| | | | 7.5–10 | 240–390 | Post-treated | 2017 | [224] |
| | | | 2–7 | 235–390 | Post-treated | 2016 | [204] |
| | TDMAZ | EG | – | 80 | | 2017 | [65] |
| | ZTB | EG | ≈0.8 | 130 | | 2019 | [417] |
| 0.8 | | | 150 | | 2014 | [126] | |
| 0.3–1.6 | | | 105–195 | | 2013 | [418] | |
| – | | | 150 | | 2013 | [230] | |
| | EG, HQ, FHQ, GL | – | 150 | | 2013 | [230] | |
| | 7-OTS | 11 (SAOL), 1.3 (ZrO ₂) | 170 | | 2009 | [419] | |
| 41 Niobium | | | | | | | |
| Nb(OEt) ₅ | HQ | 0.8–2.8 | 200–350 | | 2020 | [421] | |
| 42 Molybdenum | | | | | | | |
| Mo(CO) ₆ | EDT, BDT, 1,4-butanedithiol | 1.2 (EDT), 1.0 (1,4-butanedithiol), 1.5 (BDT) | 170 | | 2021 | [243] | |
| | | 1.3 | 155–175 | | 2018 | [242] | |
| 49 Indium | | | | | | | |
| INCA-1 (+H ₂ O ₂) | HQ | 0.43 (InO _x), 0.50 (SL) | 150 | | 2021 | [423] | |
| INCA-1 | HQ | 1.6 | 200 | | 2021 | [369] | |
| | | 1.6 | 150–200 | | 2020 | [424] | |
| | | – | – | | 2020 | [422] | |
| 50 Tin | | | | | | | |
| HS-Sn | HQ | 0.25 | 75–200 | Post-treated | 2022 | [426] | |
| TDMASn | GL | 2.5 | 100 | | 2020 | [425] | |
| | GL, EG | 0.1–1.3 (GL), 0.1 (EG) | 75–200 (GL), 100 (EG) | | 2018 | [220] | |
| 72 Hafnium | | | | | | | |
| TEMAH | HQ | 7.9 | 150 | | 2021 | [367] | |
| HfCl ₄ | 2,6-NDC | ≈6 | 260 | | 2021 | [122] | |
| TDMAH (+H ₂ O) | ED, MC | ≈0.9 (ED + MC) | 100 | | 2021 | [262] | |
| TDMAH (+DEZ) | EG | ≈1.0–1.2 | – | | 2021 | [324] | |
| TDMAH | EG | 0.4–1.2 | 105–205 | | 2014 | [420] | |
| | EG, GL, HQ, FHQ | – | 150 (EG) | | 2013 | [230] | |
| 73 Tantalum | | | | | | | |
| Ta(OEt) ₅ (+H ₂ O) | PMDA, DAH | 0.6 (Ta ₂ O ₅), 5.1 (PMDA + DAH) | 170 | | 2009 | [209] | |

based on R(thd)₃ precursors, but the tris(*N,N'*-diisopropyl-2-dimethylamido guanidinato) (DPDMG) ligand has been challenged as well (Table 6). The advantage of the DPDMG-based precursors is believed to be the all-nitrogen coordinated structure, making the precursor more reactive while preserving its thermal stability.^[208]

Regarding the organic component, only aromatic organic precursors have been employed in combination with the rare earth elements, one of the motivations being the possibility to find UV and/or visible light absorbing organic molecules as sensitizers of the characteristic luminescence of the different R ion species. For example, Y(thd)₃ has been

combined with 2,3-pyrazinedicarboxylic acid (2,3-PZD),^[214] 2,6-NDC,^[122] 1,4-NDC, BDC, 9,10-anthracenedicarboxylic acid (ADA),^[266] and La(thd)₃ with BDC,^[129] uracil and adenine,^[58] and Eu(thd)₃ with BDC,^[57,266] 3,5-PDC,^[57,428] 2,6-PDC,^[57] 1,4-NDC,^[266] ADA,^[266] and 2-amino-1,4-BDC,^[429] and Er(thd)₃ or Er(DPDMG) with 2,3-PZD,^[214] 3,5-PDC,^[208] and 2-[2-[2-chloro-3-[2-[1,3-dihydro-3,3-dimethyl-1-(4-sulfobutyl)-2*H*-indol-2-ylidene]-ethylidene]-1-cyclopenten-1-yl]-ethenyl]-3,3-dimethyl-1-(4-sulfobutyl)-3*H*-indolium hydroxide (IR-806).^[259] Different pyridine-based organic precursors yield strong bonds via N and O donor atoms with the large R³⁺ ions acting as hard acids such that the resultant hybrids usually are thermally

Table 6. ALD/MLD processes based on rare-earth elements.

| 39 Yttrium | Organic | GPC [Å per cycle] | T_{DEP} [°C] | In situ cryst. | Year | Ref. |
|--|-----------------------|---|--|----------------|------|-------|
| Y(thd) ₃ | 2,6-NDC | ≈ 2 | 260 | | 2021 | [122] |
| Y(thd) ₃ (+Eu(thd) ₃) | 1,4-NDC, BDC, ADA | – | – | | 2021 | [266] |
| (Y _{0.92} Yb _{0.04} Er _{0.04})(thd) ₃ | 2,3-PZD | 3.4 | 160–225 | (Yes) | 2018 | [214] |
| 57 Lanthanum | | | | | | |
| La(thd) ₃ | BDC | – | 220 | Yes | 2017 | [129] |
| | Uracil, adenine | 1.6 (uracil), 1.4 (adenine) | 260–320 | | 2017 | [58] |
| 60 Neodymium | | | | | | |
| Nd(thd) ₃ | BDC | 3.2 | 200 | (Yes) | 2020 | [430] |
| 63 Europium | | | | | | |
| Eu(thd) ₃ (+Y(thd) ₃) | 1,4-NDC, BDC, ADA | ≈2.4 (BDC), ≈2.8 (1,4-NDC), ≈2.7 (ADA) | 220–240 (BDC, 1,4-NDC), 250–270 (ADA) | | 2021 | [266] |
| Eu(thd) ₃ | 2-amino-1,4-BDC | – | 180–250 | Yes | 2020 | [429] |
| | 3,5-PDC, BDC, 2,6-PDC | ≈1.2 (2,6-PDC), ≈2.0 (BDC, 3,5-PDC) | 280–300 | (Yes) (BDC) | 2016 | [57] |
| | 3,5-PDC | ≈2 | 260–340 | | 2015 | [428] |
| 68 Erbium | | | | | | |
| (Yb,Er)(DPDMG) ₃ | IR-806 | 2.5 | 250–280 | | 2019 | [259] |
| (Y _{0.92} Yb _{0.04} Er _{0.04})(thd) ₃ | 2,3-PZD | 3.4 | 160–275 | (Yes) | 2018 | [214] |
| Er(DPDMG) ₃ | 3,5-PDC | 6.4 | 245–280 | | 2017 | [208] |
| 70 Ytterbium | | | | | | |
| (Yb,Er)(DPDMG) ₃ | IR-806 | 2.5 | 250–280 | | 2019 | [259] |
| (Y _{0.92} Yb _{0.04} Er _{0.04})(thd) ₃ | 2,3-PZD | 3.4 | 160–275 | (Yes) | 2018 | [214] |

stable and exhibit intense photoluminescence. Different nucleobases have been considered attractive building blocks for luminescent nanostructures for many advanced applications, such as sensors and organic light emitting diodes. Depending on the participating metal/nucleobase, the formation of various different assemblies is possible. For ytterbium, both thd^[214] and DPDMG^[259] precursors have been used, in combination with 2,3-PZD^[214] and IR-806.^[259]

The GPC values reported vary from 1 to 6 Å per cycle. Deposition temperatures vary in the range of 160–320 °C, the lowest being for the (Y,Yb,Er)-based films with 2,3-PZD, and the highest for La–uracil and La–adenine films. In situ crystalline films have been obtained only with lanthanum and europium.

5. Crystallinity of ALD/MLD Films

While the ALD/MLD approach was well established for a growing variety of metal–organic thin films already more than a decade ago, the possibility to grow in situ crystalline metal–organic thin films by ALD/MLD remained on a wish list until 2016. This is understandable as even the prototype ALD processes for aluminum and hafnium oxides yield amorphous films. However, once the first direct ALD/MLD growth of crystalline Cu-terephthalate thin films of a MOF-like structure were realized in 2016,^[61] many other successes rapidly followed; **Figure 10** summarizes the ALD/MLD processes so far found to yield crystalline metal–organic thin films.

5.1. In Situ Crystalline Thin Films

In some of the early ALD/MLD studies, one or two low-angle diffraction peaks were seen for the metal–organic products, indicating toward some kind of ordered structure. The first report is from the year 2014 for the TMA + L-glutamic acid (linear carboxylic acid) process,^[234] soon followed by similar findings for the Fe(hfa)₂TMEDA + oxalic acid process.^[207] The observed reflections did not match to the diffraction patterns expected for any relevant crystalline compound, and were therefore interpreted as indications of sheet-like ordering rather than a 3D crystal structure.

The first clearly in situ crystalline ALD/MLD films were realized in 2016 from the Cu(thd)₂ + BDC process in a very narrow deposition temperature range of 180–190 °C.^[61] Noteworthy, in the same year, Ameloot and co-workers applied another vapor phase synthesis route, named MOF–chemical vapor deposition (CVD), for crystalline zeolitic imidazolate framework (ZIF-8) thin films; this two-step route consisted of the ALD growth of a ZnO film, which was then exposed to 2-methylimidazole powder bed in a closed reactor vessel to realize the final vapor-to-solid conversion of ZnO into the ZIF-8 structured hybrid thin film.^[431]

The success in growing in situ crystalline Cu–BDC films with ALD/MLD was soon followed by other positive results; in these successful experiments, the common nominator was the electropositive metal constituent bound via ionic bonding to the organic linker. These discoveries included the processes in which either Li(thd) or Ca(thd)₂ was employed as the metal

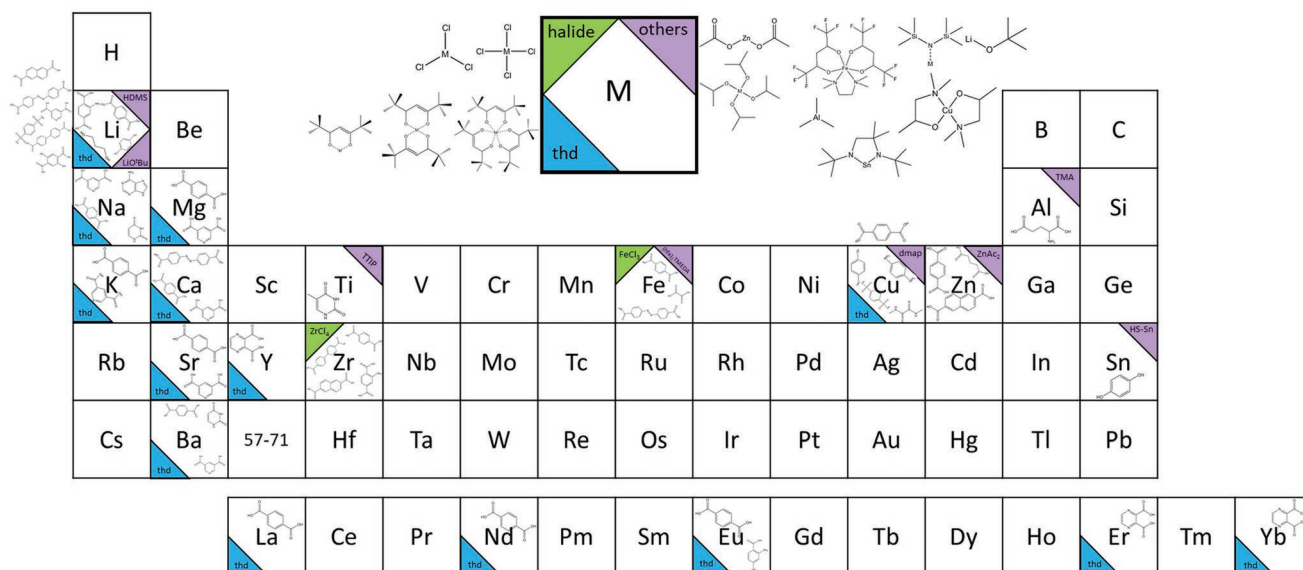


Figure 10. ALD/MLD processes that have yielded crystalline (CP- or MOF-type) metal–organic thin films, in situ or with postdeposition treatments.

precursor in combination with BDC as the organic linker.^[62,128] The Ca–BDC films were found to grow crystalline over a notably wide deposition temperature range; they were also found to absorb water molecules when exposed to ambient air, forming a well-defined crystalline water-derivative phase, which could be regenerated back to the original crystal structure through a low-temperature annealing. Moreover demonstrated was the promising mechanical properties of these films.^[62]

The repertoire of the BDC-based crystalline films was rapidly expanded to cover many other metal components; these ALD/MLD processes yielded crystalline coordination polymer thin films either in situ (Na, K, Ca, Sr, Ba, Fe, La, Eu) or after a humidity treatment (Mg).^[57,129] For the Fe–BDC film, the recorded grazing incidence X-ray diffraction (GIXRD) pattern could be matched for its main features to the so-called MOF-2 structure, the only clearly visible difference being the low-angle double peaks seen for Fe–BDC instead of the single peak expected for the MOF-2 structure.^[203]

In general, the BDC-based processes formed an excellent platform to investigate the growth modes of typical ALD/MLD processes yielding in situ crystalline metal–organic films. In **Figure 11**, atomic force microscopy (AFM) images taken after 70 and 400 deposition cycles for Li–BDC films and after 100 and 400 cycles for Ba–BDC films are shown to demonstrate that even after the initial 70 or 100 cycles, the films seem to consist

of distinct granular-shaped particles, which then gain in size upon the further deposition cycles. In between the granules, deep voids are seen, a fact which points toward an island-type growth mode. In this growth mode, the initial nucleation and growth are not uniform but distinct islands are formed, which then grow as the deposition process proceeds. A constant-growth regime is achieved only after the islands have coalesced and formed a continuous thin-film layer.^[128,129]

More recent studies demonstrated the possibilities provided by different functionalization schemes. In the two well-behaving ALD/MLD processes yielding in situ crystalline Li-2-amino-1,4-BDC^[225] and Eu-2-amino-1,4-BDC^[429] films, the BDC molecule was functionalized with an additional amino group attached to the benzene ring. The former Li-based material was found to possess a previously unknown crystal structure, whereas the Eu-based material was compatible with the UiO-66 structure. Also, nitrogen-functionalized PDC organic linkers have been applied to deposit in situ crystalline films, that is, the Li-, Na-, and K-based 3,5-PDC films reported in 2019.^[118] Among these, the Li–3,5-PDC films were of the known Li–ULMOF-4 (UL = ultralight) crystal structure, whereas the other film compositions/structures were apparently not known from previous bulk-material studies. In 2020, two new dicarboxylic-acid-based ALD/MLD hybrid materials were reported, in which the organic linker consisted of two or three benzene rings, i.e., Zr–2,6-NDC

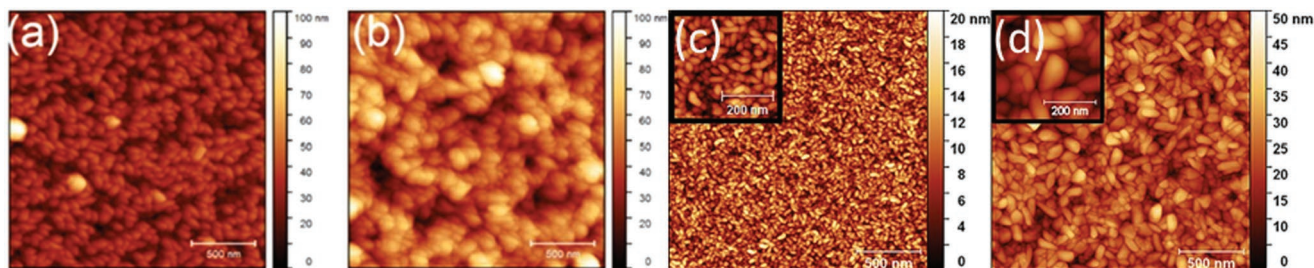


Figure 11. AFM images for in situ crystalline Li–BDC films with a) 70 and b) 400 deposition cycles. Reproduced with permission.^[128] Copyright 2016, American Chemical Society. Ba–BDC films with c) 100 and d) 400 deposition cycles. Reproduced with Permission.^[129] Copyright 2017, Wiley-VCH.

and Zr-4,4'-BPDC; these were partly crystalline after the deposition, but required an additional acetic acid vapor treatment in a sealed autoclave to yield fully crystalline films.^[106]

Besides the dicarboxylic-acid-type precursors, organic diols have been shown to yield in situ crystalline metal-organic thin films. This was seen in 2017 for HQ in combination with lithium hexamethyldisilazide.^[63] On the other hand, adenine and uracil are examples of natural nucleobase molecules, in which there are multiple possibly reactive groups (NH₂, NH, and quinone-type = O); in combination with sodium, these precursors have yielded in situ crystalline Na-adenine^[58] and Na-uracil^[223] films showing several sharp diffraction peaks in GIXRD patterns. For the Ba-uracil films,^[58] only one clear low-angle peak was seen besides some broad features at the higher angles. Positive indications (with few diffraction peaks) of crystallinity have been observed for other ALD/MLD processes as well, e.g., for zinc glutarate,^[253] (Y,Yb,Er)-pyrazine,^[214] Cu-PPDA,^[206] and Ti-thymine,^[136] these findings of certain degree of crystallinity are often referred to as “nanocrystallinity”^[206] or “layered structure.”^[136]

Exciting results have been obtained also with the photo-switchable azobenzene dicarboxylic acid precursor, which has yielded in situ crystalline ALD/MLD films with Li,^[67] Ca,^[67] and Fe.^[263] Interestingly, when mixed with BDC, crystalline hetero-organic Fe-(AZO,BDC) films could be deposited which maintained their crystallinity even better than the binary Fe-AZO films upon the UV-driven photoisomerization of the azobenzene moieties.^[67]

The most recent reports from the last two years are for various lithium-based ALD/MLD processes yielding in situ crystalline Li-PD^[271] (with highly oriented growth on the crystalline silicon wafer), Li-DHTP^[270] (with crystallinity reliant on the Li-precursor pulse length), and Li-BDC, Li-3,5-PDC, Li-2,6-NDC, Li-4,4'-BPDC, and Li-AZO films with so-called intercalated-metal-organic-framework (iMOF)-type structures.^[411] Also, 1D CP-type Cu-DMD films were grown recently; the attractive feature of these films was the semiconductor-to-metal transition achieved with a postdeposition reductive annealing.^[119]

5.2. Postdeposition-Treated Crystalline Thin Films

In 2013, Ritala and co-workers pioneered in the fabrication of crystalline metal-organic thin films through ALD/MLD;

however, the in situ amorphous Zn-BDC films required a post-deposition treatment in a humidity-controlled chamber (relative humidity (RH) 60%; 12 h) followed by recrystallization with *N,N*-dimethylformamide (DMF) in an autoclave (150 °C; 2 h) for the crystallization of the material in the cubic MOF-5 (or so-called IRMOF-1) structure, consisting of Zn₄O clusters connected with rigid benzene dicarboxylate linkers.^[117] Later (in 2015), this work was followed with studies of IRMOF-8 structured thin films, obtained from the as-deposited amorphous Zn-2,6-NDC films through a postdeposition treatment at RT in RH 70% first for an unknown crystalline phase with a large unit cell, and then recrystallized into IRMOF-8 structure in an autoclave with DMF as the solvent.^[229] In 2016, a similar process was reported for amorphous Zr-BDC films which were crystallized into the UiO-66 structure by treating them in acetic acid vapor.^[204] In a later study, these UiO-66 films were applied as arrow coatings.^[205] Also, it was demonstrated that Zr-BDC films deposited without acetic acid modulation showed an excess of BDC,^[204] but when acetic acid pulsing was used during deposition, this no longer was the case.^[224]

Most recently, two new processes of Zr-2,6-NDC and Zr-4,4'-BPDC of partly in situ crystalline films were developed. These films were further crystallized to form MOF-like structures by heat treatment in acetic acid vapor in a sealed autoclave (160 °C; 24 h).^[106] These postdeposition crystallization processes can be conveniently followed by scanning electron microscope (SEM) imaging, see **Figure 12** for the Zr-2,6-NDC and Zr-4,4'-BPDC films as an example; the as-deposited only partly crystalline films are relatively flat, while the postdeposition-treated crystalline samples have rough surfaces with large crystallites.^[106]

Simple postdeposition humidity treatments have been employed in various ways for the conversion between anhydrous and water-containing forms of ALD-/MLD-grown films; this is often also a play between amorphous and crystalline films. For example, the as-deposited amorphous Mg-BDC films were found to instantaneously absorb water, forming thereby a crystalline water-derivative phase; in this case, the desorption of the absorbed water disrupted the crystal structure and the films became amorphous again.^[129] Somewhat differently, Ca-BDC^[62,129] and Sr-BDC^[129] films were found to reversibly absorb water molecules forming well-defined crystalline water-derivative and anhydrous phases. For Li-BDS and Cu-BDS, the ALD/MLD products were crystalline films with hydration water. In the latter case, the crystal structure matched with

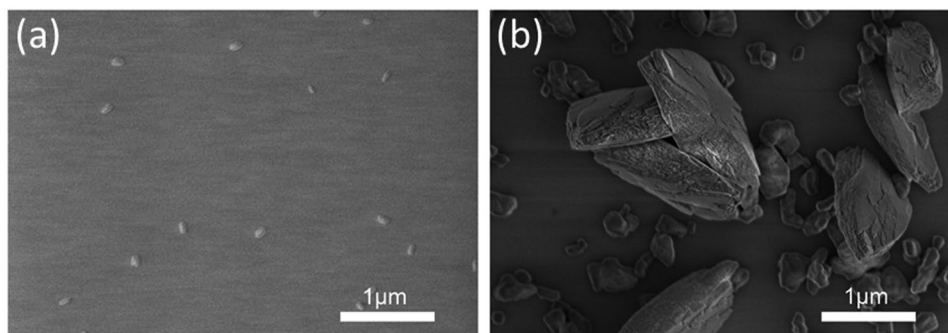


Figure 12. SEM images for a) a mostly amorphous (partly crystalline) as-deposited Zr-2,6-NDC thin film and b) the same film sample after an autoclave treatment for the crystallization. Reproduced with Permission.^[106] Copyright 2020, Royal Society of Chemistry.

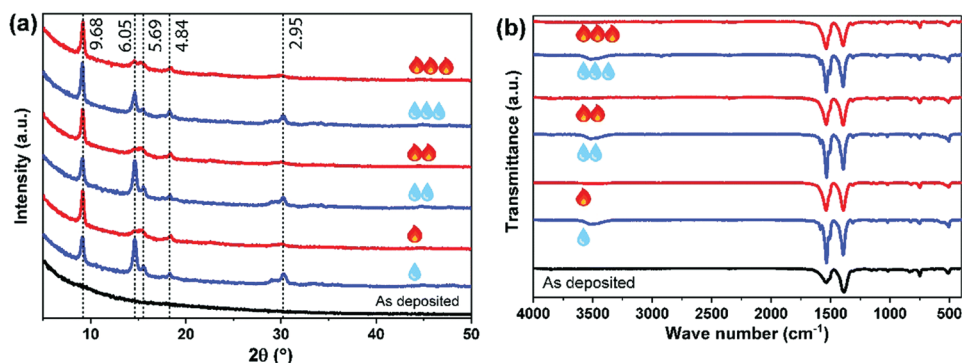


Figure 13. a) GIXRD patterns, and b) FTIR spectra for an as-deposited Nd-BDC film (black), and for the same thin film after three consecutive humidity (blue droplets) and heat (red flames) treatment cycles. Reproduced with permission.^[430] Copyright 2020, Royal Society of Chemistry.

previously reported bulk-synthesized hydrated Cu-BDS, but for the former case, no previous reports were found from literature. Interestingly, the as-deposited Li-BDS films were found to readily release the hydrated water, and remained crystalline and stable.^[121]

Yet another interesting behavior was seen for Nd-BDC films which were initially amorphous but crystallized when treated under humid conditions. Then, a subsequent heat treatment completely removed the coordinated water molecules but retained the crystallinity. This reversible guest water molecule intake and release could be repeated several times without losing the crystalline coordination network structure, see **Figure 13**.^[430]

There are even more examples of interesting water-absorption-induced changes. The as-deposited Cu-HQ films are amorphous and strongly air and moisture sensitive; these films were found to crystallize into a previously unknown crystalline phase upon reaction with water.^[206] Similarly, the as-deposited amorphous Mg-, Ca-, Sr-, and Ba-based 3,5-PDC films crystallized into water-containing structures through a postdeposition humidity treatment. In this case, the water-absorption-/desorption-derived changes could be repeated several times without breaking the basic metal-organic structure.^[118] For the sodium counterpart, the as-deposited anhydrous Na-3,5-PDC films were crystalline, of the crystal structure not previously reported. During the humidity treatments, this structure then changed into a previously known four-hydrated structure.^[432] Interestingly, the postdeposition treatment can be based on annealing only, as was recently demonstrated for Sn-HQ films which were initially weakly nanocrystalline but could be better crystallized through a postdeposition annealing.^[426]

5.3. Factors Promoting In Situ Crystallinity

A clear majority of the in situ crystalline ALD/MLD films grown so far are based on the electropositive s-block metals. Tentatively, this has been attributed to the fact that the resultant non-oriented ionic bonds connecting the metal cations and organic linkers possess more spatial freedom to adjust to the coordination requirements of the specific crystal structure compared to the more strictly oriented covalent bonds that are rather predetermined to a certain spatial coordination symmetry.

In the case of the higher-valent (transition) metal species, it seems to be advantageous to look for inorganic precursors with as small ligands as possible. Bulkier ligands of the inorganic precursor may hinder the in situ crystallization of the growing film. For example, the Na(thd) + nucleobase processes with an inorganic precursor with one thd ligand were found to yield highly crystalline films, whereas the Ba(thd)₂ + nucleobase processes with two thd ligands yielded partly crystalline films and the La(thd)₃ + nucleobase processes with three thd ligands resulted in completely amorphous films.^[58] Another example demonstrates that crystalline Fe-BDC films (with a crystal structure resembling the MOF-2 structure) could be obtained when FeCl₃ with small halide ligands was employed as the iron source, whereas depositions based on the bulkier Fe(acac)₃ precursor yielded amorphous films.^[105,203] The steric hindrance caused by the bulky ligands apparently complicates the building-up of the new coordination bonds and thereby the coordination network structure.^[203] There are also cases where the explanation is not so straightforward. For example, the Cu(thd)₂ + BDC process was found to yield crystalline films, whereas with Cu(dmap)₂, amorphous Cu-BDC films were obtained.^[206] In some cases, the precursor pulse length defines whether the process yields crystalline or amorphous films, viz. the Li(thd) + DHTP process yielding crystalline less-lithiated films with short Li(thd) pulses and amorphous fully lithiated films with longer Li(thd) pulses.^[270]

It also seems that the in situ crystalline 3D structure is possibly easier to obtain with multidentate organic linkers due to the higher degree of freedom for possible coordination modes provided by the involvement of the different binding sites of the molecule.^[118] Here we note that, pyridinedicarboxylic acids are particularly interesting organic linker molecules with their rigid skeletons and multiple coordination sites, as they can act in a multidentate fashion, their N and O acceptors can participate in hydrogen-bonding interactions, and they may also exhibit π - π interactions between the stacked benzene rings.^[432]

5.4. Crystal Structure Highlights

Considering the crystal structures so far realized for the ALD/MLD grown thin films, some are well-known from literature for the corresponding bulk samples (typically synthesized

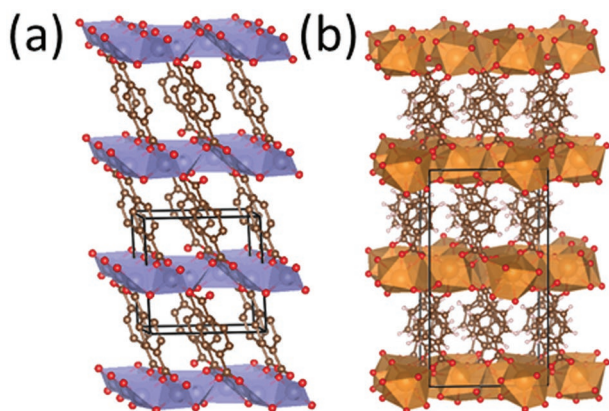


Figure 14. Layered CP structures of a) Li-BDC^[433] and b) Ba-BDC;^[434] structures drawn with VESTA.^[435]

through solution-based routes), while some structures are previously unseen. Many of the alkali-metal- and alkaline-earth-metal-based hybrids with ionic bonds (between metal cations and oxygen sites in the organic linker) possess known layered CP-type crystal structures. Examples of those are Li-BDC and Ba-BDC shown in **Figure 14**.

There are also few cases for which the diffraction pattern recorded for the hybrid film closely corresponds to a pattern reported/calculated for a well-known MOF structure. An important example is the in situ crystalline Cu-BDC films with strong similarity to the MOF-2 structure.^[61] Another example, is the ULMOF-4 structured^[436] Li-3,5-PDC films; in this case, the 3,5-PDC linker coordinates to the Li⁺ ions in a multidentate fashion enabling the 3D crystal structure (**Figure 15**).

The hybrid films of the most attractive MOF-5 structure required a post-ALD/MLD treatment for the crystallization. The as-deposited Zn-BDC films were initially amorphous but crystallized readily in ambient humidity into an unknown phase; recrystallization of this phase into the desired MOF-5 phase was then achieved in an autoclave using DMF as the solvent. The crystallites of the MOF-5 film were visible in optical microscope images as the smooth film surface turns granular (**Figure 16**).^[117]

Possibly, the most exciting structures are those not attained before (**Figure 17**). The prime example is the new Li-HQ phase.^[63] For this material, the structure was predicted (starting

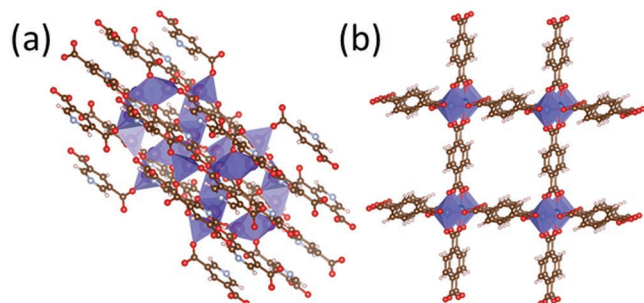


Figure 15. a) Li-3,5-PDC with ULMOF-4^[436] structure having pyridinedicarboxylate coordinating in a multidentate fashion. b) Cu-BDC with a structure similar to MOF-2;^[437] structures drawn with VESTA.^[435]

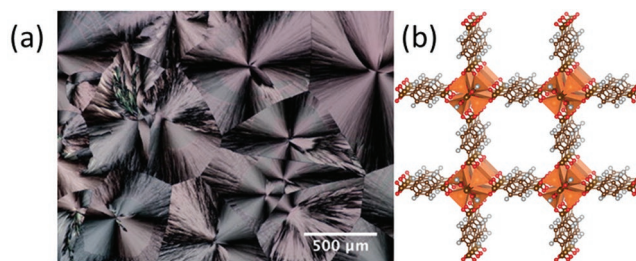


Figure 16. a) Optical microscope image of the crystals formed upon the crystallization of an initially amorphous Zn-BDC film in ambient humidity. b) The MOF-5 structure formed when crystalline Zn-BDC film was treated in an autoclave. Reproduced with permission.^[117] Copyright 2013, Elsevier Inc. MOF-5^[2] structure drawn with VESTA.^[435]

from a structure known for Na-HQ) with density functional theory (DFT) calculations, and then verified by comparing the calculated and experimental X-ray diffraction (XRD) patterns. The undercoordinated (three-coordinated) Li site in the structure explains why this phase had not been reached through conventional solution synthesis routes: this site is also readily accessible by the solvent molecules. Another example is the Li-AZO structure with the UV-active 4,4'-azobenzene dicarboxylate moieties. For this previously unknown structure, a plausible model was obtained by assuming the same monoclinic $P2_1/c$ space group as for the Li-BDC, Li-2,6-NDC, and Li-4,4'-BPDC carboxylates,^[411] and indexing the major diffraction peaks accordingly to corroborate the monoclinic symmetry and for the estimation of the unit cell parameters. Additional support for this crystal arrangement was obtained from the X-ray reflectivity (XRR)-determined film density value which was perfectly in line with the value calculated from the structure model.

There are also several cases in which the crystal structure is known for the corresponding water-coordinated form, but the anhydrous parent structure is realized through the ALD/MLD synthesis for the first time. Here, an excellent example is the in situ crystalline and anhydrous Na-3,5-PDC phase with unknown crystal structure.^[118] The postdeposition humidity treatment then transformed the crystal structure to the previously known four-hydrated structure (**Figure 18**).^[432] This is one of the examples where ALD/MLD indeed can be an important tool for the stabilization of new anhydrous metal-organic

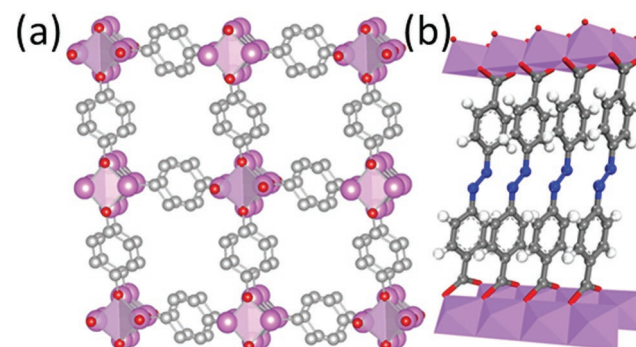


Figure 17. Crystal structures proposed for the a) Li-HQ^[63] (drawn with VESTA^[435]) and b) Li-AZO films. Reproduced with permission.^[411] Copyright 2020, American Chemical Society.

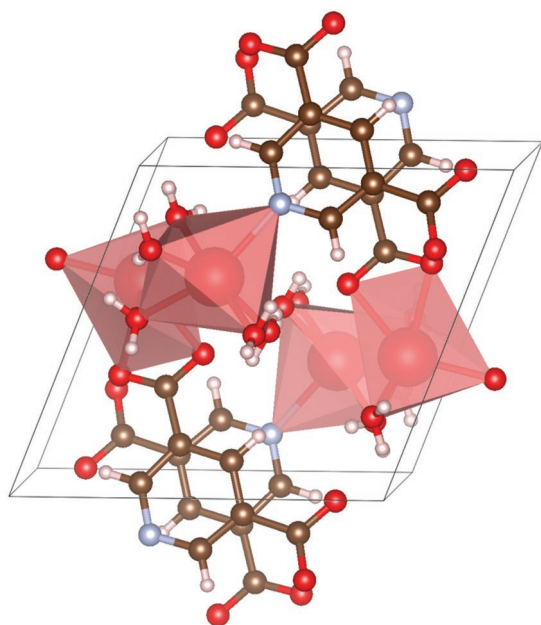


Figure 18. Crystal structure for the four-hydrated Na-3,5-PDC^[432] realized for the as-deposited (anhydrous) film after humidity treatment; structure drawn with VESTA.^[435]

framework structures owing to its beneficial solution-free conditions.

Finally, there is also a recent example of thin films grown with ALD/MLD for which a novel long-range ordered 1D polymer chain structure could be realized (Figure 19).^[119] The films were of the *N,N*-dimethyl dithiooxamidato-copper (Cu-DMD) composition and possessed high degree of out-of-plane ordering suggesting the formation of a well-ordered secondary structure by the parallel alignment of the 1D polymer chains.

5.5. Film Density

Crystallinity of the ALD/MLD hybrid films is often reflected in their density values (typically determined from XRR data), such that the density is usually lower for the crystalline films compared to the related amorphous films. This is understood by the certain porosity level of the crystal structure, while the varied bond lengths/angles in amorphous films often lead to the

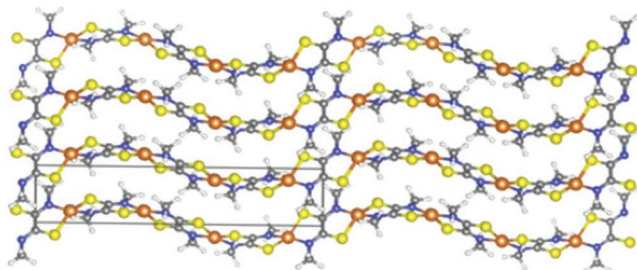


Figure 19. Geometry-optimized structure of the Cu-DMD thin films along the (100) plane. Reproduced with permission.^[119] Copyright 2021, American Chemical Society.

denser packing. This was most straightforwardly seen for the Cu-BDC films which grew in situ crystalline (MOF-2-like structure) at the lower deposition temperatures (180–190 °C) and amorphous at the higher deposition temperatures (>190 °C); the density values were ≈ 1.5 and 2.1 g cm^{-3} , respectively.^[61] Similar trend was seen for the in situ crystalline Li₂DHTP films having density value of 1.52 g cm^{-3} being lower than for the amorphous Li₄DHTP films with density of 1.73 g cm^{-3} .^[270] The density value for the crystalline Cu-BDC film (1.5 g cm^{-3}) is little higher than the ideal value calculated for the MOF Cu-BDC structure (1.4 g cm^{-3}).^[437] However, the common trend observed for most of the crystalline ALD/MLD films is that the actual density value is slightly lower than the ideal density; this is presumably due to the polycrystalline nature of these films, e.g., the XRR-derived density values for alkali- and alkaline-earth-metal-BDC thin films are systematically slightly lower than the ideal values calculated from the reported crystal structures ($\approx 0.2 \text{ g cm}^{-3}$).^[129] In some cases, the film density values have been also found to be slightly film-thickness-dependent; for example, in the case of the crystalline Li-2-amino-1,4-BDC films, the density was found to decrease from 1.59 g cm^{-3} for the film deposited with 100 cycles, to 1.40 – 1.44 g cm^{-3} for films deposited with 200 to 400 cycles.^[225] Here, the most straightforward explanation is that the degree of crystallinity is lower for the thinnest film.

An interesting comparison can be made among different amorphous M-BDC films deposited at 200 °C. For M = Mn, Co, and Cu, the density values were in the range of 1.6 – 1.9 g cm^{-3} , while for the M = Ni film, the density was 1.4 g cm^{-3} ; this clearly lower density was tentatively taken as indication toward the Ni-BDC films being crystalline in nanoscale.^[120] However, additional test depositions to obtain crystalline films at the “nonideally” low deposition temperature of 170 °C (lower than the evaporation temperature of the BDC precursor) yielded GIXRD-amorphous films, unfortunately.

The choice of the organic linker moiety has naturally a clear effect on the density. For example, compared to the corresponding BDC phases, the 3,5-PDC phases are often less dense; this is seen, e.g., for the Na-3,5-PDC (1.5 g cm^{-3}) and Na-BDC (1.7 g cm^{-3}) films.^[118] Similarly, the choice of the metal component affects the density, following the expected trend considering the metal atom masses and ion sizes, e.g., Li-AZO (1.40 g cm^{-3}), Ca-AZO (1.45 g cm^{-3}), and Fe-AZO (1.50 g cm^{-3}).^[67]

In some (alkali- and alkaline-earth-metal-based) systems, the water inclusion seems to create more empty space within the structure decreasing the density of the film.^[118,129] As an example, the density of Ca-BDC drops from 1.7 to 1.4 g cm^{-3} when the water-coordinated Ca-BDC(H₂O)₃ phase is formed, and in the case of Sr-BDC, the density drops from 1.9 to 1.8 g cm^{-3} when the Sr-BDC(H₂O)₃ phase is formed.^[129] Similarly, for Na-BDC, the densities of the anhydrous/hydrated forms are $1.7/1.3 \text{ g cm}^{-3}$.^[118] The same phenomenon could be seen for the as-deposited iron-azobenzene film having density of 1.51 g cm^{-3} . Upon the first humidity treatment, when some of the carboxylate groups were protonated and the structure was slightly modified, the density decreased to 1.27 g cm^{-3} .^[263] On the other hand, for the Nd-BDC films, which were initially amorphous, the first water intercalation step and consequent crystallization decreased the density from 2.15 to 2.09 g cm^{-3} ;

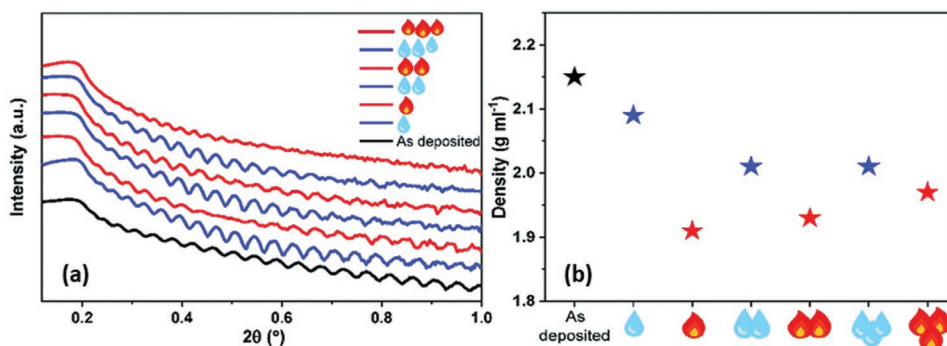


Figure 20. a) XRR curves, and b) film density values determined from the XRR data for an as-deposited amorphous Nd-BDC thin film (black), and for the same sample after three consecutive humidity (blue droplets) and heat (red flames) treatment cycles. Reproduced with permission.^[430] Copyright 2020, Royal Society of Chemistry.

this was taken as an indication of the porosity (at least to some degree) of the formed crystal structure. Then, after the initial crystallization, the density systematically decreased when water was removed from the crystal structure and increased again upon the water loading (Figure 20).^[409] In this case, this trend is reasonable, as the crystal structure is porous and the intercalated water molecules are just filling the pores, without forming strong coordination bonds (and without significantly changing the crystal structure).

5.6. Bonding Structure

Fourier transform infrared spectroscopy (FTIR) is a convenient tool for a quick detection/evaluation of the following three important hybrid film characteristics: i) degree of crystallinity, ii) carboxylate bonding mode (and other functional groups), and iii) water absorption (distinguishing coordinating water from absorbed water). Illustrative examples are shown in Figures 21 and 22 for different metal carboxylate films. First, the sharpness of the peaks provides us an indication of the degree of crystallinity, the sharper peaks naturally pointing toward crystalline films and the broader peaks toward amorphous films with a wider variation in the metal-organic bonding (Figure 21).^[234]

For the metal-carboxylate films, the different bonding modes of the carboxylate group can be assessed (for both crystalline and amorphous films) from the distance (Δ) between the two characteristic carboxylate absorption bands in the 1400–1600 cm^{-1} range, as follows: unidentate coordination $\Delta > 200 \text{ cm}^{-1}$ (Figure 22a,b), bidentate bridging coordination $130 < \Delta < 200 \text{ cm}^{-1}$ (Figure 22c,d), and bidentate chelating coordination $50 < \Delta < 150 \text{ cm}^{-1}$ (Figure 22e–g).^[234,438] Figure 22h illustrates as an example the bidentate and monodentate coordinations of Zr-BDC, while for Zr-2-amino-1,4-BDC, only the bidentate coordination (Figure 22i) is possible due to steric hindrance. Monodentate coordination is not possible indicating that the steric hindrance from the amino group prevents an excess amount of 2-amino-1,4-BDC to form a monodentate coordination with Zr.^[224]

The s-block-metal-based CP structures in particular are prone to absorb guest water molecules.^[439] Moreover, owing to the ionic network, these structures are relatively flexible for small structural rearrangements upon the intercalation/deintercalation of coordinated water molecules.^[440] The absorbed water is visible in the FTIR spectra around 3400 cm^{-1} , and from the sharpness of this peak, it can be judged whether the water molecules are only absorbed (wider peak) into the film or coordinated (sharper peak) to the structure, see Figure 23 for various s-block metal-BDC films.

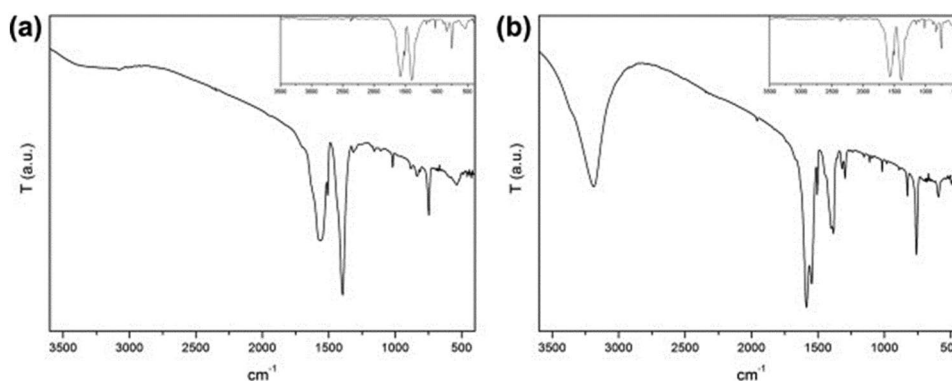


Figure 21. FTIR spectra for two Zn-BDC films: a) the as-deposited amorphous film, and b) crystalline humidity-treated film of the MOF-5 structure, the latter crystalline film showing clearly sharper peaks. Reproduced with permission.^[177] Copyright 2013, Elsevier Inc.

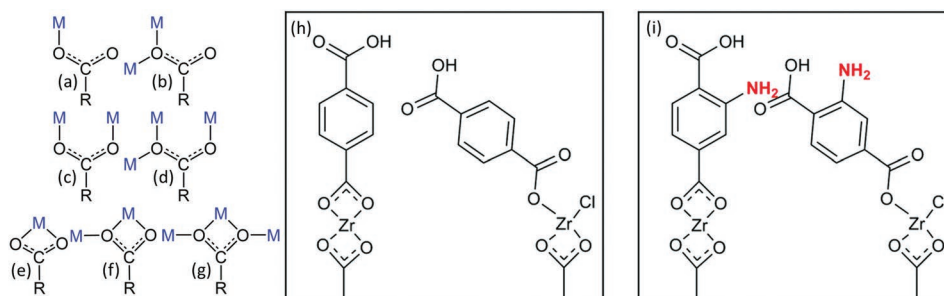


Figure 22. Different bonding modes of ligands with a carboxylate group: a) unidentate, b) monoatomic bridging, c) bridging bidentate, d) monoatomic bridging with additional bridging, e) chelating, f) monoatomic bridging with additional chelation, and g) monoatomic bridging with additional chelation and bridging. Illustrations of h) the monodentate and bidentate coordinations of BDC, and i) the bidentate coordination of 2-amino-1,4-BDC; note that for the amino-functionalized molecule only the bidentate coordination is possible due to steric hindrance.^[224] (h) and (i) Reproduced with permission.^[224] Copyright 2017, Royal Society of Chemistry.

5.7. Film Porosity

There are very little efforts so far reported to investigate the porosities of crystalline ALD/MLD grown thin films, presumably due to the difficulties in characterization of small sample amounts for the porosity. This is a pity, as several of them have some potential to possess high specific porosities required for applications such as separation membranes and sensors in microelectronics. The techniques so far used for the porosity characterization of the ALD/MLD films are: quartz crystal microbalance (QCM),^[106] palladium loading,^[229] isopropanol adsorption,^[117] N_2 adsorption,^[416] and porosity ellipsometry.^[136]

The palladium loading technique was employed for the through-porosity measurement of IRMOF-8 (Zn-2,6-NDC) films to confirm their porosity, using $Pd(thd)_2$ as the precursor.^[229] Porosity ellipsometry was applied to detect the limited or insignificant porosity of crystalline Ti-thymine films; the results revealed that the porosity was higher for the Ti-thymine (4%) films compared to the amorphous Ti-uracil (1%) and Ti-adenine (1%) films.^[136] Isopropanol adsorption was applied for MOF-5-structured Zn-BDC films showing a change in the refractive index at the low and the high

isopropanol pressures evidencing the micro- and macroporosity.^[117] The N_2 adsorption isotherm technique was applied for UiO-66- NH_2 (Zr-2-amino-1,4-BDC) films deposited on glass wool fiber substrate having total nitrogen uptake larger than that of the uncoated glass wool substrate.^[416]

For the QCM characterization, the QCM crystals coated with Zr-2,6-NDC and with Zr-4,4'-BPDC were placed back in the ALD reactor where they were heated to 120 °C for 2 h in a vacuum to remove any water from the pores in the films (Figure 24a–c), after which the reactor was cooled to room temperature and left unopened overnight to ensure the complete temperature stabilization. Finally, the films were exposed to a 1 min water pulse, the effect of which was registered by the QCM crystal. The porosity of the film was then evaluated by the amount of water absorbed; it was shown that the effect of the film on the amount of absorbed water was significant compared to the uncoated QCM crystal.^[106] Moreover, the QCM technique could distinguish the difference between the regular Zr-BDC and amino-functionalized Zr-2-amino-1,4-BDC films. The longer stabilization time needed for the amino-functionalized UiO-66 films was tentatively explained to be due to a combination of increased adsorption to the amino group and reduction

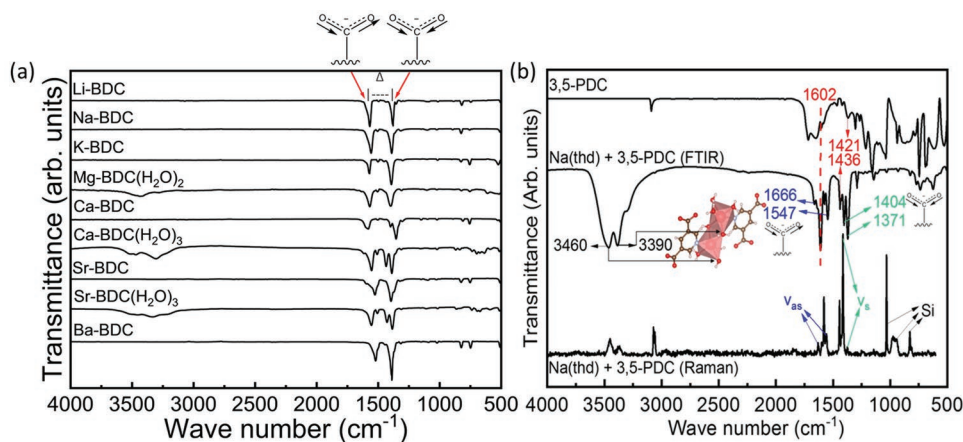


Figure 23. a) FTIR spectra for anhydrous and hydrated metal-BDC films in which different water derivative phases are seen for Ca-BDC and Sr-BDC. Reproduced with permission.^[129] Copyright 2017, Wiley-VCH. b) FTIR and Raman spectra for a hydrated Na-3,5-PDC thin film (and FTIR spectrum for the 3,5-PDC precursor powder for comparison), interpreted based on the known $Na_2-3,5-PDC(H_2O)_4$ structure.^[432] The FTIR peaks 3457 and 3390 cm^{-1} are due to $\nu(O-H)$ vibrations of the terminal and μ_2 -bridging-type coordinated water molecules.^[432] Reproduced with permission.^[118] Copyright 2019, Wiley-VCH.

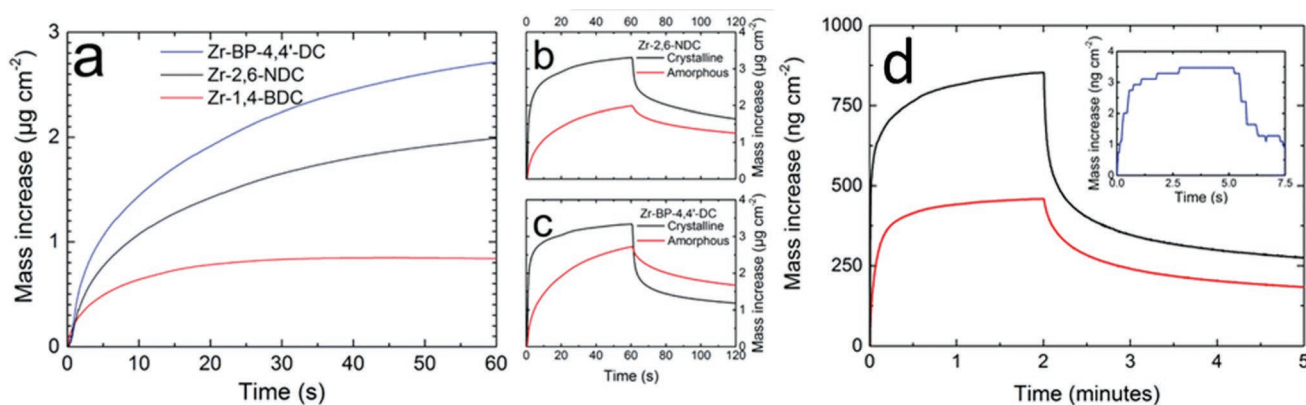


Figure 24. Porosity tests by QCM. Reproduced with permission.^[106] Copyright 2020, Royal Society of Chemistry. a) Comparison between amorphous Zr-BDC, Zr-2,6-NDC, and Zr-4,4'-BPDC films for their water uptake over a 60 s water pulse. b,c) Comparison between amorphous and crystalline Zr-2,6-NDC and Zr-4,4'-BPDC film for their water uptake and release over a 60 s water pulse and 60 s purge. d) Comparison between amorphous (as-deposited) and crystalline (postdeposition-treated) Zr-2-amino-1,4-BDC films for their water uptake over a 2 min water pulse; the inset shows the water uptake for an uncoated QCM crystal during a 5 s water pulse as a reference.

in the pore size where the amino–water complex slows down the diffusion of subsequent water molecules entering the film. Both the amorphous and crystalline films were found porous and have a much larger water uptake than the uncoated crystals, and the crystallization process almost doubles the porosity.^[224]

6. Modeling and Prediction

6.1. Process Modeling

Computational efforts have been made to understand the surface reactions during the ALD/MLD film growth. First of all, for the two simple aliphatic organic precursors, EG and GL, commonly employed in ALD/MLD, DFT calculations have shown that the expected ligand elimination processes are indeed favorable.^[56,219] When combined with TMA for the Al-based metal–organic thin films, both of these organic precursor molecules tend to lie flat and react through two terminal hydroxyl groups with the surface fragments creating so-called double surface reactions. This eventually diminishes the number of active hydroxyl sites and inhibits the further film growth in the case of EG (diol), but not with GL (triol) as its third hydroxyl group remains available for the further film growth.^[219] Most interestingly, this scheme may also depend on the metal precursor. Namely, when combined with the Mg-based precursor at the MgCp-terminated MgO surface, the same aliphatic alcohols behave somewhat differently, that is, EG still prefers to orient in a flat configuration, while the GL species prefer to lie in an upright position. This yields thicker GL-based films, consistent with the experimental observations.^[56]

The DFT method has also been employed to investigate the reactivities of aromatic (phenyl-based) organic precursors with the three different functional groups, OH, NH₂, and NO₂, in combination with TMA. In the first efforts, these reactions were investigated using gas phase models without taking the surface and substrate into account;^[338] these calculations underlined the lower reactivities of NH₂ and NO₂ (with TMA) in comparison to the OH group. In a very recent work, the reactivities of

OH- and NH₂-terminated aromatic molecules were investigated on a post-TMA pulse methyl-terminated Al₂O₃ surface, considering both homo- and hetero-bifunctional aromatic compounds: HQ, PPDA, and 4-aminophenol (4-AP).^[365] It was found that all these precursor molecules bind favorably to the methyl terminated Al₂O₃, via formation of Al–O and Al–N bonds and CH₄ elimination. Reaction energetics suggested a higher reactivity of the OH group with TMA compared to the NH₂ group. This enables the unwanted double reactions for HQ, while for the NH₂-containing PPDA and 4-AP molecules, the double reactions are reduced and the organic molecules are self-assembled in an upright configuration, which leads to thicker and more flexible hybrid films. Therefore, aromatic molecules with NH₂ terminal active groups can be considered as a promising option to promote the ALD/MLD film growth. In the same DFT study, two new organic MLD precursors, hydroquinone bis(2-hydroxyethyl)ether and 1,1'-biphenyl-4,4'-diamine, were investigated for their interactions with the methyl-terminated Al₂O₃ surface; the results revealed that these not-yet-experimentally challenged aromatic molecules react favorably with TMA and are in general promising precursors for the deposition of novel metal–organic thin films.^[365] Finally, it should be mentioned that regarding the relative reactivities of the OH and NH₂ groups, very similar results were obtained for the Ti-based processes between TiCl₄ and HQ, PPDA, or 4-AP as the organic precursor.^[390]

6.2. Structure and Property Modeling

Besides the deposition processes, also the structures and material properties of ALD/MLD grown thin films have been modeled through DFT calculations. A prime example is the case with the in situ crystalline lithium aryloxide thin films obtained from an ALD/MLD process based on LiHMDS and HQ precursors.^[63] For this material, no previous records of any kind of successful synthesis were found. Hence, DFT calculations were performed to predict the crystal structure; the predicted structure was then verified by comparing the calculated and experimental XRD patterns (Figure 25) and FTIR spectra. The crystal

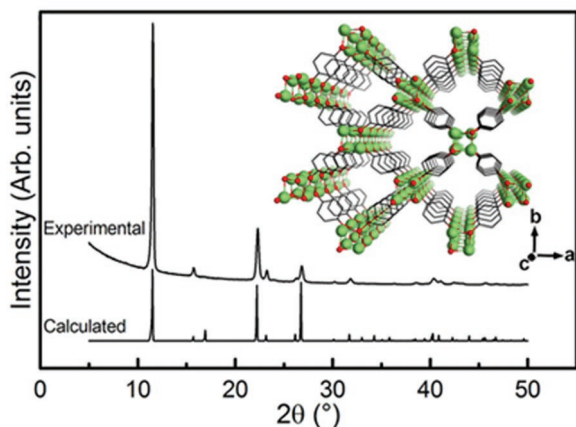


Figure 25. Comparison between the experimental and calculated XRD patterns of Li_2HQ films. Reproduced with permission.^[63] Copyright 2017, Wiley-VCH. The proposed crystal structure (drawn along the c -axis with VESTA^[435]) is shown in inset.

structure of the new Li-aryloxide material appeared to be closely related to the structures previously reported for bulk samples of Na_2HQ and K_2HQ . The lithium site in this Li_2HQ structure is coordinatively undersaturated (3-coordinated), which explains the high water (or other small molecules) absorption tendency of the films in ambient air, and also the fact that the synthesis of this material had not been succeeded through conventional solution-based routes.

In another example, quantum chemical methods were employed to derive atomic-level structural models for different $\text{ZnO}:\text{HQ}$ superlattice (SL) films, in particular for the bonding structures at the inorganic-organic interfaces (Figure 26).^[377] Based on the structure models, the band structures and infrared spectra could be derived as well. Most importantly, the modeling provided useful guidelines for the band structure

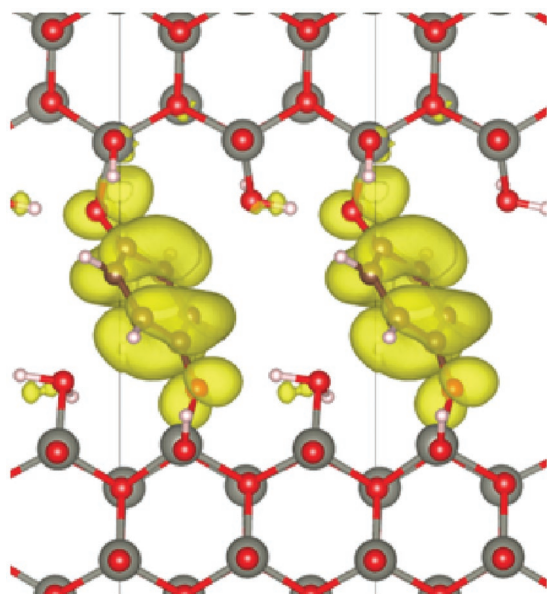


Figure 26. Band-projected electron densities for a $\text{ZnO}:\text{HQ}$ superlattice. Reproduces with permission.^[377] Copyright 2015, American Chemical Society.

engineering through small and experimentally feasible modifications of the organic constituent. For the physical property modeling of the same series of $\text{ZnO}:\text{HQ}$ SL films precisely fabricated through ALD/MLD layer-engineering, quantum chemical methods were used to address their thermal conductivity and thermoelectric properties. Systematic comparisons with bulk ZnO data revealed significantly reduced lattice thermal conductivities for the SL structures, in agreement with the experimental data.^[366]

6.3. Prediction of ALD-/MLD-Feasible Porous Metal-Organic Materials

As already emphasized in previous sections of this review, one of the recent hot topics in the field of porous MOF materials has been their fabrication in high-quality thin-film form using advanced vapor-phase thin-film techniques.^[11,61,117,441] Since the ALD/MLD technique provides us an elegant way to deposit metal-organic materials directly from gaseous precursors, it should in principle be an excellent approach to MOF thin films as well. However, among the in situ crystalline ALD/MLD metal-organic films grown so far, only few cases are potential candidates for porous MOF films: i) copper 1,4-benzenedicarboxylate (Cu-BDC) films,^[437] ii) Zr-2-amino-1,4-BDC films,^[224] and iii) Fe-BDC films.^[203]

To motivate the future efforts to challenge the in situ ALD/MLD growth of porous MOF thin films, we have collected in Table 7 few examples of metal-organic materials for which literature reports conventional bulk samples with a verified porous MOF-type crystal structure and which we consider highly feasible for the ALD/MLD fabrication, in principle. The estimated values for the surface area and pore dimensions given in Table 7 were calculated using the software Zeo++.^[442] To specifically highlight some of these materials, the isostructural series of metal 2,5-dihydroxyterephthalate (M-DHTP ; $\text{M} = \text{Mg}, \text{Mn}, \text{Fe}, \text{Co}, \text{Ni}, \text{Zn}$) coordination polymers, also known as CPO-27-M or M-MOF-74 materials, possess so-called accessible open metal sites that are desirable for various applications. Among the known M-DHTP compounds especially interesting is Zn-DHTP for which these sites remain accessible even after the complete removal of the solvent; accordingly, Zn-DHTP has been investigated as a high affinity sorbent material for CO_2 .^[443] For the Zn-DHTP structure,^[444] the Zeo++ calculation revealed the surface area at $1476 \text{ m}^2 \text{ cm}^{-3}$ and the pore dimensions at 11.6, 10.8, and 11.6 Å. Similarly, for the desolvated Fe-DHTP structure,^[445] our Zeo++ analysis estimated the surface area at $1486 \text{ m}^2 \text{ cm}^{-3}$ and the pore dimensions at 11.6, 10.8, and 11.6 Å; for the bulk samples of Fe-DHTP, reversible low-temperature oxygen adsorption properties have been investigated.^[445] Both Zn-DHTP and Fe-DHTP should be highly relevant for the ALD/MLD fabrication, as the most evident inorganic precursor candidates for these depositions, i.e., $\text{Zn}(\text{acac})_2$ and FeCl_3 , have been already successfully employed for the in situ crystalline Zn- and Fe-organic thin films with other organic components.^[67,117,203,229,253,263] Moreover, very recently, the volatility and reactivity of the organic DHTP precursor was confirmed under ALD/MLD conditions in combination with $\text{Li}(\text{thd})$ as the metal precursor.^[270]

Table 7. Examples of metal–organic materials synthesized in bulk form through conventional synthesis but not yet with ALD/MLD; examples selected based on their feasibility for the ALD/MLD synthesis (with suggested ALD and MLD precursors). The surface area and pore dimension values were calculated (based on the structures reported for bulk samples) using the software Zeo++.

| Targeted metal–organic material (synthesized in bulk form) Application potential/interesting feature | Calculated by Zeo++ Surf. area [m ² cm ⁻³] Pore dim. [Å] | Suggested MLD precursor | Suggested ALD precursor |
|--|--|----------------------------------|--|
| Zn–DHTP – Accessible sites after solvent removal ^[443] – Sorbent for CO ₂ ^[444] | Surf. area: 1476 Pore: 11.6, 10.8, 11.6 ^[443] | DHTP ^[270] | Zn(acac) ₂ ^[117,229,253] |
| Fe–DHTP – Reversible low- <i>T</i> oxygen adsorption ^[445] | Surf. area: 1486 Pore: 11.6, 10.8, 11.6 ^[445] | DHTP ^[270] | FeCl ₃ ^[67,203,263] |
| Cu–DHTP – Sorbent for CO ₂ ^[446] | Surf. area: – Pore: 4.4, 3.5, 4.4 ^[446] | DHTP ^[270] | Cu(thd) ₂ ^[61,206] |
| Co–DHTP – Stable after water removal ^[443,444,447,448] | Surf. area: 1743 Pore: 11.5, 11.0, 11.5 ^[443] | DHTP ^[270] | Co(thd) ₂ ^[201] |
| Ni–DHTP – Stable after water removal ^[444,449] | Surf. area: 1804 Pore: 11.5, 10.7, 11.5 ^[449] | DHTP ^[270] | Ni(dmamb) ₂ ^[257] |
| Mg–DHTP – CPO-27, MOF-74 ^[444] | Surf. area: – Pore: 1.8, 1.0, 1.8 ^[450] | DHTP ^[270] | Mg(thd) ₂ ^[118,129] |
| Na–4,4′-BPDC – Anode for battery ^[451] | Surf. area: 141 Pore: 0.96, 0.60, 0.92 ^[451] | 4,4′-BPDC ^[106,411] | Na(thd) ₂ ^[58,118,129] |
| Ca–4,4′-BPDC – Anode for battery ^[451] | Surf. area: – Pore: 2.0, 0.9, 2.0 ^[452] | 4,4′-BPDC ^[106,411] | Ca(thd) ₂ ^[67,118,129] |
| Mg–2,6-NDC – Desolvated crystalline structure exists, porous with solvent ^[453] | Surf. area: – Pore: 2.8, 1.4, 2.8 ^[453] | 2,6-NDC ^[106,229,411] | Mg(thd) ₂ ^[118,129] |
| Fe–1,3,5-BTC – Water as solvent including MIL-100(Fe) with very large pores and interesting in catalysis ^[454] | Surf. area: 14 560 Pore: 82, 64, 80 ^[454] | 1,3,5-BTC | FeCl ₃ ^[67,203,263] |
| Al–1,3,5-BTC – Promising adsorbent ^[455] | Surf. area: – Pore: 8.3, 0.9, 7.5 ^[456] | 1,3,5-BTC | TMA |
| Ca–1,3,5-BTC | Surf. area: – Pore: 2.7, 1.4, 2.7 ^[457] | 1,3,5-BTC | Ca(thd) ₂ ^[67,118,129] |

Finally, we like to emphasize once more the possibility to convert the as-deposited amorphous ALD/MLD films into crystalline films of a MOF-like structure, as already demonstrated, e.g., by utilizing humidity treatments followed by DMF-autoclave crystallization,^[117,229] or acetic acid vapor treatments.^[204] Commonly for these structures, the subsequent removal of the solvent molecules do not break the porous crystal structure thus also leaving the open metal sites untouched. Owing to the wide variety of possible inorganic and organic building block combinations to be explored, the prospects to discover novel ALD-/MLD-enabled MOF materials are huge. Indeed, only a fraction of these exciting thin-film materials have been realized/verified so far.

7. Highlights of Properties/Application Potential of ALD/MLD Thin Films

The shift from inorganic and silicon-based devices toward organic and hybrid inorganic–organic devices is a rapidly growing trend in microelectronics. The relevance of the MOF-type materials for such future applications is already widely understood. For these devices, the MOF material needs to be fabricated in high-quality thin-film form with the precise control over the thickness and conformality and the

possibility for easy patterning. Indeed, among the different thin-film deposition approaches, the vapor phase deposition techniques including the ALD/MLD technique are the most desirable ones.^[11]

Moreover, many of the metal–organic materials grown through different ALD/MLD processes are fundamentally new materials; in the most attractive case, this approach allows even materials not accessible by conventional synthesis techniques. Hence, the ALD/MLD fabrication is likely to lead us to truly unique materials allowing the ingenious fusion of metal and organic moieties in such a way that the hybrid material may show even mutually contradictory combinations of properties, in other words, “make impossible possible.” Such materials with new compositions and/or crystal structures are likely to reveal unorthodox chemistry features and therefore new properties and functionalities. The remarkable technological bonus is that the ALD/MLD technique has the capacity to deliver these new materials as high-quality thin films of the level required not only in microelectronics but also in other advanced applications.

7.1. Battery Applications

The Li-ion battery field is one of the application areas where we can expect significant impact from the ALD/MLD

metal–organic materials. With ALD/MLD, both electrode and coating materials have been developed having the eyes on the next-generation lithium-ion battery applications.

Most straightforwardly, ALD/MLD coatings could be beneficial as artificial solid-electrolyte interphase (SEI) layers deposited on top of the negative electrode (anode) prior to the battery assembly to prevent the less controllable natural-SEI formation. Namely, when a Li-ion battery is taken into operation, a SEI layer forms during the first charge/discharge cycles on top of anode as a result of interfacial anode/electrolyte reactions. This SEI is a crucial but poorly understood/controlled battery component. It passivates the anode against further unwanted side reactions, but the drawback is that it depletes the capacity of the battery by consuming part of the initial lithium load. In the best case, the prefabricated SEI coating could – besides stabilizing the anode and minimizing the loss of loaded lithium – endure the large volume changes that some of the battery materials suffer from. Indeed, the ALD/MLD technique should be optimal for the growth of mechanically flexible and conformal ultrathin artificial SEI layers. Considering the optimal composition for these artificial SEI layers, it is important to note that the commercial Li-ion batteries are based on carbonate-based electrolytes, which upon reacting with the anode form lithium alkyl carbonates.^[458] Carbon dioxide has been used in conventional ALD for inorganic metal carbonate films,^[127] but only recently as a third precursor in an ALD/MLD process. These ALD/MLD films grown from Li–HMDS, ethylene glycol, and CO₂ yielded lithium ethyl carbonate films,^[413] thus perfectly mimicking the organic component in naturally forming SEI layers. So far, however, these coatings have not been tested in real battery environment.

Another promising coating material is Li 1,4-benzenedisulfonate, which could be considered as a prototype of so-called solid polymeric single Li-ion conductors with immobilized (sulfonate) anions; such materials have been highlighted as promising solid-state conductors for the Li-ion battery. Very recently, such films were grown in situ crystalline from Li(thd) and BDS precursors, and the ionic conductivity of the films was determined to be in the range of 4.1×10^{-9} – 6.4×10^{-8} S cm⁻¹ at 80–118 °C.^[121] Similarly, Li-containing “lithicone” thin films with room-temperature ionic conductivity have been deposited using lithium *tert*-butoxide and EG precursors.^[412]

Materials made through ALD/MLD possess highly attractive features for the next-generation Li-ion battery technologies, not only as coatings as discussed above but also as active organic electrode materials for ultrathin and integrable components for miniaturized energy storage devices for, e.g., wireless sensors and medical and IoT devices. A thin-film microbattery could deliver energy locally; it would also be safer than the conventional wet-cell battery, and once made of organics, also mechanically flexible. The biggest obstacles with the Li–organic electrode materials in general are their solubility in the commonly employed liquid electrolytes and their notably poor electronic conductivity. In a thin-film battery configuration, these obstacles are naturally circumvented: the dissolution issue is completely avoided by replacing the liquid electrolyte by a solid one, while the reduced dimensions in thin films contribute toward mitigating the effect of the low electronic conductivity of organics. For practical applications, the thin-film microbatteries should be shaped into 3D high-active-surface-area architectures

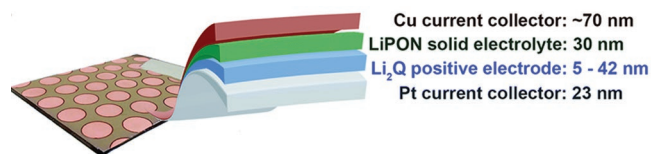


Figure 27. Schematic presentation of the Li₂HQ/LiPON/Cu cells used to evaluate the electrochemical performance of Li₂HQ. Reproduced with permission.^[59] Copyright 2018, Royal Society of Chemistry.

to reach sufficiently high energy density values, which underlines the reason why ALD/MLD is not only a scientifically elegant but also the only technologically feasible fabrication technique for these next-generation batteries. Moreover, in thin-film form, it is possible to investigate the intrinsic behaviors of Li–organics as no additives (such as conductive carbon) are needed.

The first all-ALD-/MLD-made Li–organic microbattery consisted of Li–benzoquinone (Li–HQ) cathode (importantly, in situ grown in its lithiated state) and Li–terephthalate (Li–BDC) anode, separated with an ALD–lithium phosphorus oxynitride (LiPON) layer as the electrolyte.^[59] The battery worked also without the Li–terephthalate layer (**Figure 27**), as the lithium metal layer intrinsically formed/consumed during the charge/discharge could also act as an efficient anode. For these thin-film cells with ultrathin Li–benzoquinone and LiPON layers, ultrahigh redox reaction rates were realized; the charge/discharge times as short as ≈ 0.25 s (plus energy/power densities of ≈ 100 mWh cm⁻³ and ≈ 500 W cm⁻³) are promising, considering that the setup was far from optimized yet (**Figure 28**). However, while the rate capabilities were superior, the energy densities were miserable; here, to increase the active material amount (and thereby the energy density), an evident solution is to go from planar to 3D nanotemplate designs,^[128] which has not been challenged yet. On the other hand, to control the redox potentials of the electrodes, an effective approach is to functionalize the organic backbone by electron-donating or electron-withdrawing groups; proof of the concept for this was demonstrated with the Li–BDC anode whose redox potential was decreased by 0.14 V by adding an electron-donating amino group in the benzene backbone of the BDC moiety.^[225]

Finally, there are interesting layer-structured and redox-active Li–organic materials made through ALD/MLD. These so-called intercalate-type iMOF structures are highly attractive in the sense that they experience only minimal changes in crystal structure upon Li-ion (de)intercalation,^[459–464] and are thereby beneficial to overcome one of the notorious drawbacks of conventional metal oxide electrode materials in Li-ion battery technology, i.e., the capacity decay on cycling, due to the substantial volume changes during the Li-ion intercalation. Promising ALD/MLD processes have been developed for a number of feasible iMOF material candidates,^[411] which moreover were demonstrated to be electrochemically active (**Figure 29**): the lithiation was seen for Li–BDC (0.81 V), Li–2,6-NDC (0.73 V), Li–4,4′-BPDC (0.66 V), and Li–AZO (1.48 V).

The unique benefits of ALD and MLD in the battery field, such as the atomic/molecular level rational material design, in situ growth of uniform, conformal, and pinhole-free films, and relatively low process temperatures serve as an important

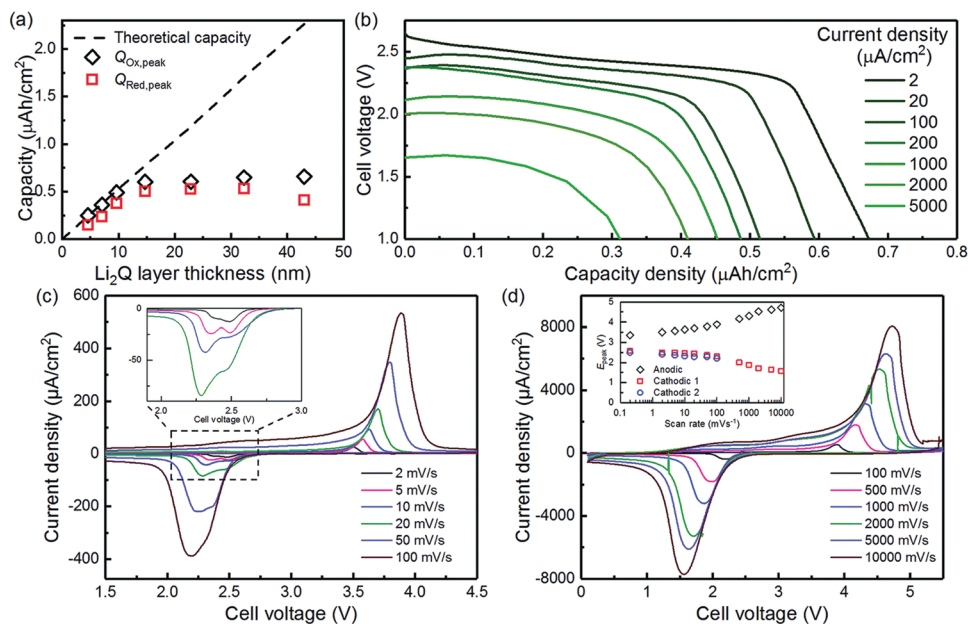


Figure 28. a) Integrated capacity corresponding to the redox peaks of solid-state cells as a function of Li_2Q layer thickness; experimental values follow the theoretical maximum (dashed line) up to 10 nm Li_2Q layers. b) Discharge voltage curves with current density ranging from $2 \mu\text{A cm}^{-2}$ ($\approx 2.6\text{C}$) to $5000 \mu\text{A cm}^{-2}$ (6500C) for 15 nm Li_2Q . c,d) Cyclic voltammograms between 2 and 100 and 100–10 000 mV s^{-1} , with 10 nm Li_2Q ; inset in (c) highlights the cathodic peak for the scan rates between 2 and 20mV s^{-1} , whereas inset in (d) shows the redox peak separation as a function of the scan rate. Reproduced with permission.^[59] Copyright 2018, Royal Society of Chemistry.

motivation to explore the aforementioned approaches further.^[102,291,331] Currently, there are strong drive to extend these efforts to Na-, K-, Zn-, Al-, and Mg-based batteries as well.^[91] Other interesting materials for electrochemical applications

include the Sn–GL films with high electrochemical activity toward Li storage,^[425] and the annealed Mn–EG films with a greater stability to restructuring during electrochemical testing with a clear promise for use as electrodes in thin-film batteries.^[60]

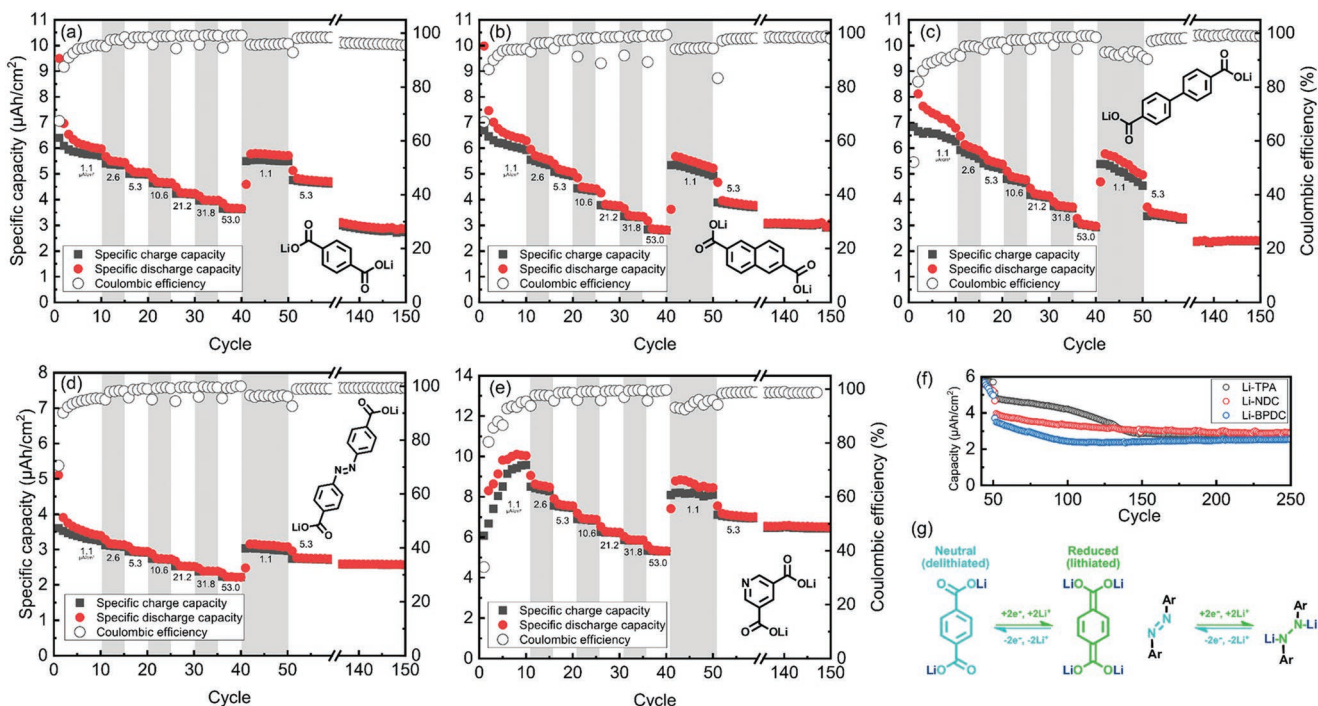


Figure 29. Galvanostatic cycling data with various current densities for a) Li–BDC, b) Li–2,6–NDC, c) Li–4,4'–BPDC, d) Li–AZO, and e) Li–3,5–PDC. f) Decreasing capacity of Li–BDC (black), Li–2,6–NDC (red), and Li–4,4'–BPDC (blue) after the experiment. g) Redox reactions of Li–BDC and Li–AZO. Reproduced with permission.^[411] Copyright 2020, American Chemical Society.

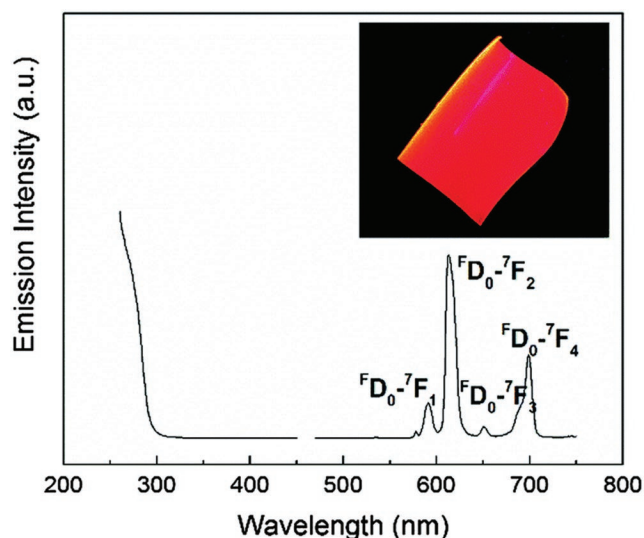


Figure 30. Photoluminescence excitation ($\lambda_{\text{em}} = 615 \text{ nm}$) and emission ($\lambda_{\text{ex}} = 270 \text{ nm}$) spectra for a 100 nm thick Eu-hybrid thin film deposited on a quartz glass substrate; the inset shows a photo taken under 270 nm UV illumination of a similarly deposited film on an indium tin oxide-coated PET substrate. Reproduced with permission.^[428] Copyright 2015, Royal Society of Chemistry.

7.2. Other Applications

Several studies have focused on the photoluminescence properties of lanthanide-based ALD/MLD thin films. In particular, the characteristic red Eu^{3+} luminescence has been realized for a number of Eu-organic films;^[57,266,429] the mechanical flexibility expected for these films was demonstrated as well (Figure 30).^[428] An interesting notion is that, while in purely inorganic matrices, such as $(\text{Y,Eu})_2\text{O}_3$, the Eu^{3+} activator concentration typically needs to be strongly diluted due to the well-known concentration quenching phenomenon, in the ALD/MLD-grown Eu-organic films, the spacious organic linkers seem to take care of this issue, as intense luminescence emission has been achieved for these films even with 100% occupation of the Ln site with Eu.^[57] Moreover, by controlling the size of the organic backbone (e.g., BDC, 1,4-NDC, ADA, 3,5-PDC, 2,6-NDC, 2-amino-1,4-BDC) or including additional

functional groups/bonding sites into the backbone both the absorption/excitation wavelength range and the emission intensity of these Eu-organic films have been successfully tailored.^[57,266] Other highlights among the ALD/MLD Ln-organic family of luminescence thin films are the MOF-structured (UiO-66) Eu-2-amino-1,4-BDC^[429] films and the erbium-based Er-3,5-PDC^[208] films.

Tailored luminescence properties have been reported for d-block-transition-metal-based metal-naphthalene films as well, i.e., Ti-2,6-NDC, Zr-2,6-NDC, Hf-2,6-NDC, and Y-2,6-NDC, that are potentially beneficial for applications such as antimicrobial coatings in photodynamic therapy or optical sensors.^[122] These experiments demonstrated that it is possible to tune the light absorption toward the visible wavelength range by using metals with a high charge density. The Zr-, Hf-, and Y-based films were found to yield intense blue photoluminescence upon UV excitation, while the emission energy and intensity depended on the metal component. In particular, the presence of Y clusters was found to enhance the luminescence intensity, whereas Zr and Hf shifted the emission toward the higher wavelengths.

Another interesting application area has been proposed for Na-uracil films, as these films exhibited widely excitation-wavelength-dependent fluorescence in the visible region (Figure 31).^[58,222] Time-resolved measurements revealed the connection of the excitation-dependent fluorescence to the so-called red-edge excitation shift effect.^[58] This finding could open up new possibilities in photonic applications as the emission wavelength can be simply changed by choosing a different excitation wavelength.^[222]

Besides the UV-active photoluminescence materials, ALD/MLD has been exploited for the fabrication of upconverting lanthanide-organic films in which Yb, Er, and Ho serve as the active metal components. Most excitingly, intense IR-to-vis upconversion in the entire visible (blue-green-red) spectral range was observed for the (Y,Yb,Er)-pyrazine films upon laser excitation at 974 nm. This is remarkable, as conventional Ln-organic complexes often suffer from excitation energy losses caused by the high-energy phonons of their organic ligands. Apparently, the network of interconnected pyrazine molecules serves as an excellent matrix to avoid the energy losses and support the Yb^{3+} -to- Er^{3+} excitation energy transfer

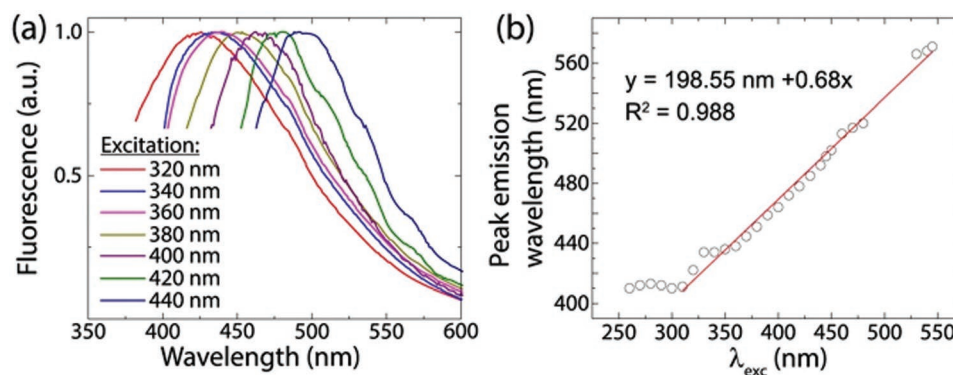


Figure 31. Broad excitation-dependent fluorescence of Na-uracil thin films: a) normalized emission spectra recorded with various excitation wavelengths, and b) the linear dependency of the emission wavelength on the excitation wavelength. Reproduced under the terms of the CC-BY 4.0 license.^[222] Copyright 2017, Published by Springer Nature.

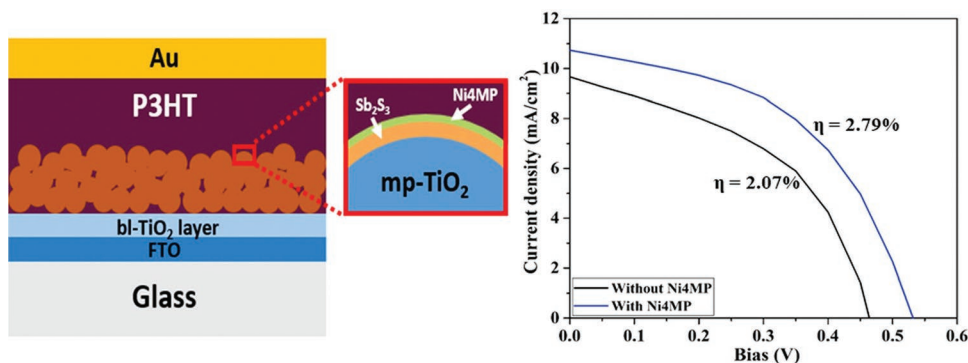


Figure 32. Enhanced photovoltaic performance for Sb_2S_3 -sensitized mesoporous TiO_2 solar cells by ALD/MLD grown Ni-4MP interlayer. Reproduced with permission.^[257] Copyright 2019, Elsevier.

allowing both two- and three-photon near-infrared (NIR)-to-visible excitation processes.^[214]

Upconverting ALD/MLD (Yb,Er)-IR-806 films with a wide absorption band in the near-infrared region and green and red upconversion emission were highlighted as potential candidates for use as, e.g., temperature sensors.^[259] Another potential application for the upconverting ALD/MLD films is found in the field of photovoltaics. For the current solar cell technologies, a fundamental restriction is their wavelength operation range, limited to the visible portion of the solar spectrum only. The performance could be enhanced by integrating the solar cell with an upconverting component capable in converting IR radiation into visible light. Here, the proper choice of the upconverting lanthanide ions is important: Yb^{3+} and Er^{3+} with the main absorption in the range 800–1000 nm are promising in the case of the wide-bandgap perovskite, dye-sensitized and organic solar cells, but not in combination with the narrow-bandgap Si-based solar cells, as Si absorbs up to 1100 nm itself; for the crystalline-Si cells, Ho^{3+} (with the major NIR absorption band in the 1150–1230 nm range) is more appropriate for efficient upconversion enhancement.^[465] Indeed, recently this was demonstrated for ALD-grown $(\text{Er,Ho})_2\text{O}_3$ -coated c-Si solar cells.^[427] Besides the upconverting materials, ALD-/MLD-grown Ni-4MP films have been shown to be beneficial as interlayers to enhance the power conversion efficiency in solar cells (Figure 32).^[257]

As an entirely different application area, lightweight and mechanically flexible ALD-/MLD-fabricated metal-organic magnets could be attractive alternatives for the conventional heavy and rigid inorganic magnets based on critically rare elements (Sm, Nd), especially in applications benefitting from the thin-film form factor. Already relatively long time ago, Epstein and co-workers demonstrated the growth of (Co,V)-TCNE films with magnetic ordering temperatures up to 300 K and a coercive field of 50 Oe at 5 K and 30 Oe at 300 K (Figure 33). In these films, the presence of metallic Co^0 islands contributes to the magnetic properties. Compared to materials previously synthesized by solution or CVD methods, these films were found smooth and pinhole-free.^[236,237]

In catalytic applications, the high film roughness can be the key feature as it increases the surface area. This was the case for the ALD-/MLD-grown Zn-glutaric acid films for which increased catalytic activity toward the copolymerization

reaction of propylene oxide and CO_2 was revealed.^[253] Similarly, Mo-thiolate films grown from molybdenum hexacarbonyl and 1,2-ethanedithiol were found catalytically active for the hydrogen evolution reaction. Here, the positive results were attributed to the fact that the films contained MoS_2 -like domains interspersed with organic linkers. Additionally, films comprised of MoS_2 domains in a porous carbon matrix were obtained by annealing the as-deposited Mo-thiolate films in $\text{H}_2\text{S}/\text{H}_2$ gas at 350 °C. Both the as-deposited and annealed Mo-thiolate-based films were found superior to the flat MoS_2 reference sample.^[242]

Ultrathin and conformal ALD/MLD hybrid films are excellent candidates for different barrier and protective coatings as well. The specific requirements, e.g., for the stability/reactivity then depend on the targeted application. For example, Detavernier and co-workers developed ALD/MLD processes for magnesium-based Mg-EG and Mg-GL films, having their use in reactive barrier layers (requiring water uptake and swelling) and solid composite electrolytes (requiring transformability into porous metal oxide) in mind.^[56] In another study, Sun and co-workers deposited Zr-EG films for nanoscale protective layers on lithium to achieve stable and long-life Li metal anodes, and demonstrated enhanced air stability, electrochemical performance, and high rate capability in symmetrical cell testing.^[417]

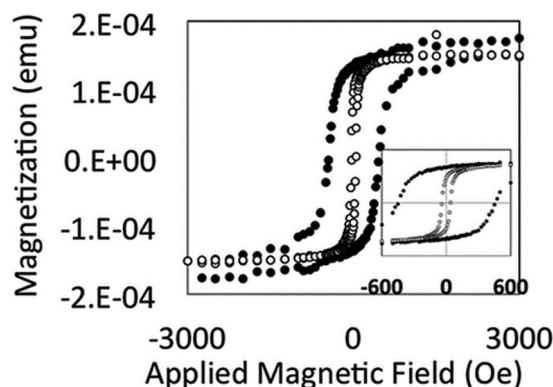


Figure 33. Magnetization of Co-TCNE film as a function of the applied magnetic field at 5 K (solid circles) and 300 K (hollow circles) of samples parallel to the magnetic field. The inset is closer view. Reproduced with permission.^[236] Copyright 2014, Royal Society of Chemistry.

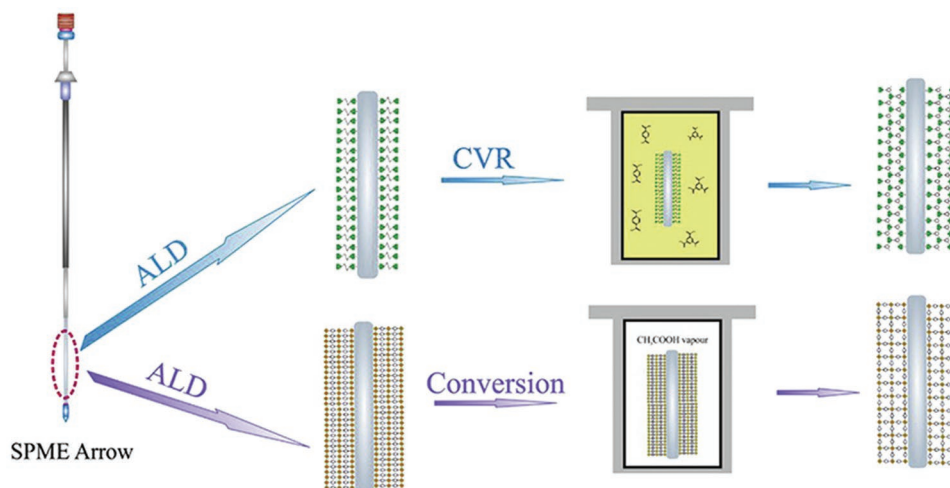


Figure 34. Chemical vapor reaction (CVR) and atomic layer deposition (ALD) conversion methods were utilized for preparation of MOF coatings of solid phase microextraction (SPME) arrow. Zr–BDC films with the UiO-66 structure were suitable for the extraction of, e.g., aromatic compounds. Reproduced with permission.^[205] Copyright 2018, Elsevier.

Organic moieties can be also used to bring added functionalities for the hybrid material as a whole. An early example is from Nilsen and co-workers; they demonstrated the hydrophobicity of the Al–L-glutamic acid films in which the hydrophobic organic backbone faced outward from the film surface, increasing the surface roughness and thereby the hydrophobicity of the films.^[234] A more recent example is the successful introduction of UV-active azobenzene moieties in Li–AZO, Ca–AZO, and Fe–AZO films, opening up new photoswitching possibilities;^[67,263,414] it is noteworthy that the *trans*–*cis* photoisomerization reaction of azobenzene is rarely realized in bulk metal–AZO samples.

Finally, we foresee remarkable application possibilities for the in situ crystalline MOF-like hybrid films; one of the evident areas is in different extraction applications. Recently, Zr–BDC films with the UiO-66 structure were proven to be suitable for the extraction of small polar compounds, aromatic compounds, and long chain polar compounds, such as acetic acid, pyridine, and trimethylamine (Figure 34).^[205] Similarly, Zr-2-amino-BDC films with the UiO-66–NH₂ structure deposited on glass wool

fiber substrates were demonstrated for their toxic gas retention by capturing ammonia and catalytically degrade different nerve agents via hydrolysis.^[416]

7.3. Superlattices and Nanolaminates

Since both ALD and MLD are modular processes, it is possible to build up different multilayer structures in which MLD-grown organic layers can be embedded within the ALD-grown inorganic layers with any predetermined pattern. Indeed, the ALD/MLD approach allows any arbitrary combination of ALD and MLD pulses (Figure 35), and has already been utilized in the fabrication of regular SL-, irregular-/graded-, and nanolaminate (NL)-type thin films. In particular, this has been exploited to introduce extra functionalities such as mechanical flexibility, bandgap tunability, carrier doping, photoswitchability, or heat-transport blocking within different inorganic matrices.

While it is rather unsurprising that organic fragments enhance the mechanical properties of intrinsically rigid

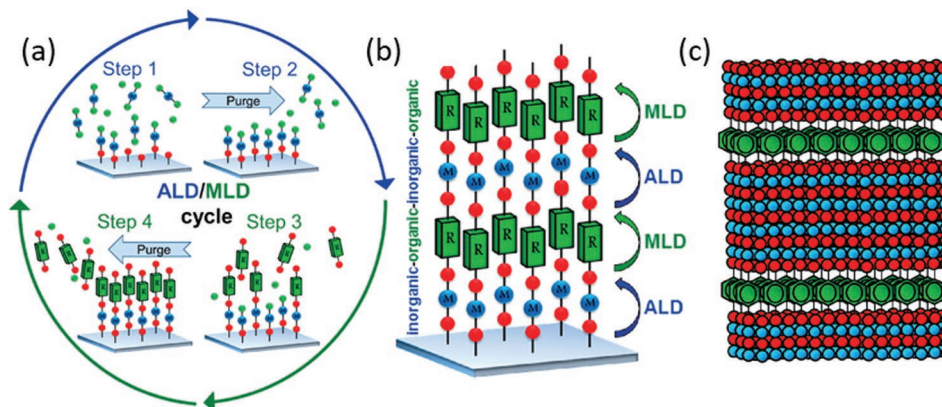


Figure 35. a) ALD/MLD cycle consisting of the four precursor pulse and purge steps. b) Schematic structure of the ordinary 1:1 hybrid metal–organic thin film fabricated by the ALD/MLD technique. c) Schematic structure of an inorganic–organic superlattice thin film deposited by controlling the sequence of the individual ALD and MLD cycles (blue = metal, red = oxygen, green = organic). Reproduced with permission.^[377] Copyright 2015, American Chemical Society.

inorganics, the results obtained through nanoindentation and tensile testing experiments for a series of ϵ -Fe₂O₃:BDC superlattice films were impressive as they demonstrated that even just few monomolecular organic layers embedded within a 100 nm ϵ -Fe₂O₃ film could make the films significantly more flexible, suppressing the elastic modulus and increasing the crack onset strain by several factors.^[124] This was important as it enabled the enhanced flexibility while keeping the individual ϵ -Fe₂O₃-layer thickness in the SL structure thick enough (\approx 20 nm) not to deteriorate their unique magnetic properties.^[123] This approach should be readily transferable to many other ALD-/MLD-grown multilayer films with different inorganic and organic combinations.

By inserting monomolecular organic layers within inorganic semiconductor matrix, it is also possible to tailor the optical bandgap. This has been demonstrated – besides the aforementioned ϵ -Fe₂O₃:BDC films^[202,263] – for TiO₂ films with either HQ^[248] or curcumin^[135] layers. Most importantly, the bandgap tailoring sensitized the TiO₂ films for visible light absorption, which is important, e.g., for their potential application in photocatalysis or as an antimicrobial coating. Regarding the latter application, it is exciting to note that curcumin is also known for its antimicrobial properties. We hypothesize that selecting the organic component optimally, ALD–TiO₂ films can be optimized for a number of exciting applications deriving from its light absorption capability.

The choice of the organic component plays an important role in controlling the properties of the resultant superlattice as a whole. This has been demonstrated for ZnO:organic SLs showing that BDC and HQ within the ZnO matrix turn the film orientation to different directions and affect the electrical transport properties differently. While the BDC layers depress electrical conductivity, adding the HQ layers enhances the carrier concentration, effective mass, and electrical conductivity.^[133] Moreover, the density difference at the ZnO/organic interfaces naturally depends on the choice of the organic component; this is important for the suppression of the thermal transport and thereby highly relevant for the optimization of the ZnO films for their thermoelectric characteristics.^[245,389] Namely, ZnO as an n-type wide bandgap semiconductor is a good candidate for critical-element-free thermoelectrics, except for its too high thermal conductivity dominated by the phonon part of thermal conductivity. Through smart design of the organic component itself and the frequency pattern, it is introduced within the ZnO film, the thermal conductivity of ZnO films has been suppressed by the factor of 50 without compromising the electrical transport properties.^[64,245,375] Another unique feature of the ALD-/MLD-grown ZnO:organic SL films is the fact that they can be deposited in a conformal manner on textile fibers so that the entire textile piece becomes an active part of the device; this is highly promising considering the potential wearable thermoelectric devices.^[55]

An attractive new organic component for the multifunctional SL structures is the photoresponsive azobenzene moiety which undergoes reversible *trans*–*cis*–*trans* photoisomerization reactions upon successive UV and visible light illuminations. Highly promising results have been obtained for the azobenzene moieties embedded within thin films of ferrimagnetic ϵ -Fe₂O₃ – the rarest but possibly the most exciting trivalent iron oxide

polymorph with an exceptionally high coercive field (up to 20 kOe at room temperature). The recently developed ALD process (based on FeCl₃ + H₂O) for rather stable ϵ -Fe₂O₃ films^[466] served as the starting point, and the added MLD azobenzene dicarboxylate cycles were used to combine nanoscale ϵ -Fe₂O₃ and azobenzene layers into well-defined SL structures.^[444] Interestingly, the few embedded azobenzene layers not only added the photoswitching functionality but was even found to enhance the magnetic performance of the ϵ -Fe₂O₃ matrix in overall. Most importantly, in this inorganic–organic matrix, the azobenzene moieties were shown to have enough freedom to undergo their characteristic *trans*–*cis*–*trans* photoisomerization reactions. This fusion and interplay between magnetism and photocontrollability could pave the way to the realization of novel lightweight, stretchable, photoswitchable, device-integrable, and sustainable thin-film magnets, for example, for the next-generation data storage.

There are attractive application possibilities for inorganic/metal–organic nanolaminate structures as well. In an early study, Al₂O₃/Al–organic NL films were investigated as gas barrier layers on biopolymer substrates.^[312] Thin ALD–Al₂O₃ coatings alone are efficient barriers against gases and vapors; however, these films are brittle and straining them generates defects that impair the barrier properties. Enhancing the flexibility by inserting nanoscale Al–EG layers was shown to decrease the number and size of defects compared to the thicker homogeneous Al₂O₃ films after straining, and hence straining deteriorated the oxygen barrier properties less when applied to the NL films than when applied to the Al₂O₃ coatings.

Other examples of interesting nanolaminates include the Ta₂O₅/polyimide nanolaminates with improved dielectric properties and elasticity compared to the bare Ta₂O₅ and polyimide films,^[209] and the ZrO₂/Zr–organic films investigated as thin-film encapsulation layers for organic light-emitting devices (OLEDs) to achieve a significantly longer lifetime.^[65] For the latter ZrO₂/Zr–organic NL films, the density, refractive index, elastic modulus, and hardness values could be tailored. Similar ZrO₂/Zr–organic films have been also used as a dielectric layer in capacitor structures; they exhibited a low leakage current and a high field effect mobility.^[418] The prepared self-assembled organic layer (SAOL)–ZrO₂ organic–inorganic nanohybrid films exhibited good mechanical stability, excellent insulating properties, and relatively high dielectric constant k (\approx 16). They were then used as a 23 nm thick dielectrics for low voltage pentacene-based thin-film transistors, which showed a maximum field effect mobility of 0.63 cm² V^{−1} s^{−1}, operating at −1 V with an on/off current ratio of \approx 10³.^[419]

7.4. Patents

We could identify all together around 160 ALD-/MLD-related patents (**Figure 36**); these are collected in Table S5 (Supporting Information). Here, we highlight just some representative examples. The early patents often focused on ALD-/MLD-fabricated (amorphous) aluminum alkoxide or so-called alucone films, suggested for various purposes, e.g., for a semiconductor device where the alucone film is deposited over the stack structure of a liner.^[467] Interestingly, there are also patents for the ALD/MLD

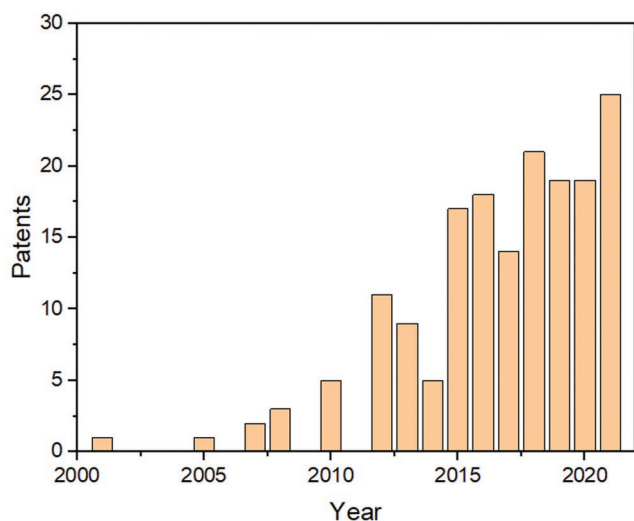


Figure 36. Annually filed ALD-/MLD-related patents.

fabrication of crystalline MOF films from an organometallic precursor and at least one additional organic ligand.^[468]

Many of the patents aim at battery applications. One of these describes a potential electrode for a lithium battery built up as a nanolaminate stack from metal oxide layers (TiO_2 or MnO_2) separated by a decoupling layer deposited from an organic precursor.^[469] In another battery-related patent, a manufacturing method is introduced for a solid-state thin-film battery comprising of lithium–organic electrodes (anode and cathode) and an ALD-grown solid-state electrolyte deposited between the cathode and the anode films.^[470]

The ALD/MLD technique is promising for flexible and conformal coatings as well. For example, one patent describes a flexible laminate made by repeating at least twice the sequence of an inorganic layer and an organic layer, the latter comprising of either primary amine, aromatic amine, or aromatic amine with a hydroxyl group.^[471] Another invention covers the ALD/MLD deposition on a 3D substrate to form an organic optoelectronic device, comprising of a 3D-curved organic functional layer assembly.^[472]

An attractive application area is also seen in different barrier and encapsulation coatings. The patented ALD/MLD protective coatings include gas permeation barrier materials,^[473] organic electronic devices,^[474] and packaging structures for OLEDs to protect against oxygen and water vapor transmission.^[475] For encapsulation, an interesting example is the material to be used for a slow-release medical treatment and composing of a core made with the active component (pharmaceutical or nutraceutical compound) and a multilayer shell deposited by MLD.^[476] Moreover, ALD/MLD films are also envisioned for antireflective coating application, wherein the organic compound absorbs light at the selected wavelength range.^[477]

Several inventions utilize postdeposition-treated hybrid films, based on, e.g., titanium,^[478–481] or zinc,^[482] and annealed at elevated temperatures to remove the organic part, yielding materials beneficial for solar cell battery,^[478] dye-sensitized solar cell,^[479] nanocatalyst,^[482] photocatalytic activity,^[481] or water purification.^[480]

Finally, an interesting patent related to selective deposition was published recently; it describes the selective growth of

polymer thin films on a metallic surface in comparison to a dielectric surface. Selectivity could be further improved by etching of the film.^[483]

8. Conclusions and Outlook

The research exploiting the combined ALD/MLD technique has been progressively gaining momentum within its “decade plus” long history. Initially the focus was on Al-, Zn-, and Ti-organic hybrid materials derived from the three metals best known from the parent ALD technology. The metal precursors used in these processes were also adopted from the existing ALD precursor library, i.e., trimethyl aluminum, diethyl zinc, and titanium tetrachloride. The most commonly employed organic precursors in the early ALD/MLD works were simple aliphatic organic alcohols such as ethylene glycol with two terminal hydroxyl groups as the reactive groups, in an analogy to the water molecule commonly used as the coreactant in the ALD processes of metal oxide thin films. Accordingly, in the resultant metal–organic thin films, the metal nodes were bonded to the organic backbone via oxygen atoms, such that the products could be considered as metal alkoxides or so-called “metalcones.”

Later on, the research has rapidly expanded to cover – regarding the metal component – the periodic table already relatively widely (s-block metals, d-block transition metals, p-block metals, lanthanides), and to involve – regarding the organic precursor – molecules ranging from the simple aliphatic alcohols to both synthetic and natural aromatic organics with different reactive groups. The choice of the reactive group in the organics (OH, COOH, NH_2 , SO_3H , or SH) is important in the sense that it defines the bonding site (O, N, or S) in the resultant hybrid material. Interestingly, combining two different reactive groups into a single heterobifunctional precursor molecule seems to – according to both experimental observations and computational modeling – well prevent the unwanted double surface reactions sometimes seen for the homo-bifunctional organic molecules with a flexible aliphatic carbon backbone. The choice of the organic component may also affect the thermal/chemical stability of the hybrid film; in the early works, the simplest metal alkoxide films were often reported to be unstable in atmospheric conditions, while most of the hybrids based on aromatic organics have been found appreciably stable. Organic precursors may be tricky to utilize also because of their considerably lower vapor pressures in comparison to the well-established inorganic precursors.

The smart design of the organic precursor is of vital importance, not only for the feasibility of the ALD/MLD growth process and the stability of the resultant thin-film product, but also for the important functional properties of the targeted metal–organic material. The most important decision is naturally the choice of the backbone in the organic precursor, as it is the part of the precursor molecule that remains as the actual organic moiety in the final metaorganic material. The other parameter to play with is the atom species via which the metal and organic components are bound together. There are already many exciting studies reported in which the organic backbone has brought important additional functionalities

(besides the most straightforwardly expected spacing and flexibility) into the hybrid material as a whole; intriguing examples include the different carrier doping, optical bandgap tuning, and light-absorption properties of the organics, and possibly most excitingly, the photoswitching functionality of the *trans-cis* isomerization active azobenzene moiety.

An amazing new dimension for the ALD/MLD research emerged when it was realized that some of the processes yielded in situ crystalline thin films, even with compositions and/or crystal structures not previously reported for bulk materials produced through conventional synthesis routes. One of the highlights is the case with so-called coordinatively unsaturated metal sites; these sites attract small guest molecules and are hence highly beneficial in applications based on absorption of small molecules, such as H₂O, H₂, CH₄, CO₂, or O₂. In the solution-based synthesis, it is difficult if not impossible to avoid the filling of these sites with the solvent molecules, but in the gas-phase ALD/MLD synthesis, this issue is perfectly circumvented.

Some of the in situ crystalline metal–organics yielded from ALD/MLD synthesis resemble the well-known MOF materials. The research on MOF materials in general has been blooming for the last two decades, motivated by their huge technological potential in applications ranging from gas capture, storage, and separation to sensing, catalysis, optics, and electronics. The MOF material family realized in bulk form is enormous, and already well tailored for their composition, crystal structure, porosity, and surface/interface features. However, the true application breakthroughs of the MOF materials – in particular in sensors, membranes, nonlinear optics, and electronics – critically require that these materials can be produced as high-quality thin films and coatings, which can be integrated with the other components in the actual device configurations. The ALD/MLD approach is highly promising, as it could allow the deposition of these materials as conformal coatings on large-area and high-aspect-ratio substrates. There are also exciting extensions of the MOF material family that are highly relevant for ALD/MLD, that is, so-called intercalated-type iMOFs and amorphous MOFs (aMOFs). The iMOFs are layer-structured redox-active metal–organic materials showing only minimal changes in crystal structure upon metal-ion (de)intercalation; they could thus provide us novel solutions to overcome one of the notorious drawbacks of conventional metal oxide electrode materials in Li-ion battery technology, i.e., the capacity decay on cycling, due to the substantial volume changes during the Li-ion intercalation. For the aMOFs, on the other hand, novel phenomena could be expected around the amorphous–crystalline transition.

Since mixing of several different ALD and MLD cycles with arbitrary frequencies is rather straightforward, it is relatively easy to fabricate elaborated heterostructures and superlattices not necessarily attainable with conventional synthesis techniques. This allows the fusion of different inorganic and organic building blocks with even contradicting properties, to realize unforeseen material functions which could – ultimately – lead us even to entirely new application areas. The literature already reports highly promising results for various metal-oxide:organic superlattice structures; these successful proof-of-the-concept results include the bandgap engineering

of photocatalytic TiO₂ films, thermal conductivity suppression and simultaneous electrical conductivity enhancement of thermoelectric ZnO films, and mechanical property enhancement of magnetic ϵ -Fe₂O₃ films achieved by introducing just few monomolecular organic layers within the inorganic metal oxide matrix.

Currently, the ALD/MLD technique is a well-established branch of the ALD technology, having, for example, dedicated sessions in essentially all international ALD conferences as well as in many other major conferences related to materials. In the history of the parent ALD technology, fundamental research conducted by the academic community has rapidly attracted the interest of industry as well. From this background, technological breakthroughs should be possible for the ALD-/MLD-fabricated inorganic–organic thin films as well. The ALD/MLD films are biocompatible, lightweight, and bendable, and could thus pave the way toward novel solutions in, e.g., wearable applications. Moreover, taking an analogy to their ALD counterparts, it is anticipated that the ALD/MLD films are compatible with the current microelectronics technologies. Definitely, considerable amount of research and development work is required to prove this in practice. There are a number of drawbacks – partly common with the parent ALD technology – such as the slowness of the industrial manufacturing and the necessity for vacuum chamber and accordingly the higher cost. These drawbacks naturally need to be properly considered and addressed to be able show that the benefits of adopting a novel ALD/MLD process could outweigh the drawbacks. This should be easiest in applications where ultrathin, high-quality, and conformal metal–organic coatings are needed, or in cases where there is no alternative technique to fabricate the desired superior functional material.

To summarize, the fundamental excitement on ALD/MLD arises from the fact that it can be used as a unique designer's tool to link different metal nodes or nanoscale inorganic layers with organic moieties into novel metal–organics and inorganic:organic multilayer structures with unforeseen property palette. Through smart design, the thus realized novel materials should lead us to intriguing material functions as well, significantly beyond those challenged before. The huge outstanding technical advantage is that the ALD/MLD synthesis has the capacity to yield these adventurous functional materials as high-quality conformal coatings on demanding surface chemistries and architectures, thus opening up new avenues in the application space as well.

Supporting Information

Supporting Information is available from the Wiley Online Library or from the author.

Acknowledgements

This work has received funding from the European Research Council under the European Union's Seventh Framework Programme (FP/2007-2013)/ERC Advanced Grant Agreement (No. 339478) and also from the Academy of Finland (Prof3, PREIN).

Conflict of Interest

The authors declare no conflict of interest.

Keywords

atomic layer deposition/molecular layer deposition (ALD/MLD), crystalline metal–organic thin films, metal–organic materials

Received: January 26, 2022

Revised: March 9, 2022

Published online: April 20, 2022

- [1] S. Kitagawa, M. Kondo, *Bull. Chem. Soc. Jpn.* **1998**, *71*, 1739.
- [2] O. M. Yaghi, H. Li, *J. Am. Chem. Soc.* **1995**, *117*, 10401.
- [3] S. R. Batten, N. R. Champness, X. M. Chen, J. Garcia-Martinez, S. Kitagawa, L. Öhrström, M. O’Keeffe, M. P. Suh, J. Reedijk, *Pure Appl. Chem.* **2013**, *85*, 1715.
- [4] J. L. C. Rowsell, O. M. Yaghi, *Microporous Mesoporous Mater.* **2004**, *73*, 3.
- [5] M. D. Allendorf, A. Schwartzberg, V. Stavila, A. A. Talin, *Chem. - Eur. J.* **2011**, *17*, 11372.
- [6] L. E. Kreno, K. Leong, O. K. Farha, M. Allendorf, R. P. Van Duyne, J. T. Hupp, *Chem. Rev.* **2012**, *112*, 1105.
- [7] Y. Chen, S. Ma, *Rev. Inorg. Chem.* **2012**, *32*, 81.
- [8] I. Stassen, N. Burtch, A. Talin, P. Falcaro, M. Allendorf, R. Ameloot, *Chem. Soc. Rev.* **2017**, *46*, 3185.
- [9] D. Zacher, O. Shekhah, C. Wöll, R. A. Fischer, *Chem. Soc. Rev.* **2009**, *38*, 1418.
- [10] O. Shekhah, J. Liu, R. A. Fischer, C. Wöll, *Chem. Soc. Rev.* **2011**, *40*, 1081.
- [11] C. Crivello, S. Sevim, O. Graniel, C. Franco, S. Pané, J. Puigmartí-Luis, D. Muñoz-Rojas, *Mater. Horiz.* **2021**, *8*, 168.
- [12] S. M. George, *Chem. Rev.* **2010**, *110*, 111.
- [13] T. Suntola, J. Antson, *US005485919A*, **1977**.
- [14] “2018 Millennium Technology Prize for Tuomo Suntola for enabling smart technology,” <https://millenniumprize.org/stories/2018-millennium-technology-prize-for-tuomo-suntola-finnish-physicists-innovation-enables-manufacture-and-development-of-information-technology-products/> (accessed: December 2021).
- [15] T. Yoshimura, S. Tatsuura, W. Sotoyama, *Appl. Phys. Lett.* **1991**, *59*, 482.
- [16] M. Bohr, R. Chau, T. Ghani, K. Mistry, *IEEE Spectrum* **2007**, *44*, 29.
- [17] S. Yoshida, T. Ono, M. Esashi, *Micro Nano Lett.* **2010**, *5*, 321.
- [18] M. Putkonen, J. Harjuoja, T. Sajavaara, L. Niinistö, *J. Mater. Chem.* **2007**, *17*, 664.
- [19] L. Yan, M. Zhang, S. Zhao, T. Sun, B. Zhang, M. Cao, Y. Qin, *Chem. Eng. J.* **2020**, *382*, 122860.
- [20] S. Xiong, T. Sheng, L. Kong, Z. Zhong, J. Huang, Y. Wang, *Chin. J. Chem. Eng.* **2016**, *24*, 843.
- [21] P. Yang, G. Wang, Z. Gao, H. Chen, Y. Wang, Y. Qin, *Materials* **2013**, *6*, 5602.
- [22] T. Bitzer, N. Richardson, *Appl. Surf. Sci.* **1999**, *144–145*, 339.
- [23] Y. Du, S. M. George, *J. Phys. Chem. C* **2007**, *111*, 8509.
- [24] N. M. Adamczyk, A. A. Dameron, S. M. George, *Langmuir* **2008**, *24*, 2081.
- [25] Q. Peng, K. Efimenko, J. Genzer, G. N. Parsons, *Langmuir* **2012**, *28*, 10464.
- [26] B. C. Welch, O. M. McIntee, A. B. Ode, B. B. McKenzie, A. R. Greenberg, V. M. Bright, S. M. George, *J. Vac. Sci. Technol., A* **2020**, *38*, 052409.
- [27] D. J. Higgs, J. W. DuMont, K. Sharma, S. M. George, *J. Vac. Sci. Technol., A* **2018**, *36*, 01A117.
- [28] A. Kubono, N. Yuasa, H.-L. Shao, S. Umemoto, N. Okui, *Thin Solid Films* **1996**, *289*, 107.
- [29] R. A. Nye, A. P. Kelliher, J. T. Gaskins, P. E. Hopkins, G. N. Parsons, *Chem. Mater.* **2020**, *32*, 1553.
- [30] A. Csenki, *Reliab. Eng. Syst. Saf.* **2007**, *92*, 685.
- [31] A. Nagai, H. Shao, S. Umemoto, T. Kikutani, N. Okui, *High Perform. Polym.* **2001**, *13*, S169.
- [32] S. Haq, N. V. Richardson, *J. Phys. Chem. B* **1999**, *103*, 5256.
- [33] H. Zhou, S. F. Bent, *J. Vac. Sci. Technol., A* **2013**, *31*, 040801.
- [34] J. Y. Lee, A. Kim, W.-S. Oh, B. Shong, *Int. J. Quantum Chem.* **2017**, *117*, e25341.
- [35] T. Yoshimura, *Macromol. Symp.* **2016**, *361*, 141.
- [36] D. C. Cameron, T. V. Ivanova, *ECS Trans.* **2013**, *58*, 263.
- [37] Y. Sun, Y. Zhao, J. Wang, J. Liang, C. Wang, Q. Sun, X. Lin, K. R. Adair, J. Luo, D. Wang, R. Li, M. Cai, T.-K. Sham, X. Sun, *Adv. Mater.* **2019**, *31*, 1806541.
- [38] H. Zhou, J. M. Blackwell, H.-B.-R. Lee, S. F. Bent, *ACS Appl. Mater. Interfaces* **2013**, *5*, 3691.
- [39] Y. Li, D. Wang, J. M. Buriak, *Langmuir* **2010**, *26*, 1232.
- [40] A. Lushington, J. Liu, M. N. Bannis, B. Xiao, S. Lawes, R. Li, X. Sun, *Appl. Surf. Sci.* **2015**, *357*, 1319.
- [41] K. Ashurbekova, K. Ashurbekova, I. Saric, E. Modin, M. Petravić, I. Abdulagatov, A. Abdulagatov, M. Knez, *Chem. Commun.* **2020**, *56*, 8778.
- [42] L. Ju, V. Vemuri, N. C. Strandwitz, *J. Vac. Sci. Technol., A* **2019**, *37*, 030909.
- [43] A. Markov, K. Greben, D. Mayer, A. Offenhäusser, R. Wördenweber, *ACS Appl. Mater. Interfaces* **2016**, *8*, 16451.
- [44] K. T. Wong, S. N. Chopra, S. F. Bent, *J. Phys. Chem. C* **2012**, *116*, 12670.
- [45] B. H. Lee, K. R. Min, S. Y. Choi, K. H. Lee, S. Im, M. M. Sung, *J. Am. Chem. Soc.* **2007**, *129*, 16034.
- [46] O. Nilsen, K. Klepper, H. Nielsen, H. Fjellvåg, *ECS Trans.* **2008**, *16*, 3.
- [47] S. M. George, B. Yoon, A. A. Dameron, *Acc. Chem. Res.* **2009**, *42*, 498.
- [48] Q. Peng, B. Gong, R. M. VanGundy, G. N. Parsons, *Chem. Mater.* **2009**, *21*, 820.
- [49] A. Sood, P. Sundberg, J. Malm, M. Karppinen, *Appl. Surf. Sci.* **2011**, *257*, 6435.
- [50] T. V. Ivanova, P. S. Maydannik, D. C. Cameron, *J. Vac. Sci. Technol., A* **2012**, *30*, 01A121.
- [51] H. Zhou, S. F. Bent, *ACS Appl. Mater. Interfaces* **2011**, *3*, 505.
- [52] P. W. Loscutt, H.-B.-R. Lee, S. F. Bent, *Chem. Mater.* **2010**, *22*, 5563.
- [53] P. Sundberg, M. Karppinen, *Beilstein J. Nanotechnol.* **2014**, *5*, 1104.
- [54] T. Tynell, I. Terasaki, H. Yamauchi, M. Karppinen, *J. Mater. Chem. A* **2013**, *1*, 13619.
- [55] G. Marin, R. Funahashi, M. Karppinen, *Adv. Eng. Mater.* **2020**, *22*, 2000535.
- [56] J. Kint, F. Mattelaer, S. S. T. Vandenbroucke, A. Muriqi, M. M. Minjauw, M. Nisula, P. M. Vereecken, M. Nolan, J. Dendooven, C. Detavernier, *Chem. Mater.* **2020**, *32*, 4451.
- [57] Z. Giedraityte, L.-S. Johansson, M. Karppinen, *RSC Adv.* **2016**, *6*, 103412.
- [58] Z. Giedraityte, J. Sainio, D. Hagen, M. Karppinen, *J. Phys. Chem. C* **2017**, *121*, 17538.
- [59] M. Nisula, M. Karppinen, *J. Mater. Chem. A* **2018**, *6*, 7027.
- [60] D. S. Bergsman, J. G. Baker, R. G. Closser, C. MacIsaac, M. Lillethorup, A. L. Strickler, L. Azarnouche, L. Godet, S. F. Bent, *Adv. Funct. Mater.* **2019**, *29*, 1904129.
- [61] E. Ahvenniemi, M. Karppinen, *Chem. Commun.* **2016**, *52*, 1139.
- [62] E. Ahvenniemi, M. Karppinen, *Chem. Mater.* **2016**, *28*, 6260.
- [63] M. Nisula, J. Linnera, A. J. Karttunen, M. Karppinen, *Chem. - Eur. J.* **2017**, *23*, 2988.
- [64] F. Krahl, A. Giri, J. A. Tomko, T. Tynell, P. E. Hopkins, M. Karppinen, *Adv. Mater. Interfaces* **2018**, *5*, 1701692.

- [65] Z. Chen, H. Wang, X. Wang, P. Chen, Y. Liu, H. Zhao, Y. Zhao, Y. Duan, *Sci. Rep.* **2017**, 7, 40061.
- [66] J. Huang, A. T. Lucero, L. Cheng, H. J. Hwang, M. W. Ha, J. Kim, *Appl. Phys. Lett.* **2015**, 106, 123101.
- [67] A. Khayyami, A. Philip, J. Multia, M. Karppinen, *Dalton Trans.* **2020**, 49, 11310.
- [68] C. Z. Leng, M. D. Losego, *Mater. Horiz.* **2017**, 4, 747.
- [69] C. Zhu, K. Han, D. Geng, H. Ye, X. Meng, *Electrochim. Acta* **2017**, 251, 710.
- [70] J.-P. Niemelä, G. Marin, M. Karppinen, *Semicond. Sci. Technol.* **2017**, 32, 093005.
- [71] E. O. Cobos Torres, P. R. Pagilla, *J. Dyn. Syst., Meas., Control* **2017**, 139, 051003.
- [72] F. Gao, A. V. Tepyakov, *Appl. Surf. Sci.* **2017**, 399, 375.
- [73] M. Wang, X. Wang, P. Moni, A. Liu, D. H. Kim, W. J. Jo, H. Sojoudi, K. O. Gleason, *Adv. Mater.* **2017**, 29, 1604606.
- [74] H. Van Bui, F. Grillo, J. R. van Ommen, G. Ozin, J. Aizenberg, I. O. Protod'yakonov, S. He, A. T. I. Yoong, Y. Yang, Y. Zhu, Y. Zeng, H. Wang, L. Gagliardi, J. T. Hupp, O. K. Farha, H. Terrones, M. Terrones, H. Kim, M. Kaiser, M. Tuominen, *Chem. Commun.* **2017**, 53, 45.
- [75] K. Gregorczyk, M. Knez, *Prog. Mater. Sci.* **2016**, 75, 1.
- [76] C. Ban, S. M. George, *Adv. Mater. Interfaces* **2016**, 3, 1600762.
- [77] X. Liang, A. W. Weimer, *Curr. Opin. Solid State Mater. Sci.* **2015**, 19, 115.
- [78] S.-B. Son, B. Kappes, C. Ban, *Isr. J. Chem.* **2015**, 55, 558.
- [79] B. J. O'Neill, D. H. K. Jackson, J. Lee, C. Canlas, P. C. Stair, C. L. Marshall, J. W. Elam, T. F. Kuech, J. A. Dumesic, G. W. Huber, *ACS Catal.* **2015**, 5, 1804.
- [80] R. Long, M. L. Dunn, *J. Appl. Phys.* **2014**, 115, 233514.
- [81] B. H. Lee, B. Yoon, A. I. Abdulagatov, R. A. Hall, S. M. George, *Adv. Funct. Mater.* **2013**, 23, 532.
- [82] D. M. King, X. Liang, A. W. Weimer, *Powder Technol.* **2012**, 221, 13.
- [83] M. Leskelä, M. Ritala, O. Nilsen, *MRS Bull.* **2011**, 36, 877.
- [84] S. M. George, B. H. Lee, B. Yoon, A. I. Abdulagatov, R. A. Hall, *J. Nanosci. Nanotechnol.* **2011**, 11, 7948.
- [85] G. N. Parsons, S. M. George, M. Knez, *MRS Bull.* **2011**, 36, 865.
- [86] J.-S. Park, H. Chae, H. K. Chung, S. I. Lee, *Semicond. Sci. Technol.* **2011**, 26, 034001.
- [87] B. H. Lee, V. R. Anderson, S. M. George, *ECS Trans.* **2011**, 41, 131.
- [88] D. M. King, X. Liang, A. W. Weimer, *ECS Trans.* **2009**, 25, 163.
- [89] H. Kim, H.-B.-R. Lee, W.-J. Maeng, *Thin Solid Films* **2009**, 517, 2563.
- [90] S. George, A. Dameron, Y. Du, N. M. Adamczyk, S. Davidson, *ECS Trans.* **2007**, 11, 81.
- [91] X. Meng, *J. Mater. Res.* **2021**, 36, 2.
- [92] Y. Zhao, L. Zhang, J. Liu, K. Adair, F. Zhao, Y. Sun, T. Wu, X. Bi, K. Amine, J. Lu, X. Sun, *Chem. Soc. Rev.* **2021**, 50, 3889.
- [93] J. Liu, J. Wang, *Front. Energy Res.* **2021**, 9, 244.
- [94] M. Madadi, J. Heiska, J. Multia, M. Karppinen, *ACS Appl. Mater. Interfaces* **2021**, 13, 56793.
- [95] Q. Sun, K. C. Lau, D. Geng, X. Meng, *Batteries Supercaps* **2018**, 1, 41.
- [96] S. M. George, B. Yoon, *Mater. Matters* **2008**, 5, 18326.
- [97] J.-P. Niemelä, A. J. Karttunen, M. Karppinen, *J. Mater. Chem. C* **2015**, 3, 10349.
- [98] A. W. Weimer, *J. Nanopart. Res.* **2019**, 21, 9.
- [99] A. Perrotta, O. Werzer, A. M. Coclite, *Adv. Eng. Mater.* **2018**, 20, 1700639.
- [100] J. Cai, Q. Sun, X. Meng, *AIMS Mater. Sci.* **2018**, 5, 957.
- [101] Y. Zhao, X. Sun, *ACS Energy Lett.* **2018**, 3, 899.
- [102] X. Meng, *J. Mater. Chem. A* **2017**, 5, 18326.
- [103] J. Liu, X. Sun, *Nanotechnology* **2015**, 26, 024001.
- [104] J. Multia, A. Khayyami, J. Heiska, M. Karppinen, *J. Vac. Sci. Technol., A* **2020**, 38, 052406.
- [105] P. Sundberg, M. Karppinen, *Eur. J. Inorg. Chem.* **2014**, 2014, 968.
- [106] K. B. Lausund, M. S. Olsen, P.-A. Hansen, H. Valen, O. Nilsen, *J. Mater. Chem. A* **2020**, 8, 2539.
- [107] B. Yoon, Y. Lee, A. Derk, C. Musgrave, S. George, *ECS Trans.* **2019**, 33, 191.
- [108] W. Zhou, J. Leem, I. Park, Y. Li, Z. Jin, Y.-S. Min, *J. Mater. Chem.* **2012**, 22, 23935.
- [109] B. Yoon, D. Seghete, A. S. Cavanagh, S. M. George, *Chem. Mater.* **2009**, 21, 5365.
- [110] T. Suntola, *Mater. Sci. Rep.* **1989**, 4, 261.
- [111] A. A. Dameron, D. Seghete, B. B. Burton, S. D. Davidson, A. S. Cavanagh, J. A. Bertrand, S. M. George, *Chem. Mater.* **2008**, 20, 3315.
- [112] K. Van de Kerckhove, F. Mattelaer, D. Deduytsche, P. M. Vereecken, J. Dendooven, C. Detavernier, W. L. Vasconcelos, C. Detavernier, B.-Z. Li, X.-P. Qu, *Dalton Trans.* **2016**, 45, 1176.
- [113] K. Van de Kerckhove, F. Mattelaer, J. Dendooven, C. Detavernier, *Dalton Trans.* **2017**, 46, 4542.
- [114] K. B. Klepper, O. Nilsen, H. Fjellvåg, *Dalton Trans.* **2010**, 39, 11628.
- [115] H. Lee, U. Choi, H. Kim, J. S. Lee, *Bull. Korean Chem. Soc.* **2020**, 41, 54.
- [116] M. D. Groner, F. H. Fabreguette, J. W. Elam, S. M. George, *Chem. Mater.* **2004**, 16, 639.
- [117] L. D. Salmi, M. J. Heikkilä, E. Puukilainen, T. Sajavaara, D. Grosso, M. Ritala, *Microporous Mesoporous Mater.* **2013**, 182, 147.
- [118] J. Penttinen, M. Nisula, M. Karppinen, *Chem. - Eur. J.* **2019**, 25, 11466.
- [119] M. Nisula, A. J. Karttunen, E. Solano, G. C. Tewari, M. Karppinen, M. Minjauw, H. S. Jena, P. Van Der Voort, D. Poelman, C. Detavernier, *ACS Appl. Mater. Interfaces* **2021**, 13, 10249.
- [120] A. Philip, S. Vasala, P. Glatzel, M. Karppinen, *Dalton Trans.* **2021**, 50, 16133.
- [121] J. Heiska, O. Sorsa, T. Kallio, M. Karppinen, *Chem. - Eur. J.* **2021**, 27, 8799.
- [122] M. Rogowska, P.-A. Hansen, H. H. Sønsteby, J. Dziadkowiec, H. Valen, O. Nilsen, *Dalton Trans.* **2021**, 50, 12896.
- [123] A. Philip, J.-P. Niemelä, G. C. Tewari, B. Putz, T. E. J. Edwards, M. Itoh, I. Utke, M. Karppinen, *ACS Appl. Mater. Interfaces* **2020**, 12, 21912.
- [124] J. P. Niemelä, A. Philip, N. Rohbeck, M. Karppinen, J. Michler, I. Utke, *ACS Appl. Nano Mater.* **2021**, 4, 1692.
- [125] Y.-S. Park, H. Kim, B. Cho, C. Lee, S.-E. Choi, M. M. Sung, J. S. Lee, *ACS Appl. Mater. Interfaces* **2016**, 8, 17489.
- [126] R. A. Hall, S. M. George, Y. Kim, W. Hwang, M. E. Samberg, N. A. Monteiro-Riviere, R. J. Narayan, *JOM* **2014**, 66, 649.
- [127] O. Nilsen, V. Miikkulainen, K. B. Gandrud, E. Østreng, A. Ruud, H. Fjellvåg, *Phys. Status Solidi* **2014**, 211, 357.
- [128] M. Nisula, M. Karppinen, *Nano Lett.* **2016**, 16, 1276.
- [129] J. Penttinen, M. Nisula, M. Karppinen, *Chem. - Eur. J.* **2017**, 23, 18225.
- [130] J. P. Guthrie, *Can. J. Chem.* **1978**, 56, 2342.
- [131] G. P. Panasyuk, L. A. Azarova, G. P. Budova, A. P. Savost'yanov, *Inorg. Mater.* **2007**, 43, 951.
- [132] A. Mietrach, T. W. T. Muesmann, J. Christoffers, M. S. Wickleder, *Eur. J. Inorg. Chem.* **2009**, 2009, 5328.
- [133] R. Ghiyasi, G. C. Tewari, M. Karppinen, *J. Phys. Chem. C* **2020**, 124, 13765.
- [134] A. Khayyami, M. Karppinen, *Chem. Mater.* **2018**, 30, 5904.
- [135] A. Philip, R. Ghiyasi, M. Karppinen, *ChemNanoMat* **2021**, 7, 253.
- [136] L. Momtazi, H. H. Sønsteby, O. Nilsen, *Beilstein J. Nanotechnol.* **2019**, 10, 399.
- [137] L. Qin, N. Yan, H. Hao, T. An, F. Zhao, H. Feng, *Appl. Surf. Sci.* **2018**, 436, 548.
- [138] X. Tong, P. Yang, Y. Wang, Y. Qin, X. Guo, *Nanoscale* **2014**, 6, 6692.
- [139] Y. Takahashi, M. Iijima, K. Inagawa, A. Itoh, *J. Vac. Sci. Technol., A* **1987**, 5, 2253.
- [140] L. Yan, L. Li, X. Ru, D. Wen, L. Ding, X. Zhang, H. Diao, Y. Qin, *Carbon* **2021**, 173, 145.

- [141] T. Miyamae, K. Tsukagoshi, O. Matsuoka, S. Yamamoto, H. Nozoye, *Jpn. J. Appl. Phys.* **2002**, *41*, 746.
- [142] S. Yoshida, T. Ono, M. Esashi, *Nanotechnology* **2011**, *22*, 335302.
- [143] Y. Chen, Z. Gao, B. Zhang, S. Zhao, Y. Qin, *J. Power Sources* **2016**, *315*, 254.
- [144] R. R. Amashaev, I. M. Abdulagatov, M. K. Rabadanov, A. I. Abdulagatov, *Russ. J. Phys. Chem. A* **2021**, *95*, 1439.
- [145] T. J. Myers, S. M. George, *J. Vac. Sci. Technol., A* **2021**, *39*, 052405.
- [146] B. C. Welch, O. M. McIntee, T. J. Myers, A. R. Greenberg, V. M. Bright, S. M. George, *Desalination* **2021**, *520*, 115334.
- [147] H.-I. Shao, S. Umemoto, T. Kikutani, N. Okui, *Polymer* **1997**, *38*, 459.
- [148] J. M. Wallas, B. C. Welch, Y. Wang, J. Liu, S. E. Hafner, R. Qiao, T. Yoon, Y.-T. Cheng, S. M. George, C. Ban, *ACS Appl. Energy Mater.* **2019**, *2*, 4135.
- [149] M. Junige, S. M. George, *J. Vac. Sci. Technol., A* **2021**, *39*, 023204.
- [150] F. S. M. Hashemi, C. Prasittichai, S. F. Bent, *J. Phys. Chem. C* **2014**, *118*, 10957.
- [151] C. Prasittichai, K. L. Pickrahn, F. S. Minaye Hashemi, D. S. Bergsman, S. F. Bent, *ACS Appl. Mater. Interfaces* **2014**, *6*, 17831.
- [152] Y. Chen, B. Zhang, Z. Gao, C. Chen, S. Zhao, Y. Qin, *Carbon* **2015**, *82*, 470.
- [153] H.-J. Kim, U.-J. Choi, H. Kim, K. Lee, K.-B. Park, H.-M. Kim, D.-K. Kwak, S.-W. Chi, J. S. Lee, K.-B. Kim, *Nanoscale* **2019**, *11*, 444.
- [154] U.-J. Choi, H. Kim, Y.-S. Park, J. S. Lee, *Bull. Korean Chem. Soc.* **2018**, *39*, 119.
- [155] D. S. Bergsman, R. G. Closser, S. F. Bent, *Chem. Mater.* **2018**, *30*, 5087.
- [156] R. G. Closser, D. S. Bergsman, L. Ruelas, F. S. M. Hashemi, S. F. Bent, *J. Vac. Sci. Technol., A* **2017**, *35*, 031509.
- [157] D. Bergsman, H. Zhou, S. F. Bent, *ECS Trans.* **2014**, *64*, 87.
- [158] S. M. Matveev, D. D. Dlott, P. Hanusova, J. P. Maria, R. Nye, G. Parsons, *AIP Conf. Proc.* **2020**, *2272*, 050017.
- [159] R. A. Nye, S. Wang, S. Uhlenbrock, J. A. Smythe, G. N. Parsons, *Dalton Trans.* **2022**, *57*, 1838.
- [160] P. W. Loscutoff, H. Zhou, S. B. Clendenning, S. F. Bent, *ACS Nano* **2010**, *4*, 331.
- [161] A. Kim, M. A. Filler, S. Kim, S. F. Bent, *J. Am. Chem. Soc.* **2005**, *127*, 6123.
- [162] H. Zhou, M. F. Toney, S. F. Bent, *Macromolecules* **2013**, *46*, 5638.
- [163] Y.-S. Park, S.-E. Choi, H. Kim, J. S. Lee, *ACS Appl. Mater. Interfaces* **2016**, *8*, 11788.
- [164] C. Prasittichai, H. Zhou, S. F. Bent, *ACS Appl. Mater. Interfaces* **2013**, *5*, 13391.
- [165] J. S. Lee, Y. J. Lee, E. L. Tae, Y. S. Park, K. B. Yoon, *Science* **2003**, *301*, 818.
- [166] F. Fug, A. Petry, H. Jost, A. Ahmed, M. Zamanzade, W. Possart, *Appl. Surf. Sci.* **2017**, *426*, 133.
- [167] T. Yoshimura, S. Ito, T. Nakayama, K. Matsumoto, *Appl. Phys. Lett.* **2007**, *91*, 033103.
- [168] T. Yoshimura, S. Tatsuura, W. Sotoyama, A. Matsuura, T. Hayano, *Appl. Phys. Lett.* **1992**, *60*, 268.
- [169] T. Yoshimura, A. Oshima, D.-I. Kim, Y. Morita, *ECS Trans.* **2009**, *25*, 15.
- [170] T. Yoshimura, R. Ebihara, A. Oshima, *J. Vac. Sci. Technol., A* **2011**, *29*, 051510.
- [171] T. Yoshimura, S. Ishii, *J. Vac. Sci. Technol., A* **2013**, *31*, 031501.
- [172] T. Yoshimura, Y. Kudo, *Appl. Phys. Express* **2009**, *2*, 015502.
- [173] S. E. Atanasov, M. D. Losego, B. Gong, E. Sacht, J.-P. Maria, P. S. Williams, G. N. Parsons, *Chem. Mater.* **2014**, *26*, 3471.
- [174] D. H. Kim, S. E. Atanasov, P. Lemaire, K. Lee, G. N. Parsons, *ACS Appl. Mater. Interfaces* **2015**, *7*, 3866.
- [175] S. Ghafourisaleh, G. Popov, M. Leskelä, M. Putkonen, M. Ritala, *ACS Omega* **2021**, *6*, 17545.
- [176] A. A. Volk, J.-S. Kim, J. Jamir, E. C. Dickey, G. N. Parsons, *J. Vac. Sci. Technol., A* **2021**, *39*, 032413.
- [177] J. S. Kim, G. N. Parsons, *Chem. Mater.* **2021**, *33*, 9221.
- [178] J. Gil-Font, M.-A. Hatte, M. R. Bailey, N. Navarrete, J. Ventura-Espinosa, A. Goulas, D. La Zara, J. R. van Ommen, R. Mondragón, L. Hernández, *Appl. Therm. Eng.* **2020**, *178*, 115559.
- [179] D. La Zara, F. Zhang, F. Sun, M. R. Bailey, M. J. Quayle, G. Petersson, S. Folestad, J. R. van Ommen, *Appl. Mater. Today* **2021**, *22*, 100945.
- [180] D. La Zara, M. R. Bailey, P.-L. Hagedoorn, D. Benz, M. J. Quayle, S. Folestad, J. R. van Ommen, *ACS Appl. Nano Mater.* **2020**, *3*, 6737.
- [181] R. G. Closser, M. Lillethorup, D. S. Bergsman, S. F. Bent, *ACS Appl. Mater. Interfaces* **2019**, *11*, 21988.
- [182] X. Yuan, N. Wolf, D. Mayer, A. Offenhäusser, R. Wördenweber, *Langmuir* **2019**, *35*, 8183.
- [183] R. G. Closser, D. S. Bergsman, S. F. Bent, *ACS Appl. Mater. Interfaces* **2018**, *10*, 24266.
- [184] S. Chae, J. Soon, H. Jeong, T. j. Lee, J. H. Ryu, S. M. Oh, *J. Power Sources* **2018**, *392*, 159.
- [185] M. Lillethorup, D. S. Bergsman, T. E. Sandoval, S. F. Bent, *Chem. Mater.* **2017**, *29*, 9897.
- [186] S. Chae, J. B. Lee, J. G. Lee, T. j. Lee, J. Soon, J. H. Ryu, J. S. Lee, S. M. Oh, *J. Power Sources* **2017**, *370*, 131.
- [187] J. Fichtner, Y. Wu, J. Hitzenberger, T. Drewello, J. Bachmann, *ECS J. Solid State Sci. Technol.* **2017**, *6*, N171.
- [188] L. Yan, X. Wang, S. Zhao, Y. Li, Z. Gao, B. Zhang, M. Cao, Y. Qin, *ACS Appl. Mater. Interfaces* **2017**, *9*, 11116.
- [189] D. S. Bergsman, R. G. Closser, C. J. Tassone, B. M. Clemens, D. Nordlund, S. F. Bent, *Chem. Mater.* **2017**, *29*, 1192.
- [190] A. Markov, N. Wolf, X. Yuan, D. Mayer, V. Maybeck, A. Offenhäusser, R. Wördenweber, *ACS Appl. Mater. Interfaces* **2017**, *9*, 29265.
- [191] Y. Liang, J. Huang, P. Zang, J. Kim, W. Hu, *Appl. Surf. Sci.* **2014**, *322*, 202.
- [192] H. Zhou, S. F. Bent, *J. Phys. Chem. C* **2013**, *117*, 19967.
- [193] T. Bitzer, N. V. Richardson, *Appl. Phys. Lett.* **1998**, *71*, 662.
- [194] N. R. Wolf, X. Yuan, H. Hassani, F. Milos, D. Mayer, U. Breuer, A. Offenhäusser, R. Wördenweber, *ACS Appl. Bio Mater.* **2020**, *3*, 7113.
- [195] Q. Dong, F. Zhou, J. Jiang, W. L. Xu, D. Behera, B. Sengupta, M. Yu, *ACS Appl. Mater. Interfaces* **2020**, *12*, 26360.
- [196] I. Šarić, M. Kolypadi Markovic, R. Peter, P. Linić, K. Wittine, I. Kavre Piltaver, I. Jelovica Badovinac, D. Marković, M. Knez, G. Ambrožič, *Appl. Surf. Sci.* **2021**, *539*, 148254.
- [197] J. Shi, S. F. Bent, *ACS Nano* **2021**, *15*, 3004.
- [198] A. Lai, H. C. Loehde-Woolard, W. W. McNeary, J. Burger, R. Pfeiffer, A. W. Weimer, *Chem. Eng. Sci.* **2021**, *245*, 116954.
- [199] H. Tan, Y. Chu, X. Wu, W. J. Liu, D. W. Zhang, S. J. Ding, *Chem. Mater.* **2021**, *33*, 7785.
- [200] S. A. Vasudevan, Y. Xu, S. Karwal, H. G. M. E. van Ostaay, G. M. H. Meesters, M. Talebi, E. J. R. Sudhölter, J. Ruud van Ommen, *Chem. Commun.* **2015**, *51*, 12540.
- [201] E. Ahvenniemi, M. Karppinen, *Dalton Trans.* **2016**, *45*, 10730.
- [202] A. Tanskanen, M. Karppinen, *Phys. Status Solidi RRL* **2018**, *12*, 1800390.
- [203] A. Tanskanen, M. Karppinen, *Sci. Rep.* **2018**, *8*, 8976.
- [204] K. B. Lausund, O. Nilsen, *Nat. Commun.* **2016**, *7*, 13578.
- [205] H. Lan, L. D. Salmi, T. Rönkkö, J. Parshintsev, M. Jussila, K. Hartonen, M. Kemell, M.-L. Riekkola, *Anal. Chim. Acta* **2018**, *1024*, 93.
- [206] D. J. Hagen, L. Mai, A. Devi, J. Sainio, M. Karppinen, *Dalton Trans.* **2018**, *47*, 15791.
- [207] J. E. Bratvold, G. Carraro, D. Barreca, O. Nilsen, *Appl. Surf. Sci.* **2015**, *347*, 861.
- [208] L. Mai, Z. Giedraityte, M. Schmidt, D. Rogalla, S. Scholz, A. D. Wieck, A. Devi, M. Karppinen, *J. Mater. Sci.* **2017**, *52*, 6216.

- [209] L. D. Salmi, E. Puukilainen, M. Vehkamäki, M. Heikkilä, M. Ritala, *Chem. Vap. Deposition* **2009**, *15*, 221.
- [210] L. Momtazi, H. H. Sønsteby, D. A. Dartt, J. R. Eidet, O. Nilsen, *RSC Adv.* **2017**, *7*, 20900.
- [211] O. Nilsen, K. R. Haug, T. Finstad, *Chem. Vap. Deposition* **2013**, *19*, 174.
- [212] A. Raupke, F. Albrecht, J. Maibach, A. Behrendt, A. Polywka, R. Heiderhoff, J. Helzel, T. Rabe, H.-H. Johannes, W. Kowalsky, E. Mankel, T. Mayer, P. Gorrrn, T. Riedl, *ECS Trans.* **2014**, *64*, 97.
- [213] A. Rüpke, F. Albrecht, J. Maibach, A. Behrendt, A. Polywka, R. Heiderhoff, J. Helzel, T. Rabe, H.-H. Johannes, W. Kowalsky, E. Mankel, T. Mayer, P. Gorrrn, T. Riedl, *ACS Appl. Mater. Interfaces* **2014**, *6*, 1193.
- [214] Z. Giedraityte, M. Tuomisto, M. Lastusaari, M. Karppinen, *ACS Appl. Mater. Interfaces* **2018**, *10*, 8845.
- [215] V. M. Smirnov, E. G. Zemtsova, P. E. Morozov, *Rev. Adv. Mater. Sci.* **2009**, *21*, 205.
- [216] V. M. Smirnov, E. G. Zemtsova, A. A. Belikov, I. L. Zheldakov, P. E. Morozov, O. G. Polyachonok, V. B. Aleskovskii, *Dokl. Phys. Chem.* **2007**, *413*, 95.
- [217] L. Momtazi, D. A. Dartt, O. Nilsen, J. R. Eidet, *J. Biomed. Mater. Res., Part A* **2018**, *106*, 3090.
- [218] D. M. Piper, J. J. Travis, M. Young, S.-B. Son, S. C. Kim, K. H. Oh, S. M. George, C. Ban, S.-H. Lee, *Adv. Mater.* **2014**, *26*, 1596.
- [219] K. Van de Kerckhove, M. K. S. Barr, L. Santinacci, P. M. Vereecken, J. Dendooven, C. Detavernier, *Dalton Trans.* **2018**, *47*, 5860.
- [220] K. Van de Kerckhove, J. Dendooven, C. Detavernier, *J. Vac. Sci. Technol., A* **2018**, *36*, 051506.
- [221] K. B. Klepper, O. Nilsen, P.-A. Hansen, H. Fjellvåg, *Dalton Trans.* **2011**, *40*, 4636.
- [222] V. Pale, Z. Giedraityte, X. Chen, O. Lopez-Acevedo, I. Tittonen, M. Karppinen, *Sci. Rep.* **2017**, *7*, 6982.
- [223] Z. Giedraityte, O. Lopez-Acevedo, L. A. Espinosa Leal, V. Pale, J. Sainio, T. S. Tripathi, M. Karppinen, *J. Phys. Chem. C* **2016**, *120*, 26342.
- [224] K. B. Lausund, V. Petrovic, O. Nilsen, *Dalton Trans.* **2017**, *46*, 16983.
- [225] J. Heiska, M. Nisula, E.-L. Rautama, A. J. Karttunen, M. Karppinen, *Dalton Trans.* **2020**, *49*, 1591.
- [226] J. Huang, M. Lee, A. T. Lucero, L. Cheng, M.-W. Ha, J. Kim, *Jpn. J. Appl. Phys.* **2016**, *55*, 06GK04.
- [227] S.-W. Seo, E. Jung, C. Lim, H. Chae, S. M. Cho, *Thin Solid Films* **2012**, *520*, 6690.
- [228] K. S. Han, Y. Park, G. Han, B. H. Lee, K. H. Lee, D. H. Son, S. Im, M. M. Sung, *J. Mater. Chem.* **2012**, *22*, 19007.
- [229] L. D. Salmi, M. J. Heikkilä, M. Vehkamäki, E. Puukilainen, M. Ritala, T. Sajavaara, *J. Vac. Sci. Technol., A* **2015**, *33*, 01A121.
- [230] A. I. Abdulagatov, K. E. Terauds, J. J. Travis, A. S. Cavanagh, R. Raj, S. M. George, *J. Phys. Chem. C* **2013**, *117*, 17442.
- [231] D. C. Miller, R. R. Foster, Y. Zhang, S. H. Jen, J. A. Bertrand, Z. Lu, D. Seghete, J. L. O'Patches, R. Yang, Y. C. Lee, S. M. George, M. L. Dunn, *J. Appl. Phys.* **2009**, *105*, 093527.
- [232] P. Sundberg, A. Sood, X. Liu, L.-S. Johansson, M. Karppinen, *Dalton Trans.* **2012**, *41*, 10731.
- [233] T. Tynell, H. Yamauchi, M. Karppinen, *J. Vac. Sci. Technol., A* **2014**, *32*, 01A105.
- [234] K. B. Klepper, O. Nilsen, S. Francis, H. Fjellvåg, *Dalton Trans.* **2014**, *43*, 3492.
- [235] K.-H. Yoon, K.-S. Han, M.-M. Sung, *Nanoscale Res. Lett.* **2012**, *7*, 71.
- [236] C.-Y. Kao, B. Li, Y. Lu, J.-W. Yoo, A. J. Epstein, *J. Mater. Chem. C* **2014**, *2*, 6171.
- [237] C.-Y. Kao, J.-W. Yoo, Y. Min, A. J. Epstein, *ACS Appl. Mater. Interfaces* **2012**, *4*, 137.
- [238] P. Sundberg, A. Sood, X. Liu, M. Karppinen, *Dalton Trans.* **2013**, *42*, 15043.
- [239] A. Sood, P. Sundberg, M. Karppinen, *Dalton Trans.* **2013**, *42*, 3869.
- [240] K. B. Klepper, O. Nilsen, T. Levy, H. Fjellvåg, *Eur. J. Inorg. Chem.* **2011**, *2011*, 5305.
- [241] Y. Sun, C. Zhao, K. R. Adair, Y. Zhao, L. V. Goncharova, J. Liang, C. Wang, J. Li, R. Li, M. Cai, T.-K. Sham, X. Sun, *Energy Environ. Sci.* **2021**, *14*, 4085.
- [242] C. MacIsaac, J. R. Schneider, R. G. Closser, T. R. Hellstern, D. S. Bergsman, J. Park, Y. Liu, R. Sinclair, S. F. Bent, *Adv. Funct. Mater.* **2018**, *28*, 1800852.
- [243] J. Shi, L. Zeng, S. Nikzad, D. M. Koshy, A. S. Asundi, C. MacIsaac, S. F. Bent, *J. Vac. Sci. Technol., A* **2022**, *40*, 012402.
- [244] G. Luka, L. Wachnicki, B. S. Witkowski, R. Jakiela, I. S. Virt, *Mater. Des.* **2017**, *119*, 297.
- [245] T. Tynell, A. Giri, J. Gaskins, P. E. Hopkins, P. Mele, K. Miyazaki, M. Karppinen, *J. Mater. Chem. A* **2014**, *2*, 12150.
- [246] J. Liu, B. Yoon, E. Kuhlmann, M. Tian, J. Zhu, S. M. George, Y.-C. Lee, R. Yang, *Nano Lett.* **2013**, *13*, 5594.
- [247] A. J. Karttunen, L. Sarnes, R. Townsend, J. Mikkonen, M. Karppinen, *Adv. Electron. Mater.* **2017**, *3*, 1600459.
- [248] J. P. Niemelä, M. Karppinen, *Dalton Trans.* **2015**, *44*, 591.
- [249] J. W. DuMont, S. M. George, *J. Phys. Chem. C* **2015**, *119*, 14603.
- [250] B. Yoon, B. H. Lee, S. M. George, *ECS Trans.* **2011**, *41*, 271.
- [251] A. Tanskanen, M. Karppinen, *Dalton Trans.* **2015**, *44*, 19194.
- [252] S. Lee, G. H. Baek, J. H. Lee, D. W. Choi, B. Shong, J. S. Park, *Appl. Surf. Sci.* **2018**, *458*, 864.
- [253] L. D. Salmi, M. Mattinen, T. Niemi, M. J. Heikkilä, K. Mizohata, S. Korhonen, S.-P. Hirvonen, J. Räisänen, M. Ritala, *Adv. Mater. Interfaces* **2017**, *4*, 1700512.
- [254] Y.-Q. Cao, L. Zhu, X. Li, Z.-Y. Cao, D. Wu, A.-D. Li, H. Spreitzer, M. Gratzel, *Dalton Trans.* **2015**, *44*, 14782.
- [255] P. C. Lemaire, C. J. Oldham, G. N. Parsons, *J. Vac. Sci. Technol., A* **2016**, *34*, 01A134.
- [256] N. Bahlawane, D. Arl, J. S. Thomann, N. Adjeroud, K. Menguelti, D. Lenoble, *Surf. Coat. Technol.* **2013**, *230*, 101.
- [257] L. Lee, J. Park, K. Seok Han, R. Saravana Kumar, M. Mo Sung, *Appl. Surf. Sci.* **2019**, *476*, 897.
- [258] D. Choudhury, G. Rajaraman, S. K. Sarkar, *J. Vac. Sci. Technol., A* **2018**, *36*, 01A108.
- [259] M. Tuomisto, Z. Giedraityte, L. Mai, A. Devi, V. Boiko, K. Grzeszkiewicz, D. Hreniak, M. Karppinen, M. Lastusaari, *J. Lumin.* **2019**, *213*, 310.
- [260] D. C. Miller, R. R. Foster, S. H. Jen, J. A. Bertrand, D. Seghete, B. Yoon, Y. C. Lee, S. M. George, M. L. Dunn, *Acta Mater.* **2009**, *57*, 5083.
- [261] S. Zhao, J. Yang, F. Duan, B. Zhang, Y. Liu, B. Zhang, C. Chen, Y. Qin, *J. Colloid Interface Sci.* **2021**, *598*, 45.
- [262] M.-H. Tseng, D.-Y. Su, G.-L. Chen, F.-Y. Tsai, *ACS Appl. Mater. Interfaces* **2021**, *13*, 27392.
- [263] A. Khayyami, A. Philip, M. Karppinen, *Angew. Chem., Int. Ed.* **2019**, *58*, 13400.
- [264] M. Vähä-Nissi, J. Sievänen, E. Salo, P. Heikkilä, E. Kenttä, L. S. Johansson, J. T. Koskinen, A. Harlin, *J. Solid State Chem.* **2014**, *214*, 7.
- [265] A. Philip, R. Ghiyasi, M. Karppinen, *Molecules* **2021**, *26*, 3214.
- [266] M. Safdar, A. Ghazy, M. Tuomisto, M. Lastusaari, M. Karppinen, *J. Mater. Sci.* **2021**, *56*, 12634.
- [267] D. Choi, M. Yoo, H. M. Lee, J. Park, H. Y. Kim, J.-S. Park, *ACS Appl. Mater. Interfaces* **2016**, *8*, 12263.
- [268] P.-A. Hansen, O. Nilsen, *Dalton Trans.* **2021**, *50*, 8307.
- [269] J.-P. Niemelä, N. Rohbeck, J. Michler, I. Utke, *Dalton Trans.* **2020**, *49*, 10832.
- [270] J. Heiska, M. Karppinen, *Dalton Trans.* **2022**, *51*, 4246.
- [271] H. Wang, K. E. Gregorczyk, S. B. Lee, G. W. Rubloff, C.-F. Lin, *J. Phys. Chem. C* **2020**, *124*, 6830.

- [272] R. Yemini, S. Blanga, H. Aviv, I. Perelshtein, E. Teblum, S. Dery, E. Gross, Y. Mastai, M. Noked, O. Lidor-Shalev, *Adv. Mater. Interfaces* **2022**, *9*, 2101725.
- [273] L. Keskiaväli, M. Putkonen, E. Puhakka, E. Kenttä, J. Kint, R. K. Ramachandran, C. Detavernier, P. Simell, *ACS Omega* **2018**, *3*, 7141.
- [274] L. Svärd, M. Putkonen, E. Kenttä, T. Sajavaara, F. Krahl, M. Karppinen, K. Van de Kerckhove, C. Detavernier, P. Simell, *Langmuir* **2017**, *33*, 9657.
- [275] B. Gong, Q. Peng, G. N. Parsons, *J. Phys. Chem. B* **2011**, *115*, 5930.
- [276] Y. Lee, B. Yoon, A. S. Cavanagh, S. M. George, *Langmuir* **2011**, *27*, 15155.
- [277] L. Ju, B. Bao, S. W. King, N. C. Strandwitz, *J. Vac. Sci. Technol., A* **2017**, *35*, 01B136.
- [278] M. Włodarski, M. Putkonen, M. Norek, *Coatings* **2020**, *10*, 459.
- [279] B. Gong, G. N. Parsons, *ECS J. Solid State Sci. Technol.* **2012**, *1*, P210.
- [280] K. Ashurbekova, K. Ashurbekova, I. Saric, M. Gobbi, E. Modin, A. Chuvilin, M. Petravic, I. Abdulagatov, M. Knez, *Chem. Mater.* **2021**, *33*, 1022.
- [281] K. Ashurbekova, K. Ashurbekova, I. Saric, E. Modin, M. Petravic, I. Abdulagatov, A. Abdulagatov, M. Knez, *Chem. Commun.* **2021**, *57*, 2160.
- [282] S. T. Oyakhire, H. Ablat, N. E. Richey, S. F. Bent, *J. Vac. Sci. Technol., A* **2022**, *40*, 023405.
- [283] T. D. Gould, A. Izar, A. W. Weimer, J. L. Falconer, J. W. Medlin, *ACS Catal.* **2014**, *4*, 2714.
- [284] K. Ashurbekova, K. Ashurbekova, B. Alonso-Lerma, I. Šarić, L. Barandiaran, E. Modin, M. Petravić, R. Perez-Jimenez, M. Knez, *ACS Appl. Nano Mater.* **2022**, *5*, 2762.
- [285] R. L. Puurunen, *J. Appl. Phys.* **2005**, *97*, 121301.
- [286] T. Tynell, M. Karppinen, *Semicond. Sci. Technol.* **2014**, *29*, 043001.
- [287] V. Jadhav, D. P. Hoogerheide, J. Korch, M. Wanunu, *Nano Lett.* **2019**, *19*, 921.
- [288] X. Li, M. Banis, A. Lushington, X. Yang, Q. Sun, Y. Zhao, C. Liu, Q. Li, B. Wang, W. Xiao, C. Wang, M. Li, J. Liang, R. Li, Y. Hu, L. Goncharova, H. Zhang, T. K. Sham, X. Sun, *Nat. Commun.* **2018**, *9*, 4509.
- [289] Y. Zhao, Q. Sun, X. Li, C. Wang, Y. Sun, K. R. Adair, R. Li, X. Sun, *Nano Energy* **2018**, *43*, 368.
- [290] X. Li, X. Xiong, T. Li, T. Gao, Y. Wu, *IEEE Electron Device Lett.* **2018**, *39*, 1952.
- [291] Y. Zhao, L. V. Goncharova, Q. Sun, X. Li, A. Lushington, B. Wang, R. Li, F. Dai, M. Cai, X. Sun, *Small Methods* **2018**, *2*, 1700417.
- [292] C. Wang, Y. Zhao, Q. Sun, X. Li, Y. Liu, J. Liang, X. Li, X. Lin, R. Li, K. R. Adair, L. Zhang, R. Yang, S. Lu, X. Sun, *Nano Energy* **2018**, *53*, 168.
- [293] A. I. Abdulagatov, K. N. Ashurbekova, K. N. Ashurbekova, R. R. Amashaev, M. K. Rabadanov, I. M. Abdulagatov, *Russ. J. Appl. Chem.* **2018**, *91*, 347.
- [294] A. Perrotta, P. Poodt, F. J. (Fieke) van den Bruele, W. M. M. (Erwin) Kessels, M. Creatore, *Dalton Trans.* **2018**, *47*, 7649.
- [295] L. Chen, Z. Huang, R. Shahbazian-Yassar, J. A. Libera, K. C. Klavetter, K. R. Zavadil, J. W. Elam, *ACS Appl. Mater. Interfaces* **2018**, *10*, 7043.
- [296] Y. Zhao, L. V. Goncharova, Q. Zhang, P. Kaghazchi, Q. Sun, A. Lushington, B. Wang, R. Li, X. Sun, *Nano Lett.* **2017**, *17*, 5653.
- [297] B. Hwang, N. Qaiser, C. Lee, P. Matteini, S. J. Yoo, H. Kim, *J. Alloys Compd.* **2020**, *846*, 156420.
- [298] Z. Shang, X. Liang, *Nano Lett.* **2017**, *17*, 104.
- [299] A. Jaggernauth, R. M. Silva, M. A. Neto, M. J. Hortigüela, G. Gonçalves, M. K. Singh, F. J. Oliveira, R. F. Silva, M. Vila, *J. Phys. Chem. C* **2016**, *120*, 24176.
- [300] X. Li, A. Lushington, Q. Sun, W. Xiao, J. Liu, B. Wang, Y. Ye, K. Nie, Y. Hu, Q. Xiao, R. Li, J. Guo, T.-K. Sham, X. Sun, *Nano Lett.* **2016**, *16*, 3545.
- [301] W. Xiao, D. Y. Hui, C. Zheng, D. Yu, Y. Y. Qiang, C. Ping, C. L. Xiang, Z. Yi, *Nanoscale Res. Lett.* **2015**, *10*, 130.
- [302] X. Li, A. Lushington, J. Liu, R. Li, X. Sun, *Chem. Commun.* **2014**, *50*, 9757.
- [303] S. Feng-Bo, D. Yu, Y. Yong-Qiang, C. Ping, D. Ya-Hui, W. Xiao, Y. Dan, X. Kai-wen, *Org. Electron.* **2014**, *15*, 2546.
- [304] A. J. Loebel, C. J. Oldham, C. K. Devine, B. Gong, S. E. Atanasov, G. N. Parsons, P. S. Fedkiw, *J. Electrochem. Soc.* **2013**, *160*, 1971.
- [305] Z. Shang, R. L. Patel, B. W. Evanko, X. Liang, *Chem. Commun.* **2013**, *49*, 10067.
- [306] S.-H. Jen, S. M. George, R. S. McLean, P. F. Garcia, *ACS Appl. Mater. Interfaces* **2013**, *5*, 1165.
- [307] L. Ghazaryan, E.-B. Kley, A. Tünnermann, A. Viorica Szeghalmi, *J. Vac. Sci. Technol., A* **2013**, *31*, 01A149.
- [308] H. He, J. Liu, *J. Mater. Chem. A* **2020**, *8*, 22100.
- [309] M. Park, S. Oh, H. Kim, D. Jung, D. Choi, J.-S. Park, *Thin Solid Films* **2013**, *546*, 153.
- [310] S.-H. Jen, B. H. Lee, S. M. George, R. S. McLean, P. F. Garcia, *Appl. Phys. Lett.* **2012**, *101*, 234103.
- [311] B. H. Lee, B. Yoon, V. R. Anderson, S. M. George, *J. Phys. Chem. C* **2012**, *116*, 3250.
- [312] M. Vähä-Nissi, P. Sundberg, E. Kauppi, T. Hirvikorpi, J. Sievänen, A. Sood, M. Karppinen, A. Harlin, *Thin Solid Films* **2012**, *520*, 6780.
- [313] Y. Qin, Y. Yang, R. Scholz, E. Pippel, X. Lu, M. Knez, *Nano Lett.* **2011**, *11*, 2503.
- [314] M. Yu, H. H. Funke, R. D. Noble, J. L. Falconer, *J. Am. Chem. Soc.* **2011**, *133*, 1748.
- [315] X. Liang, J. Li, M. Yu, C. N. McMurray, J. L. Falconer, A. W. Weimer, *ACS Catal.* **2011**, *1*, 1162.
- [316] X. Liang, A. W. Weimer, *J. Nanopart. Res.* **2010**, *12*, 135.
- [317] X. Liang, M. Yu, J. Li, Y.-B. Jiang, A. W. Weimer, *Chem. Commun.* **2009**, 7140.
- [318] X. Liang, D. M. King, P. Li, S. M. George, A. W. Weimer, *AIChE J.* **2009**, *55*, 1030.
- [319] S. Zhang, Y. Zhao, F. Zhao, L. Zhang, C. Wang, X. Li, J. Liang, W. Li, Q. Sun, C. Yu, J. Luo, K. Doyle-Davis, R. Li, T. Sham, X. Sun, *Adv. Funct. Mater.* **2020**, *30*, 2001118.
- [320] S. Chaudhury, E. Wormser, Y. Harari, E. Edri, O. Nir, *ACS Appl. Mater. Interfaces* **2020**, *12*, 53356.
- [321] E. M. Wormser, O. Nir, E. Edri, *RSC Adv.* **2021**, *11*, 2427.
- [322] P. Ingale, C. Guan, R. Kraehnert, R. Naumann d'Alnoncourt, A. Thomas, F. Rosowski, *Catal. Today* **2021**, *362*, 47.
- [323] H. Jain, P. Poodt, *Dalton Trans.* **2021**, *50*, 5807.
- [324] N. E. Richey, S. Borhan, S. F. Bent, *Dalton Trans.* **2021**, *50*, 4577.
- [325] O. Lidor-Shalev, N. Leifer, M. Ejenberg, H. Aviv, I. Perelshtein, G. Goobes, M. Noked, Rosy, *Batteries Supercaps* **2021**, *4*, 1739.
- [326] S. Sayegh, J.-H. Lee, D.-H. Yang, M. Weber, I. Iatsunskyi, E. Coy, A. Razzouk, S. S. Kim, M. Bechelany, *Sens. Actuators, B* **2021**, *344*, 130302.
- [327] P. Abi Younes, S. Sayegh, A. A. Nada, M. Weber, I. Iatsunskyi, E. Coy, N. Abboud, M. Bechelany, *Colloids Surf., A* **2021**, *628*, 127274.
- [328] K. Kaliyappan, T. Or, Y. Deng, Y. Hu, Z. Bai, Z. Chen, *Adv. Funct. Mater.* **2020**, *30*, 1910251.
- [329] M. J. Young, D. Choudhury, S. Letourneau, A. Mane, A. Yanguas-Gil, J. W. Elam, *Chem. Mater.* **2020**, *32*, 992.
- [330] H. Wang, Z. Wang, X. Xu, W. Zhao, D. Wu, M. Muhammad, Y. Liu, C. Chen, B. Liu, Y. Duan, *Adv. Opt. Mater.* **2020**, *8*, 1901320.
- [331] Y. Zhao, M. Amirmaleki, Q. Sun, C. Zhao, A. Codirenzi, L. V. Goncharova, C. Wang, K. Adair, X. Li, X. Yang, F. Zhao, R. Li, T. Filleter, M. Cai, X. Sun, *Matter* **2019**, *1*, 1215.

- [332] G. Chen, Y. Weng, F. Sun, X. Zhou, C. Wu, Q. Yan, T. Guo, Y. Zhang, *RSC Adv.* **2019**, *9*, 20884.
- [333] D. M. Piper, Y. Lee, S.-B. Son, T. Evans, F. Lin, D. Nordlund, X. Xiao, S. M. George, S.-H. Lee, C. Ban, *Nano Energy* **2016**, *22*, 202.
- [334] D. Choudhury, S. K. Sarkar, N. Mahuli, *J. Vac. Sci. Technol., A* **2015**, *33*, 061305.
- [335] S. Hollevoet, K. B. Gandrud, M. Y. Timmermans, B. Put, Y. El Ajjour, K. Van de Kerckhove, C. Detavernier, M. Mees, P. M. Vereecken, *Adv. Mater. Interfaces* **2019**, *6*, 1901407.
- [336] J. J. Brown, R. A. Hall, P. E. Kladitis, S. M. George, V. M. Bright, *ACS Nano* **2013**, *7*, 7812.
- [337] U.-J. Choi, H. Kim, Y.-S. Park, H. Lee, J. S. Lee, *Chem. Commun.* **2018**, *54*, 3286.
- [338] F. Yang, J. Brede, H. Ablat, M. Abadia, L. Zhang, C. Rogero, S. D. Elliott, M. Knez, *Adv. Mater. Interfaces* **2017**, *4*, 1700237.
- [339] A. Lushington, C. Langford, J. Liu, K. Nie, R. Li, X. Sun, J. Guo, X. Sun, *J. Phys. Chem. C* **2017**, *121*, 11757.
- [340] L. Zhang, Y. Zhao, M. N. Banis, K. Adair, Z. Song, L. Yang, M. Markiewicz, J. Li, S. Wang, R. Li, S. Ye, X. Sun, *Nano Energy* **2019**, *60*, 111.
- [341] S. Son, L. Cao, T. Yoon, A. Cresce, S. E. Hafner, J. Liu, M. Groner, K. Xu, C. Ban, *Adv. Sci.* **2019**, *6*, 1801007.
- [342] S.-B. Son, Y. Wang, J. Xu, X. Li, M. Groner, A. Stokes, Y. Yang, Y.-T. Cheng, C. Ban, *ACS Appl. Mater. Interfaces* **2017**, *9*, 40143.
- [343] Y. Ma, J. M. Martinez de la Hoz, I. Angarita, J. M. Berrio-Sanchez, L. Benitez, J. M. Seminario, S.-B. Son, S.-H. Lee, S. M. George, C. Ban, P. B. Balbuena, *ACS Appl. Mater. Interfaces* **2015**, *7*, 11948.
- [344] Y. He, D. M. Piper, M. Gu, J. J. Travis, S. M. George, S.-H. Lee, A. Genc, L. Pullan, J. Liu, S. X. Mao, J.-G. Zhang, C. Ban, C. Wang, *ACS Nano* **2014**, *8*, 11816.
- [345] B. Gong, J. C. Spagnola, G. N. Parsons, *J. Vac. Sci. Technol., A* **2012**, *30*, 01A156.
- [346] C. J. Oldham, B. Gong, J. C. Spagnola, J. S. Jur, K. J. Senecal, T. A. Godfrey, G. N. Parsons, *J. Electrochem. Soc.* **2011**, *158*, D549.
- [347] L. Cheng, J. Lee, H. Zhu, A. V. Ravichandran, Q. Wang, A. T. Lucero, M. J. Kim, R. M. Wallace, L. Colombo, J. Kim, *ACS Nano* **2017**, *11*, 10243.
- [348] K. H. Yoon, H. S. Kim, K. S. Han, S. H. Kim, Y.-E. K. Lee, N. K. Shrestha, S. Y. Song, M. M. Sung, *ACS Appl. Mater. Interfaces* **2017**, *9*, 5399.
- [349] J. Huang, M. Lee, A. Lucero, J. Kim, *Chem. Vap. Deposition* **2013**, *19*, 142.
- [350] B. H. Lee, K. H. Lee, S. Im, M. M. Sung, *J. Nanosci. Nanotechnol.* **2009**, *9*, 6962.
- [351] B. H. Lee, K. H. Lee, S. Im, M. M. Sung, *Org. Electron.* **2008**, *9*, 1146.
- [352] K. H. Lee, J.-M. Choi, S. Im, B. H. Lee, K. K. Im, M. M. Sung, S. Lee, *Appl. Phys. Lett.* **2007**, *91*, 123502.
- [353] D. M. Piper, S.-B. Son, J. J. Travis, Y. Lee, S. S. Han, S. C. Kim, K. H. Oh, S. M. George, S.-H. Lee, C. Ban, *J. Power Sources* **2015**, *275*, 605.
- [354] X. Liang, B. W. Evanko, A. Izar, D. M. King, Y. B. Jiang, A. W. Weimer, *Microporous Mesoporous Mater.* **2013**, *168*, 178.
- [355] D. Seghete, R. A. Hall, B. Yoon, S. M. George, *Langmuir* **2010**, *26*, 19045.
- [356] D. Seghete, B. D. Davidson, R. A. Hall, Y. J. Chang, V. M. Bright, S. M. George, *Sens. Actuators, A* **2009**, *155*, 8.
- [357] J.-B. Fang, C. Liu, Y.-Q. Cao, A.-D. Li, *J. Mater. Res.* **2020**, *35*, 738.
- [358] J.-Z. Kong, Y. Chen, Y.-Q. Cao, Q.-Z. Wang, A.-D. Li, H. Li, F. Zhou, *J. Alloys Compd.* **2019**, *799*, 89.
- [359] O. Lidor-Shalev, R. Yemini, N. Leifer, R. Nanda, A. Tibi, I. Perelshtein, E. S. Avraham, Y. Mastai, M. Noked, *ACS Nano* **2019**, *13*, 10397.
- [360] J. Park, J. Seth, S. Cho, M. M. Sung, *Appl. Surf. Sci.* **2020**, *502*, 144109.
- [361] S. H. Song, S.-T. Hwang, B.-H. Choi, *Thin Solid Films* **2020**, *706*, 138082.
- [362] J.-B. Fang, Q. Ren, C. Liu, J.-A. Chen, D. Wu, A.-D. Li, *Dalton Trans.* **2021**, *50*, 511.
- [363] J. S. D. Peñaranda, M. Nisula, S. S. T. Vandenbroucke, M. M. Minjauw, J. Li, A. Werbrouck, J. Keukelier, A. I. Pitillas Martínez, J. Dendooven, C. Detavernier, *Dalton Trans.* **2021**, *50*, 1224.
- [364] M. H. Aboonaser Shiraz, E. Rehl, H. Kazemian, J. Liu, *Nanomaterials* **2021**, *11*, 1976.
- [365] A. Muriqi, M. Karppinen, M. Nolan, *Dalton Trans.* **2021**, *50*, 17583.
- [366] A. J. Karttunen, T. Tynell, M. Karppinen, *Nano Energy* **2016**, *22*, 338.
- [367] J. Lei, W.-J. Ding, C. Liu, D. Wu, W.-M. Li, A.-D. Li, *APL Mater.* **2021**, *9*, 121110.
- [368] J.-H. Han, T.-Y. Kim, D.-Y. Kim, H. L. Yang, J.-S. Park, *Dalton Trans.* **2021**, *50*, 15841.
- [369] S. Lee, H. M. Kim, G. H. Baek, J. S. Park, *ACS Appl. Mater. Interfaces* **2021**, *13*, 60144.
- [370] F. Krahl, Y. Ge, M. Karppinen, *Semicond. Sci. Technol.* **2020**, *36*, 025012.
- [371] C. Liu, J.-B. Fang, Y.-Q. Cao, D. Wu, A.-D. Li, *Appl. Phys. Lett.* **2020**, *117*, 031601.
- [372] J. Huang, H. Zhang, A. Lucero, L. Cheng, S. KC, J. Wang, J. Hsu, K. Cho, J. Kim, *J. Mater. Chem. C* **2016**, *4*, 2382.
- [373] T. Tynell, M. Karppinen, *Thin Solid Films* **2014**, *551*, 23.
- [374] B. Yoon, B. H. Lee, S. M. George, *J. Phys. Chem. C* **2012**, *116*, 24784.
- [375] F. Krahl, A. Giri, M. S. Bin Hoque, L. Sederholm, P. E. Hopkins, M. Karppinen, *J. Phys. Chem. C* **2020**, *124*, 24731.
- [376] G. Marin, T. Tynell, M. Karppinen, *J. Vac. Sci. Technol., A* **2019**, *37*, 020906.
- [377] A. J. Karttunen, T. Tynell, M. Karppinen, *J. Phys. Chem. C* **2015**, *119*, 13105.
- [378] J. Fang, Y. Cao, S. Chang, F. Teng, D. Wu, A. Li, *Adv. Funct. Mater.* **2022**, *32*, 2109682.
- [379] Y. Park, K. S. Han, B. H. Lee, S. Cho, K. H. Lee, S. Im, M. M. Sung, *Org. Electron.* **2011**, *12*, 348.
- [380] B. Zhang, Y. Chen, J. Li, E. Pippel, H. Yang, Z. Gao, Y. Qin, *ACS Catal.* **2015**, *5*, 5567.
- [381] K. S. Han, M. M. Sung, *J. Nanosci. Nanotechnol.* **2014**, *14*, 6137.
- [382] X. Xu, H. Wang, J. Wang, M. Muhammad, Z. Wang, P. Chen, W. Zhao, B. Kang, J. Zhang, C. Li, Y. Duan, *ACS Appl. Energy Mater.* **2020**, *3*, 4208.
- [383] A. Perrotta, R. Berger, F. Muralter, A. M. Coclite, *Dalton Trans.* **2019**, *48*, 14178.
- [384] X. Liang, Y.-B. Jiang, A. W. Weimer, *J. Vac. Sci. Technol., A* **2012**, *30*, 01A108.
- [385] B. Yoon, J. L. O'Patchen, D. Seghete, A. S. Cavanagh, S. M. George, *Chem. Vap. Deposition* **2009**, *15*, 112.
- [386] S. Cho, G. Han, K. Kim, M. M. Sung, *Angew. Chem., Int. Ed.* **2011**, *50*, 2742.
- [387] R. Berger, M. Seiler, A. Perrotta, A. M. Coclite, *Materials* **2021**, *14*, 1418.
- [388] T. Mu, Y. Zhao, C. Zhao, N. G. Holmes, S. Lou, J. Li, W. Li, M. He, Y. Sun, C. Du, R. Li, J. Wang, G. Yin, X. Sun, *Adv. Funct. Mater.* **2021**, *31*, 2010526.
- [389] R. Ghiyasi, M. Milich, J. Tomko, P. E. Hopkins, M. Karppinen, *Appl. Phys. Lett.* **2021**, *118*, 211903.
- [390] A. Tanskanen, P. Sundberg, M. Nolan, M. Karppinen, *Thin Solid Films* **2021**, *736*, 138896.
- [391] S. Ishchuk, D. H. Taffa, O. Hazut, N. Kaynan, R. Yerushalmi, *ACS Nano* **2012**, *6*, 7263.
- [392] Q. Dong, J. Jiang, S. Li, M. Yu, *J. Membr. Sci.* **2021**, *622*, 119040.
- [393] S. Jayanthi, D. Sarkar, D. H. Taffa, R. Yerushalmi, *Top. Catal.* **2020**, *6*, 3853.
- [394] S. Wu, Z. Wang, S. Xiong, Y. Wang, *J. Membr. Sci.* **2019**, *578*, 149.

- [395] Q. Dong, Z. Song, F. Zhou, H. Li, M. Yu, *Microporous Mesoporous Mater.* **2019**, 281, 9.
- [396] Z. Song, Q. Dong, W. L. Xu, F. Zhou, X. Liang, M. Yu, *ACS Appl. Mater. Interfaces* **2018**, 10, 769.
- [397] Z. Song, M. Fathizadeh, Y. Huang, K. H. Chu, Y. Yoon, L. Wang, W. L. Xu, M. Yu, *J. Membr. Sci.* **2016**, 510, 72.
- [398] D. Sarkar, S. Ishchuk, D. H. Taffa, N. Kaynan, B. A. Berke, T. Bendikov, R. Yerushalmi, *J. Phys. Chem. C* **2016**, 120, 3853.
- [399] R. L. Patel, Y.-B. Jiang, X. Liang, *Ceram. Int.* **2015**, 41, 2240.
- [400] D. Sarkar, D. H. Taffa, S. Ishchuk, O. Hazut, H. Cohen, G. Toker, M. Asscher, R. Yerushalmi, *Chem. Commun.* **2014**, 50, 9176.
- [401] C. Liu, Y.-Q. Cao, D. Wu, A.-D. Li, *IEEE Electron Device Lett.* **2020**, 41, 155.
- [402] Y. Q. Cao, W. Zhang, L. Xu, C. Liu, L. Zhu, L. G. Wang, D. Wu, A. D. Li, G. Fang, *Langmuir* **2019**, 35, 3020.
- [403] J. W. Jung, K. S. Han, K. H. Yoon, L. Lee, Y. E. K. Lee, C. H. Lee, S. U. Lee, M. M. Sung, *Org. Electron.* **2018**, 52, 237.
- [404] C. Chen, P. Li, G. Wang, Y. Yu, F. Duan, C. Chen, W. Song, Y. Qin, M. Knez, *Angew. Chem., Int. Ed.* **2013**, 52, 9196.
- [405] A. I. Abdulagatov, R. A. Hall, J. L. Sutherland, B. H. Lee, A. S. Cavanagh, S. M. George, *Chem. Mater.* **2012**, 24, 2854.
- [406] J.-B. Fang, S. Chang, Q. Ren, T. Zi, D. Wu, A.-D. Li, *ACS Appl. Mater. Interfaces* **2021**, 13, 32520.
- [407] J.-P. Niemelä, A. Giri, P. E. Hopkins, M. Karppinen, *J. Mater. Chem. A* **2015**, 3, 11527.
- [408] Z. C. Huertas, D. Settapani, C. Flox, J. R. Morante, T. Kallio, J. J. Biendicho, *Sci. Rep.* **2022**, 12, 137.
- [409] S. H. Cha, A. Park, K. H. Lee, S. Im, B. H. Lee, M. M. Sung, *Org. Electron.* **2010**, 11, 159.
- [410] M. Putkonen, T. Aaltonen, M. Alnes, T. Sajavaara, O. Nilsen, H. Fjellvåg, *J. Mater. Chem.* **2009**, 19, 8767.
- [411] J. Multia, J. Heiska, A. Khayyami, M. Karppinen, *ACS Appl. Mater. Interfaces* **2020**, 12, 41557.
- [412] E. Kazyak, M. Shin, W. S. LePage, T. H. Cho, N. P. Dasgupta, *Chem. Commun.* **2020**, 56, 15537.
- [413] J. Heiska, M. Madadi, M. Karppinen, *Nanoscale Adv.* **2020**, 2, 2441.
- [414] A. Philip, Y. Zhou, G. C. Tewari, S. van Dijken, M. Karppinen, *J. Mater. Chem. C* **2022**, 10, 294.
- [415] C. Chen, F. Duan, S. Zhao, W. Wang, F. Yang, W. Nuansing, B. Zhang, Y. Qin, M. Knez, *Appl. Catal., B* **2019**, 248, 218.
- [416] A. Gorzkowska-Sobas, K. B. Lausund, M. C. Koning, V. Petrovic, S. M. Chavan, M. W. Smith, O. Nilsen, *Global Challenges* **2021**, 5, 2100001.
- [417] K. R. Adair, C. Zhao, M. N. Banis, Y. Zhao, R. Li, M. Cai, X. Sun, *Angew. Chem., Int. Ed.* **2019**, 58, 15797.
- [418] B. H. Lee, V. R. Anderson, S. M. George, *Chem. Vap. Deposition* **2013**, 19, 204.
- [419] B. H. Lee, K. K. Im, K. H. Lee, S. Im, M. M. Sung, *Thin Solid Films* **2009**, 517, 4056.
- [420] B. H. Lee, V. R. Anderson, S. M. George, *ACS Appl. Mater. Interfaces* **2014**, 6, 16880.
- [421] S. Zhu, Y. Yang, J. Liu, J. Sun, *J. Mater. Chem. A* **2020**, 8, 25371.
- [422] S. Lee, M. Kim, G. Baek, H. Kim, T. T. N. Van, D. Gwak, K. Heo, B. Shong, J.-S. Park, *ACS Appl. Mater. Interfaces* **2020**, 12, 43212.
- [423] S.-H. Lee, H.-J. Jeong, K.-L. Han, G. Baek, J.-S. Park, *J. Mater. Chem. C* **2021**, 9, 4322.
- [424] S. Lee, G. Baek, J.-H. Lee, T. T. N. Van, A. S. Ansari, B. Shong, J.-S. Park, *Appl. Surf. Sci.* **2020**, 525, 146383.
- [425] H. Zhu, M. H. Aboonassar Shiraz, L. Yao, K. Adair, Z. Wang, H. Tong, X. Song, T.-K. Sham, M. Arjmand, X. Song, J. Liu, *Chem. Commun.* **2020**, 56, 13221.
- [426] G. Baek, S. Lee, H. Kim, S. H. Choi, J.-S. Park, *Dalton Trans.* **2022**, 51, 1829.
- [427] A. Ghazy, M. Safdar, M. Lastusaari, A. Aho, A. Tukiainen, H. Savin, M. Guina, M. Karppinen, *Sol. Energy Mater. Sol. Cells* **2021**, 219, 110787.
- [428] Z. Giedraityte, P. Sundberg, M. Karppinen, *J. Mater. Chem. C* **2015**, 3, 12316.
- [429] R. M. Silva, L. D. Carlos, J. Rocha, R. F. Silva, *Appl. Surf. Sci.* **2020**, 527, 146603.
- [430] A. Ghazy, M. Safdar, M. Lastusaari, M. Karppinen, *Chem. Commun.* **2020**, 56, 241.
- [431] I. Stassen, M. Styles, G. Greci, H. Van Gorp, W. Vanderlinden, S. De Feyter, P. Falcaro, D. De Vos, P. Vereecken, R. Ameloot, *Nat. Mater.* **2016**, 15, 304.
- [432] W. Huang, X. Xie, K. Cui, S. Gou, Y. Li, *Inorg. Chim. Acta* **2005**, 358, 875.
- [433] J. A. Kaduk, *Acta Crystallogr., Sect. B: Struct. Sci.* **2000**, 56, 474.
- [434] S. M. F. Lo, S. S. Y. Chui, I. D. Williams, *Acta Crystallogr., Sect. C: Cryst. Struct. Commun.* **1998**, 54, 1846.
- [435] K. Momma, F. Izumi, *J. Appl. Crystallogr.* **2011**, 44, 1272.
- [436] D. Banerjee, S. J. Kim, L. A. Borkowski, W. Xu, J. B. Parise, *Cryst. Growth Des.* **2010**, 10, 709.
- [437] C. G. Carson, G. Brunello, S. G. Lee, S. S. Jang, R. A. Gerhardt, R. Tannenbaum, *Eur. J. Inorg. Chem.* **2014**, 2014, 2140.
- [438] G. B. Deacon, *Coord. Chem. Rev.* **1980**, 33, 227.
- [439] K. M. Fromm, *Coord. Chem. Rev.* **2008**, 252, 856.
- [440] B. F. Abrahams, A. D. Dharma, M. J. Grannas, T. A. Hudson, H. E. Maynard-Casely, G. R. Oliver, R. Robson, K. F. White, *Inorg. Chem.* **2014**, 53, 4956.
- [441] T. Stassin, S. Rodríguez-Hermida, B. Schrode, A. J. Cruz, F. Carraro, D. Kravchenko, V. Creemers, I. Stassen, T. Hauffman, D. De Vos, P. Falcaro, R. Resel, R. Ameloot, *Chem. Commun.* **2019**, 55, 10056.
- [442] M. Haranczyk, <http://www.zeoplusplus.org/examples.html> (accessed: December 2021).
- [443] P. D. C. Dietzel, R. E. Johnsen, R. Blom, H. Fjellvåg, *Chem. - Eur. J.* **2008**, 14, 2389.
- [444] S. R. Caskey, A. G. Wong-Foy, A. J. Matzger, *J. Am. Chem. Soc.* **2008**, 130, 10870.
- [445] M. März, R. E. Johnsen, P. D. C. Dietzel, H. Fjellvåg, *Microporous Mesoporous Mater.* **2012**, 157, 62.
- [446] R. Sanz, F. Martínez, G. Orcajo, L. Wojtas, D. Briones, *Dalton Trans.* **2013**, 42, 2392.
- [447] P. D. C. Dietzel, Y. Morita, R. Blom, H. Fjellvåg, *Angew. Chem., Int. Ed.* **2005**, 44, 6354.
- [448] M. I. Gonzalez, J. A. Mason, E. D. Bloch, S. J. Teat, K. J. Gagnon, G. Y. Morrison, W. L. Queen, J. R. Long, *Chem. Sci.* **2017**, 8, 4387.
- [449] P. D. C. Dietzel, B. Panella, M. Hirscher, R. Blom, H. Fjellvåg, *Chem. Commun.* **2006**, 959.
- [450] P. D. C. Dietzel, R. Blom, H. Fjellvåg, *Eur. J. Inorg. Chem.* **2008**, 2008, 3624.
- [451] Y. Zhang, H. Guo, W. Li, Y. Huang, Z. Zhang, G. Liu, Y. Wang, *ChemSusChem* **2019**, 12, 4160.
- [452] C. Volkringer, J. Marrot, G. Férey, T. Loiseau, *Cryst. Growth Des.* **2008**, 8, 685.
- [453] I. Senkowska, J. Fritsch, S. Kaskel, *Eur. J. Inorg. Chem.* **2007**, 2007, 5475.
- [454] P. Horcajada, S. Surblé, C. Serre, D. Y. Hong, Y. K. Seo, J. S. Chang, J. M. Grenèche, I. Margiolaki, G. Férey, *Chem. Commun.* **2007**, 2820.
- [455] N. Zhang, X. Yang, X. Yu, Y. Jia, J. Wang, L. Kong, Z. Jin, B. Sun, T. Luo, J. Liu, *Chem. Eng. J.* **2014**, 252, 220.
- [456] T. Loiseau, L. Lecroq, C. Volkringer, J. Marrot, G. Férey, M. Haouas, F. Taulelle, S. Bourrelly, P. L. Llewellyn, M. Latroche, *J. Am. Chem. Soc.* **2006**, 128, 10223.
- [457] P.-C. Liang, H.-K. Liu, C.-T. Yeh, C.-H. Lin, V. Zima, *Cryst. Growth Des.* **2011**, 11, 699.

- [458] L. Wang, A. Menakath, F. Han, Y. Wang, P. Y. Zavalij, K. J. Gaskell, O. Borodin, D. Iuga, S. P. Brown, C. Wang, K. Xu, B. W. Eichhorn, *Nat. Chem.* **2019**, *11*, 789.
- [459] Y. Ozawa, N. Ogihara, M. Hasegawa, O. Hiruta, N. Ohba, Y. Kishida, *Commun. Chem.* **2018**, *1*, 65.
- [460] C. Li, X. Hu, X. Lou, L. Zhang, Y. Wang, J.-P. Amoureux, M. Shen, Q. Chen, B. Hu, *J. Mater. Chem. A* **2016**, *4*, 16245.
- [461] N. Ogihara, T. Yasuda, Y. Kishida, T. Ohsuna, K. Miyamoto, N. Ohba, *Angew. Chem., Int. Ed.* **2014**, *53*, 11467.
- [462] D. Banerjee, S. J. Kim, J. B. Parise, *Cryst. Growth Des.* **2009**, *9*, 2500.
- [463] T. Yasuda, N. Ogihara, *Chem. Commun.* **2014**, *50*, 11565.
- [464] N. Ogihara, Y. Ozawa, O. Hiruta, *J. Mater. Chem. A* **2016**, *4*, 3398.
- [465] A. Ghazy, M. Safdar, M. Lastusaari, H. Savin, M. Karppinen, *Sol. Energy Mater. Sol. Cells* **2021**, *230*, 111234.
- [466] A. Tanskanen, O. Mustonen, M. Karppinen, *APL Mater.* **2017**, *5*, 056104.
- [467] Z. Song, T. E. Allen, C. S. Franklin, D. Gealy, *US2015243709A1*, **2015**.
- [468] I. Stassen, R. Ameloot, D. De Vos, P. M. Vereecken, *WO2015166015A1*, **2015**.
- [469] P. Willibrordus, G. Poodt, S. Unnikrishnan, P. Vereecken, D. P. N. Moitzheim, A. M. B. Van Mol, *US11108031B2*, **2021**.
- [470] M. Nisula, M. Karppinen, *WO2018197750A1*, **2018**.
- [471] A. Maraike, F. Juergen, A. Torben, K. Stephan, *EP3048185A1*, **2016**.
- [472] A. Fleissner, A. Rausch, T. Wehlus, D. Riedel, J. Rosenberger, *WO2016180815A1*, **2016**.
- [473] P. F. Carcia, R. S. Mclean, B. H. Lee, S.-H. Jen, S. George, *US2013337259A1*, **2013**.
- [474] S. M. George, A. A. Dameron, B. B. Burton, M. D. Groner, *US2010178481A1*, **2010**.
- [475] D. Peng, X. Pan, B. Li, S. Changhong, *CN102593371A*, **2012**.
- [476] J. R. Van Ommen, *US10245233B2*, **2019**.
- [477] R. Gronheid, C. Adelman, A. Delabie, G. Winroth, *EP2770373A1*, **2014**.
- [478] D. Binghai, H. Hang, W. Shimin, C. Fengxiang, W. Li, Z. Li, L. Jing, W. Erjing, *CN105280827A*, **2016**.
- [479] W. Li, C. Fengxiang, W. Shimin, D. Binghai, H. Hang, Z. Li, L. Jing, W. Erjing, *CN105280389A*, **2016**.
- [480] Y. Miao, S. Zhuonan, *US11033860B2*, **2021**.
- [481] R. Yerushalmi, S. Ishchuk, N. Kaynan, D. H. Taffa, T. Subramani, *US2015093597A1*, **2015**.
- [482] T. Yong, Z. Bin, C. Yao, Z. Shichao, *CN105195238A*, **2015**.
- [483] E. E. Tois, H. Suemori, V. J. Pore, S. P. Haukka, V. Sharma, *US10854460B2*, **2020**.



Jenna Multia is currently writing her doctoral thesis based on her Ph.D. research carried out in the Inorganic Materials Chemistry research group at the Aalto University, School of Chemical Engineering, under the supervision of Maarit Karppinen. Her Ph.D. research has focused on developing various new ALD/MLD processes, particularly for in situ crystalline metal–organic thin films based on alkali and alkaline earth metals. Recently, she was recruited as a Process Development Engineer at Beneq.



Maarit Karppinen received her Ph.D. in 1993. Before establishing her Inorganic Materials Chemistry group at the Aalto University in 2006, she was holding a Professor Chair at the Tokyo Institute of Technology. Currently, her research is focused on new ALD/MLD enabled functional materials, for which she received ERC AdG in 2013, followed by ERC PoC grants in 2015 (flexible thermoelectrics) and 2017 (Li–organic microbattery). This multidisciplinary research covers the design and synthesis of novel inorganic–organic materials and their characterization for various emerging energy technologies. She was nominated as Academy Professor for 2009–2013, and Aalto Distinguished Professor in 2017.